UNIVERSITÀ DEGLI STUDI FIRENZE

DOTTORATO DI RICERCA IN SCIENZE BIOMEDICHE

INDIRIZZO IN BIOCHIMICA E BIOLOGIA APPLICATA

CICLO XXXI

Coordinatore Prof. Massimo Stefani

Mechanisms of cell signalling in protein misfolding and natural molecules for prevention and treatment of amyloidosis

Settore Scientifico Disciplinare BIO/10

Dottorando
Dott.ssa Elena Bruzzone

Tutor
Prof.ssa Monica Bucciantini

Coordinatore
Prof. Massimo Stefani

Anni 2017/2018

"It is our choices that show what we truly are,
far more than our abilities."

Albus Dumbledore

Abstract

Oleuropein aglycone stabilizes the monomeric α-synuclein and favours the growth of non-toxic aggregates.

α-synuclein plays a key role in the pathogenesis of Parkinson's disease (PD); its deposits are found as amyloid fibrils in the Lewy bodies and Lewy neurites, the histopathological hallmarks of PD. Amyloid fibrillation is a progressive process proceeding through the transient formation of oligomeric intermediates widely considered as the most toxic species. Consequently, a promising approach of intervention against PD might be preventing α-synuclein accumulation and aggregation. A possible strategy involves the use of small molecules able to slow down the aggregation process or to alter oligomers conformation favouring a non-pathogenic one. In this study, we show that oleuropein aglycone (OleA), an olive polyphenol, exhibits anti-amyloidogenic power by interacting with α-synuclein monomers and interfering with the formation of on-pathway oligomers, in vitro. We investigated the molecular basis of such interference by Thioflavine T and ANS binding assays together with limited proteolysis; aggregate morphology was monitored by electron microscopy. We also found that OleA reduces the cytotoxicity of α-synuclein aggregates by hindering their binding to cell membrane components and preventing the resulting cellular damages in terms of increased ROS production.

Autophagy activation induced by the first genetic variant of β2-microglobulin oligomers.

It is widely recognized that the mechanism of amyloid aggregate cytotoxicity requires the primary interaction between the aggregates and the cell membrane, resulting in functional and structural perturbation of the latter, which can induce cell death by apoptosis or autophagy.

Autophagy is the process that helps to clean the cell from an exogenous or endogenous material that is useless or harmful to cells. This mechanism involves the transport of material present at the cytoplasmic level material through specific vesicles called autophagosomes in the lysosomal compartment. Generally, autophagy is induced by cell starvation, but other stresses can be caused by the activation of this process, such as the presence of misfolded protein deposits.

Our study is focused on understanding the signaling pathway responsible for the autophagic process induced by the interaction of the first genetic variant of β2-microglobulin (β2M-D76N) aggregates with cell membranes.

We have investigated the interaction process of amyloid aggregates at different stages of aggregation with specific membrane sites characterized by the presence of GM1 and the consequent activation of the signaling cascade responsible for the autophagic process. In fact, data acquired by Western Blot and confocal microscopy techniques have confirmed the activation of autophagy in human neuroblastoma cell line, SH-SY5Y cells, treated with B2M-D76N oligomers. The formation of autophagosomes and the increase of LC3-II, the main marker of autophagy, were observed at 5 hours of treatment. At the cytoplasmic level, a precise autophagic pathway has been identified that involves AKT, ERK and GSK3β upstream of the mTOR complex, whose inhibition promotes the activation of autophagy, and P-S6 downstream.

Table of contents

Introduction **8**
Protein Folding and Misfolding 9
Structure and formation of amyloid fibrils 14
Protein-membrane interaction and cytotoxicity 18
Membrane lipid composition influences protein aggregation 21
The importance of GM1 22
Amyloid diseases 24
α - Synuclein 26
Parkinson's disease 30
β2-Microglobulin 36
β2-Microglobulin amyloidosis 37
Asp76Asn Variant β 2 –Microglobulin 40
Extra-Virgin olive oil, a cornerstone of the Mediterranean diet 43
Oleuropein aglycone, typical phenol of extra-virgin olive oil 44
Autophagy 49
Signalling pathways of autophagy 56
Autophagy and diseases 60

Aim of the study **61**

Materials and Methods **64**
Oleuropein deglycosylation 65
Expression, purification and aggregation experiments 66
Disaggregation experiments 67
Structural characterization 67
TEM and DLS analysis 68
Chemical characterization 68
Limited proteolysis 69
Fingerprinting analysis of off-pathway oligomers 69
Immortalised cell line and cell treatment 70
Cytotoxicity assay: MTT test 70
Reactive oxygen species 71
Confocal immunofluorescence 72
Analysis of autophagic vacuoles 73
Western blotting 73
Data analysis and statistics 74

Results **75**
Interaction between OleA and monomeric α-Syn 76
OleA interferes with α-Syn aggregation into amyloid fibrils 78
Mapping α-synuclein conformation during aggregation in the presence of OleA by limited proteolysis 80
Characterization of the off-pathway species arising during α-Syn aggregation in the presence of OleA 84
α-Syn aggregates grown in the presence of OleA show reduced cytotoxicity 89
OleA interferes with the interaction of α-Syn aggregates with the cell membrane 97
D76N β2M sonicated oligomers induce citoxicity and ROS production 99
Different morphology of β2 and sonicated β2 oligomers 101

Autophagy activation induced by sonicated oligomers of D76N β2M.....101
Description of the autophagy signaling pathway induced by D76N β2M sonicated oligomers.....104
The interaction of the D76N β2M sonicated oligomers with the cell membrane favors the aggregation of the latter.....106
Discussion.....108
References.....116

Introduction

Protein Folding and Misfolding

The folding of proteins into their compact three-dimensional structures is the most fundamental and universal example of biological self-assembly; understanding this complex process will therefore provide a unique insight into the way evolutionary selection has influenced the properties of a molecular system for functional advantage (Dobson, 2003). The process of protein folding has been widely studied, and for better understanding its characteristics the theory of "energy landscape" has been developed that considers the native state of a protein as the absolute minimum in the folding energy landscape that depends on a large number of degrees of freedom. The folding process allows proteins to assume their native structure correctly and achieve their physiological function. Secondary structure, including strands, helices and sheets that are found in nearly all native protein structures, is stabilized primarily by hydrogen bonding between the amide and carbonyl groups of the main chain (the so-called backbone). The formation of such structure is an important element in the overall folding process, although it might not have a role as fundamental as the establishment of the overall chain topology (Makarov & Plaxco, 2003). The folding mechanism is very fast, ranging from milliseconds to fractions of a second, so it is difficult to describe, given the multiple conformations that unfolded polypeptide chains can take (Figure1).

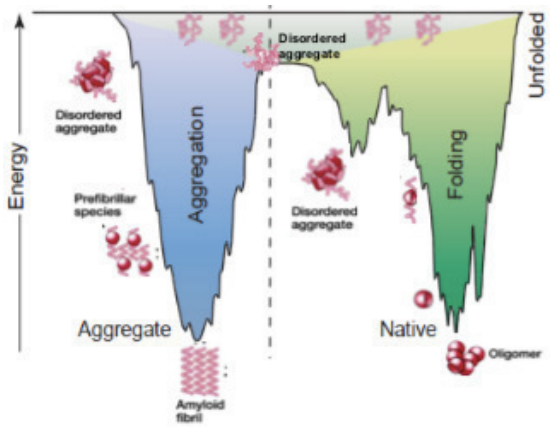

Figure1 Energy graphic of the conformational states for polypeptide chains to organize themselves in different structures during the correct folding of proteins and during the processes of protein aggregation (Jahn & Radford , 2005).

.

Levinthal, in 1969, indicated the infinity of degrees of freedom that a nascent polypeptide could display. If the protein would pass through all of these possible

conformations, it would need a time enormously greater than that measured *in vivo* (*E.coli* produces a protein of 100 amino acids in 5 seconds at 37 C). The difference that exists between the theoretical time for the correct folding to be achieved and the observed one it is known as the "Levinthal's paradox" (Levinthal , 1968).

Currently, the "core folding" of a polypeptide chain is considered to be entirely contained within its amino acid sequence; the protein folding exploits molecular dynamics that allow specific residues, although very distant in the amino acid sequence, to quickly enter in close contact. The formation of these contacts is a cooperative process, and conformational restrictions provided by an interaction will favour other interactions in a self-reinforcing process (Stefani, 2008). The inherent fluctuations in the conformation of an unfolded or incompletely folded polypeptide chain enable residues that are far in the aminoacid sequence to come into contact with other residues. Since, on average, native-like interactions between residues are more stable than non-native ones, they are more persistent and the polypeptide chain is able to find its lowest-energy structure by a trial-and-error process. Moreover, if the energy surface or 'landscape' has the right shape only a small number among all possible conformations needs to be sampled by any given protein molecule during its transition from a random coil to a native structure (Figure 2) (Dobson et al., 1998).

The energy landscape contains all conformational stages accessible to the polypeptide chain, with their entropy, free energy and fraction of native contacts. These species are heterogeneous and include highly dynamic and complex disordered conformations, whose structures are far from the native ones. Initially they form most of the secondary structure: alpha helices and β sheets. Subsequently, the increasing interactions of non-polar hydrophobic residues near the central core of the protein lead to a collapse of the polypeptide chain in a state called "Molten Globule". Molten Globules are deprived of many bonds between side chains that the protein shows in its final tertiary structure. The final steps to reach the native state include bond formation between side chains and the formation of covalent disulfide bridges.

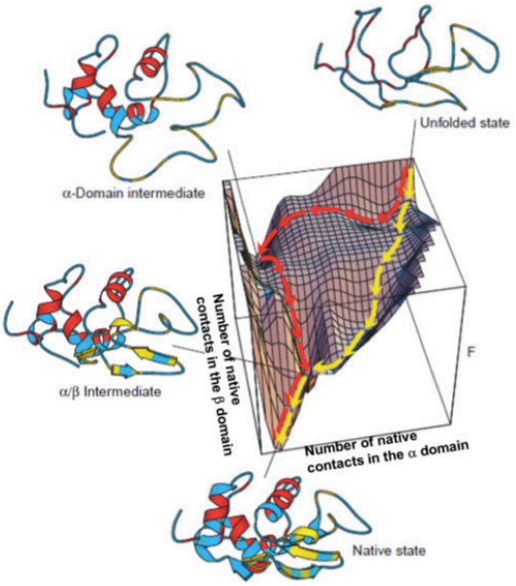

Figure 2 Schematic free-energy (F) surface representing features of the folding of hen lysozyme (a protein comprising an α and a β domain with 129 amino acid residues). Through the yellow trajectory (fast track) the α and the β domains are formed concurrently populating the intermediate only briefly. Through the red trajectory (slow track) the polypeptide chain is trapped in a long-lived intermediate with persistent structure involving only the α domain. Further folding from this intermediate involves either a transition over a higher barrier or partially unfolding (Dinner et al., 2000).

Although it is still unclear how a protein may contain information for training of its structure, it has been hypothesized that this is due to the presence of hydrophobic and polar residues, which favour the formation of specific interactions between residues ensuring the compactness of the structure. Within the cell are present both natively folded and natively unfolded proteins (NUPS). Many of these proteins are involved in cell cycle control, DNA transcription and in ribosome structure; they are characterized by low hydrophobicity and high net charge; these features make them incapable of folding in the intracellular environment and simultaneously prevent their possible aggregation (Uversky , 2002). In addition, their lack of structure favours the binding of chaperones with these proteins favouring their clearance and preventing their aggregation (Uversky , 2002). These proteins are an example of how the presence of surfaces can play an important role in facilitating the folding process. In fact, many

NUPS reach their correct three-dimensional structure upon binding to their target proteins, which have a surface adequate for NUP folding (Dedmon et al., 2002).

Probably, targets contain structural information, as charged and hydrophobic residues, required for NUP folding. Alternatively, naturally unfolded proteins undergo rapid intracellular turnover such that their unfolded state represents a mechanism of cellular control (Wright & Dyson , 1999).

Experiments carried out *in vitro* led to understand the bases of the folding process in a simple environment consisting of a buffered pH and a known ionic strength, sometimes containing a co-solvent or a denaturing agent. These conditions are very different from those present in the intracellular environment where other factors can potentially affect protein folding, misfolding or aggregation (Stefani, 2008). The intracellular protein concentration is about 300 - 400 mg / mL. This feature, known as “macromolecular crowding”, is very important in thermodynamics terms as it can affect the conformational states of proteins (Ellis , 2001). The cell membrane can promote the crowding and a reversible unfolding / refolding of specific proteins when they physiologically translocate through the membrane (Bychkova et al., 1988). Intracellular macromolecules can facilitate the folding of specific proteins. Some of these are a heterogeneous family of proteins termed “chaperones”, including prokaryotic GroES / GroEL and DnaK / DnaJ, also known in eukaryotes as Hsp70 / Hsp40. The role of chaperones is to facilitate the correct folding of other proteins, ensuring the presence of an appropriate environment, contacts with surfaces with which a protein can fold quickly and effectively and avoiding the formation of inappropriate interactions (Hartl & Hayer-Hartl, 2002). In the absence of chaperones, proteins will fail to achieve their native state (a process known as misfolding) and instead may associate with other unfolded polypeptide chains to form large aggregated structures (*in vivo*, this may result in deposition of extracellular aggregates or inclusion body formation) (Figure 3).

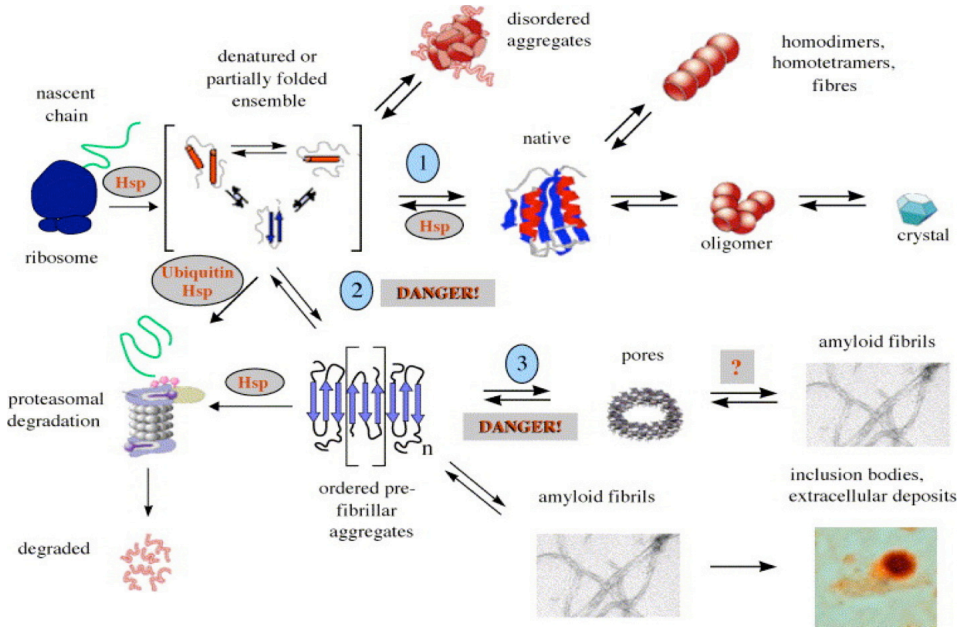

Figure 3 The possible fates of newly synthesized polypeptide chains. The equilibrium 1 between partially folded and native molecules is usually strongly in favour of the latter, except as results of mutations, chemical modifications or destabilizing solution conditions. Under normal conditions, the increased partially or completely unfolded populations are refolded by molecular chaperones (Hsp) or cleared by the ubiquitin–proteasome machinery. When these clearance machineries are impaired, disordered aggregates arise or the aggregation path (equilibrium 2) is undertaken, towards the nucleation of prefibrillar assemblies that eventually grow into mature amyloid fibrils (equilibrium 3). The formation of prefibrillar assemblies as amyloid pores could be directly related to the cytotoxic effects of amyloids (Stefani, 2004).

A similar scenario can occur when proteins acquire mutations or when they are exposed to unfavourable conditions, such as extreme heat or pH. Indeed, the presence of unfolded peptides, that expose to the aqueous environment their hydrophobic amino acid residues, induces a tendency to aggregation of hydrophobic side chains belonging to the same protein or different proteins, in the logic of decreasing the surface contact area with the solvent. In this case the polar solvent drives the formation of oligomeric protein aggregates, characterized by a high content of β-structures (Dobson, 2001). Protein folding and misfolding are associated with the regulation a wide range of cellular processes, leading to the conclusion that uncorrect folding may alter protein functionality with the consequent onset of pathologies (Stefani & Dobson, 2003). Misfolded proteins are devoid of their biological and functional activity and they are

prone to aggregate and/or interact inappropriately with other cell components, eventually leading to cell death. Some diseases often known as conformational diseases are due to misfolding and, as a consequence, the proteins acquire some normally absentoxicity (gain of function) or lose their functional activity (loss of function) (Thomas et al., 1995). Misfolding and growth of molecular aggregates with amyloid characteristics are two closely related phenomena. Indeed, it is not a coincidence that many amyloidoses are associated with mutations of specific chaperones or of proteins involved in the ubiquitin-proteasome system, that drive the polypeptide chain to a correct folding or degrade proteins that lose their correct tertiary structure, respectively (Macario & De Macario, 2001) (Layfield et al., 2001). Amyloidogenic proteins are diverse in sequence and share few characteristics, they can be large or small, have a catalytic or a structural role, be abundant or sparse. The lack of sequence or structural similarity amongst amyloidogenic proteins reinforces the notion that amyloid is a primitive structure that can be generated by many polypeptide sequences at proper conditions. Thus, it has been hypothesized that amyloid has existed as long as proteins exists, and it was probably a prominent fold in the early evolution of life (Chernoff, 2004). Recent studies have identified amyloid fibrils in bacteria, fungi, insects, invertebrates and humans that have a functional role. The functional amyloid hypothesis states that organisms have evolved to take advantage of the fact that many polypeptides can form amyloid, despite the fact that amyloid can be toxic (Mackay et al., 2001) (Fowler et al., 2006). However, the discovery of functional amyloid was surprising because amyloid has been associated solely with human diseases for over a century before its physiological role was discovered. Functional amyloid was identified initially within the past decade in several lower organisms, including bacteria (Chapman et al., 2002) (Claessen et al., 2003), fungi (Mackay et al., 2001), and insects (Iconomidou et al., 2006) and subsequently in humans (Fowler et al., 2006).

Structure and formation of amyloid fibrils

In general a protein or a peptide is termed as amyloid if, due to an alteration of its native functional state, it converts from its soluble functional state to a particular insoluble form, called the β-pleated-sheet, whose polymerization originates highly organized fibrillar aggregates. These structures are defined “amyloid fibrils” or “plaques” when

they accumulate extracellularly or as “intracellular inclusions” when they are formed inside the cell (Chiti & Dobson, 2006) (Chiti & Dobson, 2017). The presence of amyloid fibrils (either ex vivo or *in vitro*) is defined by the following three criteria (Nilson, 2004):

1. All amyloid fibrils are able to bind the dye Congo red, giving rise to an apple-green birefringence when observed under cross-polarized light.
2. All amyloid fibrils have fibrillar morphology and appear as long, straight, unbranched fibers, with a diameter of 70-120 Å and a variable length (Serpell et al., 2000), when they are investigated by electron or atomic force microscopy.
3. All amyloid fibrils are enriched in β-sheet secondary structure.

The fibrils are also stained with Thioflavin T (ThT), giving a shift in the fluorescence of the dye (LeVine, 1993) (Munishkina & Fink, 2007). Both circular dichroism (CD) and Fourier transform infra red spectroscopy (FT-IR) detect a high β-sheet content in amyloid fibrils, even when the precursor monomeric peptide or protein is substantially disordered or rich in α-helical structure. Finally, amyloid fibrils reveal a typical X-ray diffraction pattern indicating the presence of the characteristic cross-β structure in the fibril (Sunde et al., 1997).
The cross-β structure and texture is a stable structure in which the protein chains are held together by repetitive hydrogen-bonding that extends for the whole length of the fibrils. An amyloid fibril usually appears as composed by two to six 20-35 Å wide “protofilaments”, which are often twisted around each other to form supercoiled rope-like structures arranged around a hollow centre (Serpell et al., 2000). Each protofilament in such structures appears to have a highly ordered inner core that consists of polypeptide chains arranged in the characteristic cross-β structure. In this organization, the β-strands run perpendicularly to the protofilament axis, resulting in a series of β-sheets that propagate along the fibril axis (Figure 4). So the cross-β structure of the core of the amyloid aggregates is the main structural peculiarity of these assemblies.

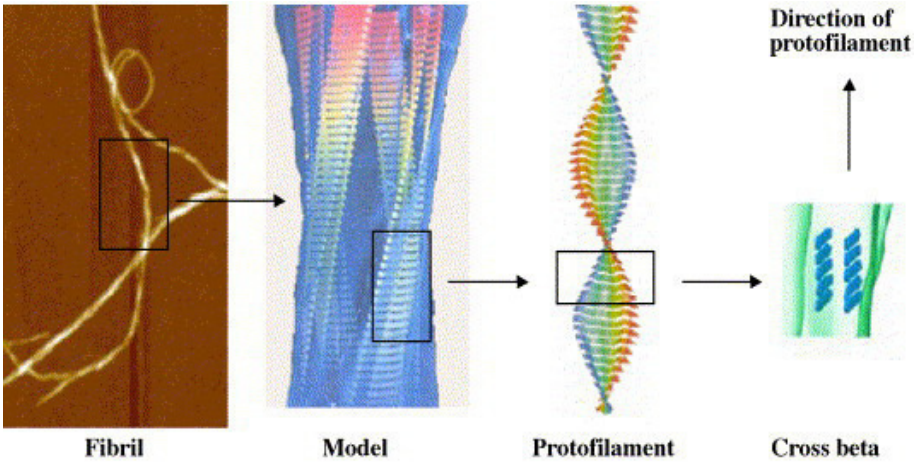

Figure 4 Close-up view of the structural organization of an amyloid fibril. Four protofilaments are wound around each other and their core structure is a row of β-sheets where each strand runs perpendicular to the fibril axis (Stefani, 2004).

The X-ray diffraction pattern characteristic of the cross-β structure consists of a sharp 4.7Å meridional reflection arising from the spacing between hydrogen-bonded β-strands within a β-sheet.

A broad reflection centred at 10 Å on the equator is also observed, which arises from the inter-sheet spacing (Figure 5). The spacing between the β-sheets depends on the size of the side-chain groups (Makin & Serpell, 2005).

So far, little is known about the detailed arrangement of the polypeptide chains into the amyloid fibrils, either those parts which form the core β-strands or the regions that connect the β-strands (Swuec et al., 2018). Many studies indicate that the sheets are relatively untwisted and they may exist, at least in some cases, in specific super secondary structure such as β-helices (Wetzel, 2002) or the α-helix (Kourie, 2001). There may be important differences in the way the strands are assembled depending on characteristics of the involved polypeptide chain, including length, sequence (Wetzel, 2002) (Chamberlain et al., 2000) and presence of intra-molecular disulfide bonds that stabilize the proteins (Frid et al., 2007).

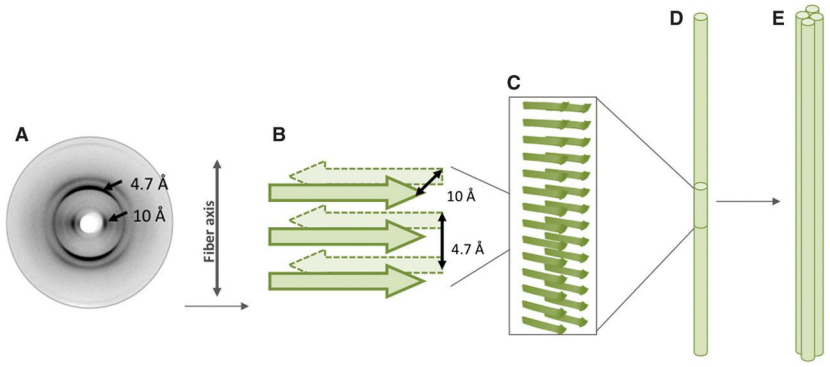

Figure 5 X-ray fibre diffraction gives information about the repetitive structure within the amyloid protofilaments. (A) the cross β diffraction pattern obtained from amyloid fibrils that arises from the (B) cross β structural core of the protofilament shown in (C). The self-associate protofilaments shown in (D) to form the mature amyloid fibril (E) (Serpell, 2014).

It is largely believed that most amyloidogenic proteins aggregate via a nucleation dependent pathway from an ensemble of partially unfolded conformations. This may occur under solution conditions (such as low pH, lack of specific ligands, high temperature, moderate concentrations of salts or co-solvents), such that the native structure is partially or completely disrupted but under which interactions such as hydrogen-bonds are not completely inhibited. However, native-like mechanisms of aggregation have also been described. For example, “lithostathine” maintains its native content of secondary structure upon aggregation into fibrils (Laurine et al., 2003). Association of protein molecules in their native-like states can therefore be the first event in the aggregation process, with the structural conversion into an amyloid conformation occurring subsequently. The time course to convert a peptide or a protein into amyloid fibrils typically includes a lag phase that is followed by a rapid exponential growth phase. The lag phase is assumed to be the time required for “nuclei” to form, where a nucleus is an ordered oligomeric amyloid species that can serve as a template for amyloid growth. When a nucleus is formed, fibril growth proceeds rapidly by further association with the nucleus of either monomers or oligomers. This protein aggregation eventually gives rise to short fibrillar structures referred to as protofibrils, which appear to be precursors of the mature fibrils and are generally shorter than the latter. Moreover, to form amyloid fibrils, proteins adopt at least in most cases, β-sheet-rich conformations. For example, in the case of the Aβ peptides, the main constituents of amyloid plaques in Alzheimer’s disease (AD), small ordered, β-sheet-rich aggregates or

"protofibrils" formed at early stages of amyloid growth have been described (Harper et al., 1997). Protofibrils have been observed in heterogeneous populations of small, roughly spherical or tubular assemblies, 2.5-5.0 nm in diameter (Lashuel et al., 2002) (Poirier et al., 2002) (Quintas et al., 2001). These species are often associated into bead-like chains or annular "doughnut"-shaped rings and appear, in most cases, to be precursors of longer protofilaments and mature fibrils that appear only at later stages of the assembly process. These "early aggregates" formed from different peptides and proteins may be very important to understand the nature and origins of the pathological properties of amyloid structures associated with neurodegenerative diseases. The soluble prefibrillar aggregates of different peptides and proteins have been shown to be equally recognised by polyclonal antibodies raised against prefibrillar assemblies grown from Aβ peptides (Kayed et al., 2003). The same antibodies, however, are unable to recognise the corresponding monomers and fibrillar aggregates, thus confirming that prefibrillar assemblies from very different peptides and proteins share common structural features which are different form those exhibited by the monomers or the mature fibrils.

Protein-membrane interaction and cytotoxicity

It is largely accepted that the toxicity of protein amyloid aggregates is mainly induced by their interaction with the cell membranes. The toxic aggregates are known to interact with cellular membranes and to compromise their integrity, by forming a range of ion channels through which they lead to imbalance of ion homeostasis and oxidative stress, eventually leading to cell death. Such a mechanism is reminiscent of the action of pore-forming proteins such as peptides found in venoms and antimicrobial secretions, bacterial toxins, perforin (Stefani & Dobson, 2003). The protein-membrane interaction is enabled by the presence, at the surface of the misfolded protein/peptide, of exposed hydrophobic residues and clusters, which prefer the hydrophobic environment of the lipid membranes (Kourie & Henry, 2002). In addition to the hydrophobic interactions, electrostatic interactions can also play an important role: amyloidogenic peptides often possess distinct positively charged regions allowing them to interact with negatively charged membranes.

The extent and the mechanism of membrane destabilization depends upon the balance of the electrostatic and hydrophobic properties and the amphipatic character of the protein. Membrane alterations induced by proteins can vary depending on the nature of the protein and lipids. Some peptides disrupt the membrane by binding through electrostatic interaction to the charged residues or regions to the charged headgroups of the phospholipids. This disturbance, likely to be reversible by itself, may be followed by insertion of hydrophobic regions of the protein into the bilayer (Evangelisti et al., 2012). Following protein insertion, the cell membrane can be affected in several ways (general electrostatic disturbance, fusion of vesicles, loss of membrane integrity, alteration in membrane thickness around the protein and/or pore formation).

The similarity between the mechanism of toxicity of pore-forming toxins (Kourie & Shorthouse, 2000) (Kourie & Henry, 2002) and the cytotoxicity of amyloid aggregates led to propose, since 1993, the "channel hypothesis" (Arispe et al., 1993); a number of experimental data, coming from both artificial lipid bilayers and cell membranes, indicate that the ability of misfolded proteins and amyloid aggregates to interact with lipid membranes is of crucial importance.

Protein aggregates can exert their toxic effect in several ways:

1) by insertion into the membrane lipid bilayer to form ion channels (Kourie & Henry, 2002) (Kourie, 2001);

2) by modifying the membrane viscosity and lipid packing thus interfering with membrane proteins (Salmona et al., 1997) (Tagliavini et al., 2001);

3) by penetrating into the cell with subsequent interaction with intracellular components (Kourie & Henry, 2002).

Many proteins have been shown to undergo changes in secondary structure upon their toxic interaction with membranes. Both α-helix to β-sheet and β-sheet to α-helix transformations, as well as secondary structure increase from a random coil conformation, have been described. For example, for some natively unfolded polypeptides like Aβ peptides, calcitonin and human amylin, the literature strongly suggests that these peptides populate an early oligomeric helical intermediate during amyloid aggregation *in vitro*. So, unfolding of the α-helix of a protein followed by refolding to β-sheet may be an important step in inducing a membrane-active structure for cytotoxic peptides, such as prion and Aβ peptides or human amylin. However, it is important to note that both β-sheet and α-helix-based protein structural changes could confer cytotoxicity to refolded proteins (Oropesa-Nuñez et al., 2016).

While it appears that no particular secondary structure confers an inherent advantage for membrane interaction, it may be that, for any particular peptide, some specific structure may allow better access of the hydrophobic residues to the membrane. This means that a change in secondary structure may undergo the ability to interact with the membrane. Anyway it is important to underline that the changes in secondary structure often arise as a consequence of the contact with the lipid environment: the hydrophobic lipids allow for lower energy exposure of hydrophobic residues, which leads to a rearrangement of the whole protein. The importance of secondary structure in hydrophobic residues exposure was shown by Gasset *et al*., who analyzed the structural requirements of α-sarcin to destabilize lipid bilayers. It was hard to explain the hydrophobic interactions of α-sarcin with a membrane, because this protein is highly polar in its native conformation. They demonstrated that, upon interaction with lipid vesicles, α-sarcin undergoes a structural change, with an increase in α-helix and decrease in β-sheet content from the most unfolded variant (Gasset et al., 1995).

The 106-126 fragment of PrP, which is the main part of the small amount of β-sheet in the normal cellular prion (PrP^c), contains a hydrophobic core sequence (residues 113-120), which is hypothesized to be involved in prion toxic properties via membrane interaction and destabilization, thus playing a key role in the pathological effect of the protein. It has been reported that β-sheet content of PrP[106-126] increases in the presence of lipids, and this structural change contributes to membrane destabilization and PrP[106-126] toxicity. The cytotoxic effect of amyloid β protein has been shown to involve the formation of ion channels within cell membranes, thus altering cell function and regulation. The Aβ peptide fragments, which are between 39 and 42 residues in length, are involved in forming these channels through a hydrophobic region at the C-terminus. The incorporation of Aβ peptides into membranes to form ion channels is thought to be determined preferentially by the presence of negatively charged, rather than by neutral, phospholipids (Alarcón et al., 2006). α-synuclein protofibrils, that are thought to be the main responsible of cell death in Parkinson's disease (PD) and form annular structures which are reminiscent of the known structures of toxin pores, have also been found to tightly bind and to permeabilize acidic phospholipid vesicles in a pore-like fashion, with a strong size selectivity in allowing molecules to cross the cell membrane (Volles et al., 2001). Calcitonin, an amyloid-forming peptide consisting of 32 residues, is known to be able to interact with membranes either directly and/or at receptor sites. Recent data showed that annular oligomers from salmon calcitonin are

able to form Ca^{2+}-permeable pores when inserted into liposomes, and that such an interaction is accompanied by an increase in the β-sheet content of the protein (Diociaiuti et al., 2006).

Mechanisms of membrane disruption other than pore formation have also been described: for example, according to some studies, human islet amyloid polypeptide (hIAPP), which is associated with death of insulin-producing pancreatic β-cells in type 2 diabetes mellitus and permeabilizes a variety of model membranes, could destroy the barrier properties of the cell membrane by extracting lipids from the latter and taking them up in the forming amyloid fibrils. It is important to note that the exact mechanism of membrane disruption by hIAPP aggregates is not known. However, lipid extraction has been shown to occur for a variety of proteins and has been proposed as a generic mechanism underlying amyloid toxicity (Sparr et al., 2004).

Membrane lipid composition influences protein aggregation

The fibrillogenic properties of membrane-bound proteins are determined by the chemical nature of membrane lipids and the mode of protein-lipid interactions. A lot of studies on membrane-mediated fibrillogenesis have been undertaken with model systems such as amyloidogenic peptides or proteins and lipid vesicles of varying composition (Bokvist et al., 2004) (Sparr et al., 2004). Membranes may be implicated not only as targets of aggregate toxicity, via disruption of membrane integrity, but also as catalyst that facilitate protein conformational changes and oligomer formation. Indeed, it is well established that lipid membranes can promote the aggregation of many different proteins/peptides. In particular, lipid composition, especially the presence of negatively charged lipids in the membrane, appears as one of the primary factors that determine the extent of membrane-mediated aggregation.

Many studies have been carried out to investigate the potential of acidic phospholipid-containing membranes in providing an environment able to enhance amyloid formation. For example, the formation of fibrous aggregates by a number of proteins in the presence of acidic, negatively-charged phospholipids, such as phosphatidylglycerol (PG), cardiolipin, or phosphatidiylserine (PS), has been described in recent studies. Membranes containing PS, an acidic phospholipid which is normally expressed in the outer surface of the plasma membrane of cancer cells and vascular endothelial cells in tumours, have been suggested to create surfaces with a high local concentration of

protons, required for aggregation (Canale et al., 2006). All these proteins share the presence of cationic residues or cationic amino acid clusters able to interact with negatively charged lipids, with subsequent fusion. Binding to acidic phospholipids neutralizes the positive charges in these proteins; accordingly, protein-protein interactions would not be counteracted by repulsion due to cationic residues, thus facilitating protein aggregation. The fibrils formed under these conditions have also been shown to incorporate lipid molecules, thus suggesting a lipid extraction by the protein on the membrane (Sparr et al., 2004). The liposome-induced fiber formation has been described as very rapid, with macroscopic structures becoming clearly visible almost instantaneously after the addition of the protein to a solution of PS-containing liposomes. Enhanced fiber formation has been seen to occur also on negatively charged mica, thus underlining the important role of these surfaces for all amyloidogenic proteins (Zhu et al., 2002).

Increasing evidence has indicated that gangliosides, particularly GM1 in lipid rafts play a pivotal role in amyloid deposition of Aβ and the related cytotoxicity in AD. Despite recent efforts to characterize Aβ-lipid interactions, the effect of Aβ aggregation on dynamic properties and organization of lipid membranes is poorly understood.

The importance of GM1

Growing evidence shows that GM1 ganglioside is involved in amyloid deposition and toxicity. Glycosphingolipids possess highly heterogeneous and diverse molecular structures in their carbohydrate chains and the lipid moieties. Based on their basic carbohydrate structures, glycosphingolipids are classified into numerous series, namely ganglio-, isoganglio-, lacto-, neolacto-, lactoganglio-, globo-, isoglobo-, muco-, gala-, neogala-, mollu-, arthro-, schisto- and spirometo-series (Table 1). Acidic glycosphingolipids containing one or more sialic acid (N-acetylneuraminic acid or N-glycolylneuraminic acid) residue(s) in their carbohydrate moiety are especially referred to as gangliosides. Gangliosides are ubiquitously found in tissues and body fluids, and are more abundantly expressed in the nervous system (Yu et al., 2009). In cells, gangliosides are primarily, but not exclusively, localized in the outer leaflet of plasma membrane.

On the cell surface, together with other membrane components such as sphingomyelin and cholesterol, gangliosides are involved in cell-cell recognition and adhesion and

signal transduction within specific cell surface microdomains, termed caveolae (Anderson, 1998), lipid rafts (Simons & Toomre, 2000) or glycosphingolipid-enriched microdomains (Hakomori et al., 1998). In addition to the cell plasma membrane, gangliosides have been shown to be present in the nuclear membrane, and they have recently been proposed to play important roles in modulating intracellular and intranuclear calcium homeostasis and the ensuing cellular functions (Ledeen & Wu, 2008).

Series	Basic structure	Abbreviation
Globo	GalNAcβ1 −3 Galα1 −4Galβ1 −4Glcβ1 −1 'Cer	Gb
Isoglobo	GalNAcβ1 −3 Galα1 −3 Galβ1 −4Glcβ1 −1 'Cer	iGb
Ganglio	Galβ1 −3 GalNAcβ1 −4Galβ1 −4Glcβ1 −1 'Cer	Gg
Isoganglio	Galβ1–3 GalNAcβ1–3 Galβ1–4Glcβ1–1'Cer	iGg
Lacto	Galβ1 −3 GlcNAcβ1 −3 Galβ1 −4Glcβ1 −1 'Cer	Lc
Neolacto	Galβ1 −4GlcNAcβ1 −3 Galβ1 −4Glcβ1 −1 'Cer	nLc
Lactoganglio	GalNAcβ1–4(GlcNAcβ1–3)Galβ1–4Glcβ1–1'Cer	LcGg
Muco	Galβ1–4Galβ1–4Glcβ1–1'Cer	Mc
Gala	Galα1–4Galβ1–1'Cer	Ga
Neogala	Galβ1–6Galβ1–6Galβ1–1'Cer	
Mollu	GlcNAcβ1–2Manα1–3Manβ1–4Glcβ1 −1'Cer	Mu
Arthro	GalNAcβ1–4GlcNAcβ1–3Manβ1–4Glcβ1–1'Cer	At
Schisto	GalNAcβ1–4Glcβ1–1'Cer	
Spirometo	Galβ1–4Glcβ1–3Galβ1–1'Cer	

Table 1 Carbohydrate structures of glycosphingolipids (Yu et al., 2011).

Gangliosides are involved in the pathology of many diseases. For example, Guillain-Barré syndrome, an acute polyradiculoneuropathy that leads to acute quadriplegia, is caused by an autoimmune response to cell surface gangliosides (Kaida et al., 2009). In influenza, a well known viral infectious disease, influenza A viruses recognize sialic acid residues of gangliosides and glycoproteins on cell surfaces as receptor molecules for cell invasion. During aging and neurodegeneration, the physicochemical properties of membranes are altered. This can result in unbalanced proportion of lipids in the membrane and/or in changed ratios of membrane lipids, which may contribute to AD pathogenesis for example (Kalanj-Bognar, 2006). In brain cells, ganglioside and lipid abnormalities, in addition to pathogenic Aβ production, may contribute to the pathological conditions found in AD (Mutoh et al., 2006).

Altered distribution of GM1 and GM2 gangliosides has been found in AD brains (Pernber et al., 2012). The interaction with GM1 has been reported to be a crucial factor

also in mediating the aggregation and toxicity of other amyloidogenic proteins and peptides (Gellermann et al., 2005) (Wakabayashi & Matsuzaki, 2009), such ashIAPP, whose aggregation and binding to the plasma membrane is thought to be the main factor determining the death of pancreatic β-cells in type II diabetes (Engel, 2009). While plasma membrane permeation and deformation have been the subject of many studies, the impairment and dysfunction caused by changes in mobility and lateral trafficking of membrane molecules induced by amyloid aggregates have been poorly investigated. Considering that amyloids can bind to a large number of biological molecules that range from glycosaminoglycans and nucleic acids to a variety of proteins and lipids, the change in membrane dynamics observed for GM1 may imply that amyloids can potentially harm all those cellular mechanisms that base their efficiency on molecules mobility (Calamai & Pavone, 2013). Actually, growing evidence shows that amyloid aggregates can alter membrane mobility of a number of proteins and other plasma membrane components, leading either to a gain or to a loss of function. For example, the binding of Sup35 amyloid fibrils to the plasma membrane can cause an accumulation of Fas receptors associated with GM1 with subsequent activation of the extrinsic apoptotic pathway (Bucciantini et al., 2012). On the other hand, sequestration of neurotransmitter receptors, such as the metabotropic glutamate mGluR5, by Aβ 1-42 oligomers has been shown to impair intracellular calcium levels and synaptic network activity (Renner et al., 2010). Within this context, an alteration of GM1 mobility may compromise its regulatory role in neurodevelopment and neuroprotection (Furukawa et al., 2011) (Yu et al., 2012), or influence cellular pathways linked to raft dynamics.

Amyloid diseases

Amyloidoses are human degenerative diseases, such as AD, PD, transmissible spongiform encephalopathies (TSEs) and non-insulin-dependent type II diabetes (NIMMD), are associated with an abnormal deposition of proteinaceous fibrillar aggregates (amyloid fibrils) in various tissues and organs (Stefani & Dobson, 2003) (Stefani, 2004). Approximately 25 different proteins and peptides are known to be able to form amyloid fibrils in various diseases. The polypeptides involved include full-length proteins (e.g. lysozyme, transthyretin), biological peptides (e.g. insulin, human amylin) and fragments of larger proteins produced by specific processing or by more

general degradation (e.g the Aβ-peptide). The peptides and proteins associated with the main amyloid diseases are listed in Table 2. These diseases can be grouped into three different categories (Chiti & Dobson, 2006):

1. neurodegenerative diseases: in which aggregation occurs in the brain (such as AD, PD, TSEs and Huntington's disease).
2. non-neuropathic localized amyloidosis: in which aggregation occurs in a single type of tissue other than the brain (such as NIMMD and medullary carcinoma of the thyroid).
3. non-neuropathic systemic amyloidosis: in which aggregation occurs in multiple tissues (such as lysozyme amyloidosis and fibrinogen amyloidosis).

Disease	Main aggregate component
Alzheimer's disease	Aβ peptides (plaques); tau protein (tangles)
Spongiform encephalopathies	Prion (whole or fragments)
Parkinson's disease	α-synuclein (wt or mutant)
Primary systemic amyloidosis	Ig light chains (whole or fragments)
Secondary systemic amyloidosis	Serum amyloid A (whole or 76-residue fragment)
Fronto-temporal dementias	Tau (wt or mutant)
Senile systemic amyloidosis	Transthyretin (whole or fragments)
Familial amyloid polyneuropathy I	Transthyretin (over 45 mutants)
Hereditary cerebral amyloid angiopathy	Cystatin C (minus a 10-residue fragment)
Haemodialysis-related amyloidosis	β_2-microglobulin
Familial amyloid polyneuropathy III	Apolipoprotein AI (fragments)
Finnish hereditary systemic amyloidosis	Gelsolin (71 amino acid fragment)
Type II diabetes	Amylin (fragment)
Medullary carcinoma of the thyroid	Calcitonin (fragment)
Atrial amyloidosis	Atrial natriuretic factor
Hereditary non-neuropathic systemic amyloidosis	Lysozyme (whole or fragments)
Injection-localised amyloidosis	Insulin
Hereditary renal amyloidosis	Fibrinogen α-A chain, transthyretin, apolipoprotein AI, apolipoprotein AII, lysozyme, gelsolin, cystatin C
Amyotrophic lateral sclerosis	Superoxide dismutase 1 (wt or mutant)

Huntington's disease	Huntingtin
Spinal and bulbar muscular atrophy	Androgen receptor [whole or poly(Q) fragments]
Spinocerebellar ataxias	Ataxins [whole or poly(Q) fragments]
Spinocerebellar ataxia 17	TATA box-binding protein [whole or poly(Q) fragments]

Table 2 A summary of the main amyloidoses and proteins or peptides involved.

It has also been demonstrated that many non-pathological peptides and proteins can aggregate *in vitro*, under appropriate conditions, into fibrils which are indistinguishable from those associated with amyloid diseases (Guijarro et al., 1998) (Litvinovich et al., 1998) (Chiti et al., 2001) (Uversky & Fink, 2004). The amyloidogenic proteins are very different in their sequence, function, size and tertiary structure, but all of them are able to form fibrils that share very similar morphological, structural and tinctorial features with amyloid. All these evidences led to the idea that the propensity to form amyloid fibrils is not an unusual feature of the small number of proteins associated with diseases, but is instead a generic property of polypeptide chains. A modification in the three-dimensional structure can be therefore sufficient to enable the production of aggregation-prone species by many proteins or peptides.

α - Synuclein

The synuclein family is constituted by α-, β- and γ-syn, but only α - Synuclein (α- Syn) has been found to be associated to human neurodegenerative diseases. α-Syn is a small neuronal protein composed by 140 amino acids, and encoded by the human SNCA gene in the chromosome 4. Figure 6 shows the α-Syn structure comprises three domains: an N-terminal domain (residues 1–60), a non-amyloid-β component of plaques (NAC) domain (residues 61–95), and a C-terminal domain (residues 96–140) (Figure 6) (Palazzi et al., 2018).

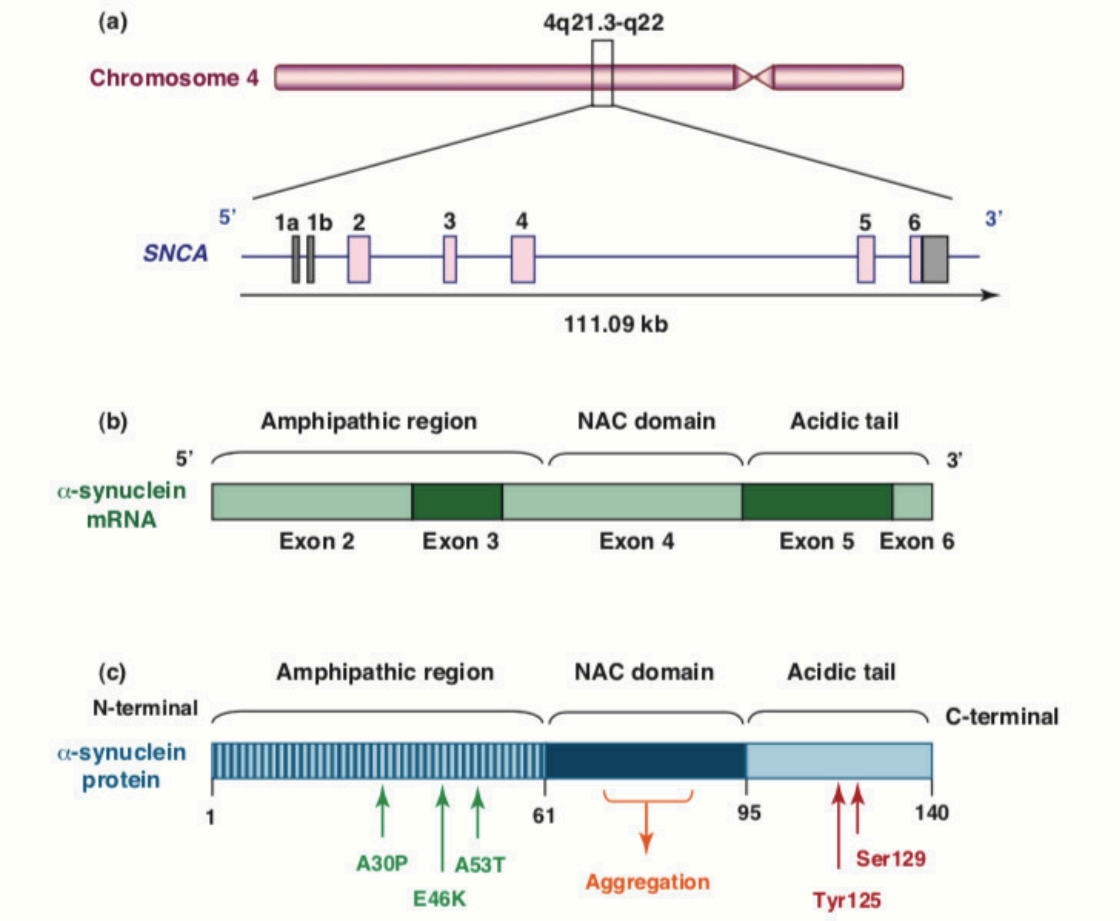

Figure 6 α-Syn is a major player in Parkinson's disease pathogenesis. (A) α-Syn is encoded by SNCA gene, located on chromosome 4. (B) From the 6 exons comprising SNCA, only the last 5 encode for α-Synuclein protein, which is composed by 140 amino acids. (C) Schematic representation of the different domains of α-Syn and the localization of the familial mutations A30P, E46K, G51D and A53T in the N-terminal domain (Vendal et al., 2010).

Several mutations segregated with PD have been already mapped to the SNCA locus. The missense mutation A53T was mapped in 1997 (Polymeropoulos et al., 1997). Subsequently two additional missense mutations were mapped: A30P and E46K (Krüger et al., 1998) (Zarranz et al., 2004). These missense mutations are located in the N-terminal domain of α-Syn, involved in the binding to membranes, and induce an increase in the propensity of this protein to misfold and form fibrillar aggregates enriched in β-sheet structure (Lemkau et al., 2012). More recently, the H50Q (Appel-Cresswell et al., 2013) and G51D (Kiely et al., 2013) missense mutations were also identified. The H50Q mutation stabilizes α-Syn fibrils, significantly increasing the

aggregation rate and the ability of this protein to form amyloid inclusions, while the G51D mutation slowdowns α-Syn aggregation, but both mutations increased the toxicity (Rutherford et al., 2014) (Fares et al., 2014). Genomic duplication or triplication of the SNCA locus, which increases α-Syn expression, also causes a form of autosomal dominant PD (Konno et al., 2016). The SNCA dosage is inversely correlated with the age of onset and directly correlated with the severity of the disease (Miller et al., 2004) (Ibáñez et al., 2004). Studies by several groups using different biophysical methods (for example, nuclear magnetic resonance (NMR), light scattering and circular dichroism (CD)) consistently showed that α-Syn purified from Escherichia coli under native or denaturing conditions exists predominantly as stable unfolded monomers (Eliezer et al., 2001). Many studies support the notion that the native and physiological form of α-Syn is the monomer, but do not rule the possibility that the protein could form functional oligomers upon interaction with other proteins or biological membranes. The apparently multifunctional properties of α-Syn may lie in its conformational flexibility, which may allow the protein to adopt different conformations upon interacting with biological membranes of different compositions, other proteins or protein complexes (Ramakrishnan et al., 2006) (Ullman et al., 2011).

It is well established that α-Syn adopts a α-helical conformation upon binding to synthetic or biological membranes in vitro. However, very little is known about the conformational state of α-Syn in the different compartments of the living cell, and there is a lack of direct evidence for a functional role of native α-Syn oligomers in biological membranes. It is conceivable that native α-Syn exists in equilibrium between different conformational and/or oligomeric states. Several factors, including oxidative stress (Hashimoto et al., 1999), post-translational modifications (Andringa et al., 2004), proteolysis (Dufty et al., 2007), as well as the concentration of fatty acids (Perrin et al., 2001) (Karube et al., 2008), phospholipids and metal ions were shown to induce and/or modulate α-Syn structure and oligomerization in vitro, which may influence this equilibrium between the monomer and oligomer state in vivo (Hashimoto et al., 1999).

Together, these studies suggest that α-Syn exists predominantly as a monomer, but do not rule out the possibility that it can form a stable multimer and/or adopt different structures under specific stress-induced conditions or upon interaction with other proteins, specific ligands, lipids and/or biological membranes (Lashuel et al., 2013).

Although the physiological function of α-Syn remains unknown, we know that this molecule is a predominantly presynaptic 140 residues natively unfolded protein.

The deficiencies in synaptic transmissions observed in response to knock down or overexpression of α-Syn suggest that α-Syn has a role in the regulation of neurotransmitter release, synaptic function and plasticity.

α-Syn interaction with membranes and lipids is also considered functionally important (Snead & Eliezer, 2014); in fact it has been suggested that α-Syn may modulate the presynaptic vesicular pool size, promote SNARE-complex assembly (Burré et al., 2010), and regulate dopaminergic neurotransmission (Lashuel et al., 2013).

Moreover, SNCA knock-out mice exhibit an impairment in hippocampal synaptic responses to prolonged trains of high-frequency stimulation that deplete the docked and reserve pool of synaptic vesicles, as well as impairments in replenishment of docked pools from the reserve pool, indicating that α-Syn may control the refilling and the trafficking of synaptic vesicles from the reserve pool to the site of synaptic vesicle release (Burré et al., 2010) (Lashuel et al., 2013) Moreover, depletion of α-Syn, through use of antisense oligonucleotides, induces a decrease in the availability of reserve synaptic vesicle pool in primary cultured hippocampal neurons (Burré et al., 2013). Finally, the possible role of α-Syn in regulating synaptic homeostasis is not exclusively related to its direct interaction with synaptic vesicles. α-Syn interacts with synaptic proteins controlling vesicle exocytosis, such as phospholipase D231 and the family of Rab small GTPases (Masuda et al., 2006). Recent studies reported that α-Syn can act as a chaperone, and controls the degradation and affects the assembly, maintenance and distribution of the pre-synaptic SNARE protein complex (Figure 7), which is directly implicated in the release of neurotransmitters, including dopamine (Hong et al., 2008). Together, these observations indicate that α-Syn has an important role in the trafficking of synaptic vesicles and in the regulation of vesicle exocytosis, and may contribute to more subtle regulatory phenomena by controlling synaptic homeostasis- associated proteins.

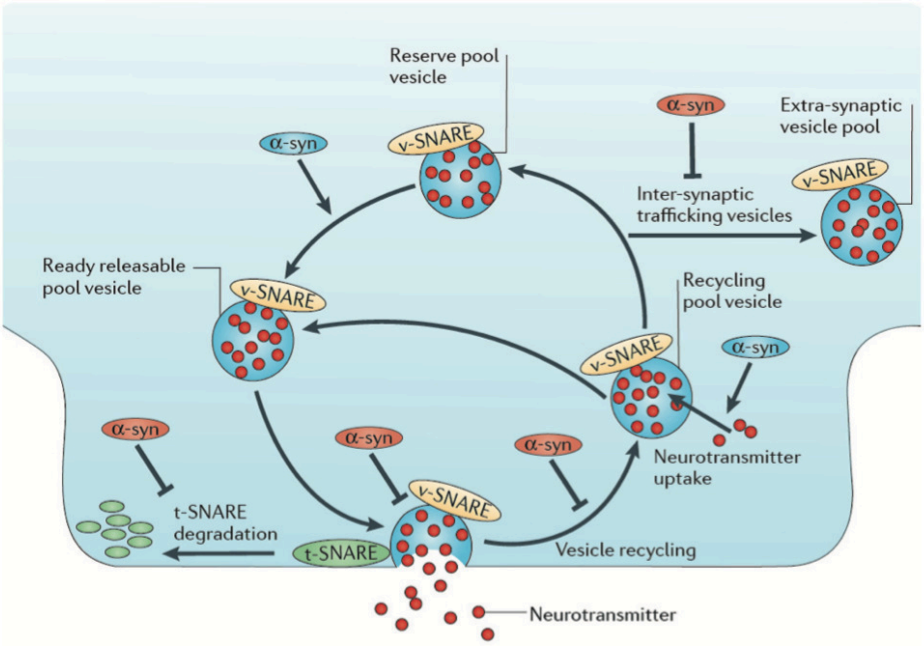

Figure 7 α-Syn modulates neurotransmitter release by regulating SNARE family proteins. α-Syn modulates the activity of v-SNARE and t-SNARE proteins, and thus vesicular trafficking at multiple stages. α-Syn in red indicates a step that is impaired due to loss of α-Syn physiological function e.g. in synucleinopathies; α-Syn in blue indicates a step where α-Syn regulates trafficking and refilling of the presynaptic vesicle (Lashuel et al., 2013).

Parkinson's disease

Parkinson's Disease (PD) was firstly described in 1817 by James Parkinson as the "shaking palsy" (Figure 8). The most prominent clinical symptoms are related to motor functions: tremor, bradykinesia (slowness of movement), rigidity and postural instability. In later stages, cognitive and behavioral functions may also be affected.

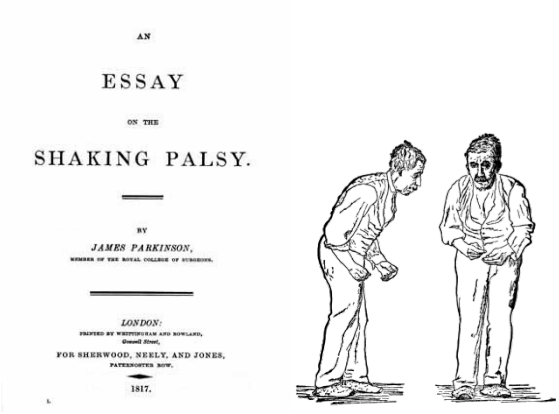

Figure 8 First scientific description of Parkinson's disease (PD) by James Parkinson in "An essay on the shanking palsy, 1817" and the illustration of this pathology by William Richard Gowers published in "A manual of diseases of the nervous system, 1886".

PD, and neurodegenerative disorders in general, constitutes an enormous socio-economic burden and the number of affected individuals is expected to increase significantly in the next decades as global population ages (Figure 9).

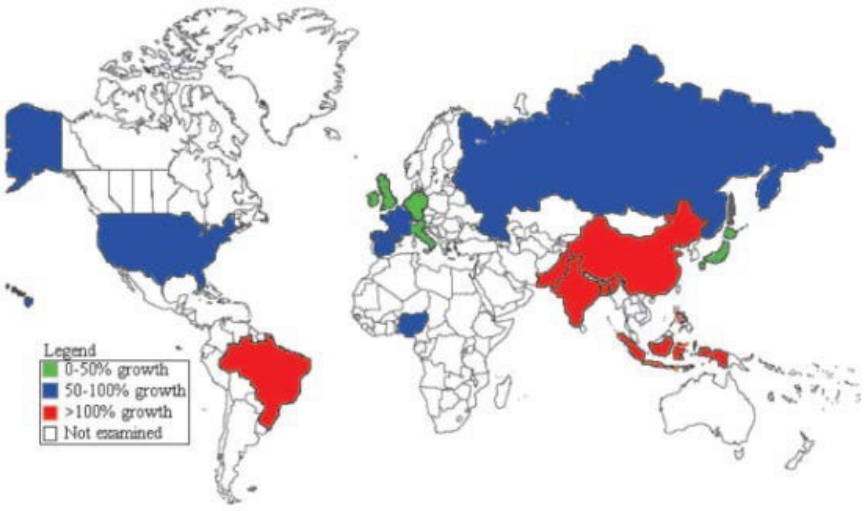

Figure 9 Number of patients suffering from PD from 2005 until 2030 (Dorsey et al., 2007).

PD incidence is usually comprised between 10 and 50/ 100,000 person-years, and its prevalence between 100 and 300/100,000 populatio. PD frequency increases sharply with age. It is rare before age 50 years, and its incidence and prevalence both increase progressively after age 60; based on a meta-analysis of prevalence studies, its prevalence rose from 107/100,000 persons between ages 50 and 59 years to 1087/100,000 persons between 70 to 79 years (Pringsheim et al., 2014). PD is usually more common in men than women, with a male-to-female ratio of about 1.5 (Wooten et al., 2004). Possible explanations for this difference include more frequent occupational exposures in men, neuroprotection from estrogens in women and X-linked genetic factors. Geographical differences in PD frequency have been reported, but are difficult to interpret because of differences in finding cases and population characteristics. A collaborative study conducted in four European countries using similar case-finding methods and diagnostic criteria did not reveal any differences (de Rijk et al., 1997). On the other hand, a meta-analysis of six studies found a lower prevalence in Africa than in either Europe or North America (Okubadejo et al., 2006), whereas there was no significant difference between African-Americans and Caucasians in the United States (Schoenberg et al., 1988). The prevalence and incidence of PD also appear to be slightly lower in Asian than in Western countries (Muangpaisan et al., 2009), although some studies have found similar estimates. It is unclear whether such differences are due to environmental factors or whether they reflect methodological differences across studies.

For the vast majority of PD patients, the syndrome only correlates with age and there is no clear explanation yet of its etiology (idiopathic PD). Only in a minority of patients, PD is caused by genetic and/or environmental factors (hereditary and symptomatic PD respectively).

Several gene loci have been implicated in autosomal dominant forms of PD including duplications or/and mutations in α-Syn (Polymeropoulos et al., 1997). Other gene loci have been found to cause autosomal recessive form of PD, such as the gene mutations in parkin (Kitada et al., 1998) and in DJ-1 (Bonifati et al., 2003). Both autosomal dominant and recessive forms of parkinsonism usually have an early onset as compared with the idiopathic PD.

There are also several environmental factors known to cause parkinsonian symptoms. Exposure to iron or manganese has been shown to generate reactive oxygen species and have been used to induce parkinsonism in laboratory animals. Two important chemical

examples are 1-methyl-4-phenyl-1,2,3,6- tetra-hydropridine (MPTP) and the herbicide paraquat, which both concentrate in dopaminergic neurons and eventually will kill them (Langston et al., 1983) (Javitch et al., 1985). MPTP was found in poorly purified MPPP, an opioid analgesic drug. It is not used in clinical practice, but has been illegally manufactured for illicit drug use. In the early 80´s Californian drug abusers were notoriously more affected with parkinsonian symptoms than the rest of the population, which led to the identification of MPTP. The MPTP metabolite MPP+ is selectively taken up by dopaminergic neurons through the dopamine transporter (DAT) (Langston et al., 1983) (Javitch et al., 1985). MPP+ inhibits the mitochondrial respiratory chain, depleting the neuron from ATP. Because of its selective uptake this neurotoxin kills SNc neurons and causes a parkinsonian-like syndrome in humans and animals. It is today the best characterized animal model for PD.

With the intention to explain idiopathic causes of PD, it has also been suggested that dopamine can be oxidized and generate a toxic derivative, dopamine quinone. In this reactive form, dopamine quinone can covalently bind to cysteins forming 5- cysteinidyl-dopamine. Cystein residues are commonly located in active sites of enzymes and the covalent modification of them might lead to a general malfunction of the neuron. In this respect high expression levels of the dopamine transporter (DAT) have been suggested to increase the toxic load of SNc neurons by increasing cytosolic dopamine (LaVoie & Hastings, 1999). These processes can occur gradually and naturally, which might up to some extent account for the late onset of the idiopathic form of PD.

Functional imaging (i.e. positron emission tomography) suggests that about 60% of the dopaminergic neurons in that region have to degenerate and about 80% of dopamine depletion has to occur before the first Parkinsonism symptoms display (Figure 10) (Dauer & Przedborski, 2003).

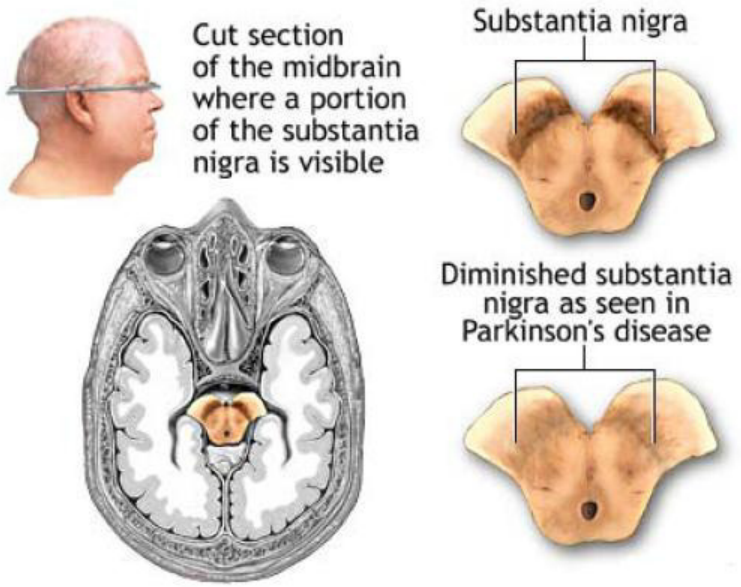

Figure 10 Comparison between the substantia nigra pars compacta in a healthy and a PD-affected brain, showing the loss of pigmentation due to prominent dopaminergic neurons death (Dauer & Przedborski, 2003).

Moreover, proteins and lipids aggregates, termed Lewy Bodies (LBs) and Lewy Neurites (LNs), were found in the post-mortem analysis of the surviving neurons in patients brains with a PD diagnosis.

LBs are eosinophilic cytoplasmic inclusions, whose main constituents are ubiquitin and, more important to this thesis, an aggregated form of the proteins α-Syn (Figure 11). Electron microscopy showed that α-Syn present in LBs and LNs is organized into filaments 200-600 nm long and with a diameter of 5-10 nm (Spillantini et al., 1998). X-ray diffraction revealed that α-Syn filaments in LBs present a β-sheet structure (Serpell et al., 2000) characteristic of amyloid fibrils.

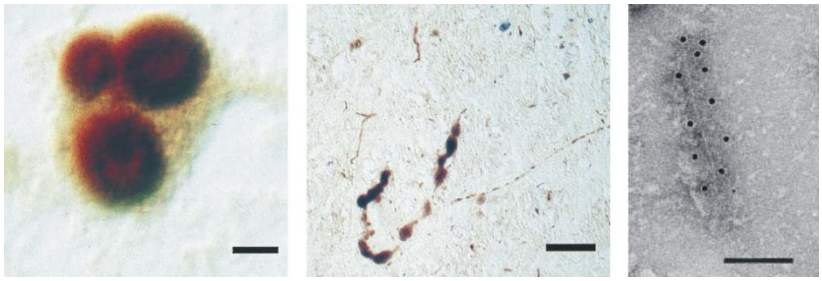

Figure 11 LBs, on the left, and LNs, in the middle, double-stained with α-Syn and ubiquitin antibodies (Scale bar 10 mm and 90 mm respectively). On the right, fibrils

purified from LBs and immunostained with aS antibody. The gold nanoparticles conjugated with the secondary antibody appears as black dots (Scale bar 100 nm). Adapted from (Spillantini et al., 1998).

Braak and co-workers associated the diffusion of LBs in different brain regions to the disease staging (Braak et al., 2003). Pathological studies of healthy and PD affected brains have shown that α-Syn inclusions form in a similar and precise order in the different regions of diseased brains, allowing the identification of six stages of LBs deposition in relationship with PD progression (Figure 12).

Interestingly, α-Syn inclusions can deposit early in the enteric nervous system and in the peripheral nervous system (Braak et al., 2003). It is quite established now that α-Syn pathology starts in some nerve and spreads in a prion-like manner. However, the mechanism(s) by which the pathology diffusion occurs is still unclear and several possibilities were proposed in the literature (Goedert et al., 2013).

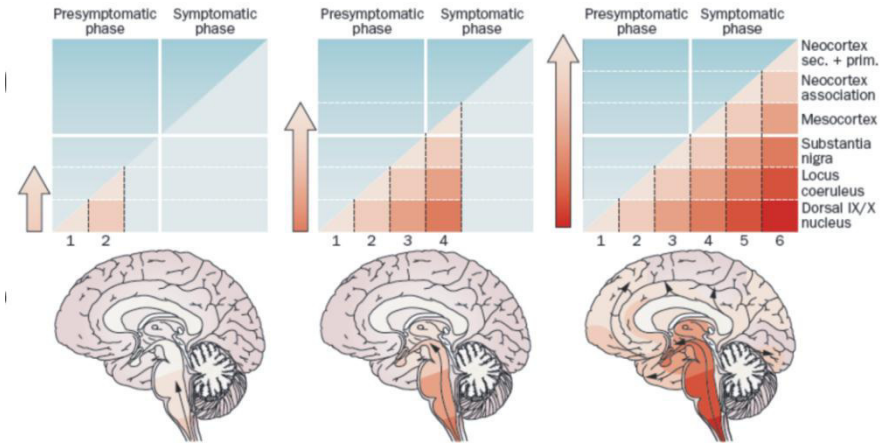

Figure 12 Six stages of PD pathology. Patients with α-Syn deposition belong to one of these stages and disease spreading means involvement of additional brain regions and symptoms worsening. Stage 1: LBs are observed in the olfactory bulb, the anterior olfactory nucleus and/or the dorsal motor nuclei of the vagal and glossopharyngeal nerves in brainstem. Stage 2: lesions occur in the pontine tegmentum. Stage 3: LBs are found in pedunculopontine nucleus, the cholinergic magnocellular nuclei of the basal forebrain, the pars compacta of the substantia nigra. Stage 4: the hypothalamus, portions of the thalamus and the anteromedial temporal mesocortex (first cortical region). First

PD symptoms occur during stage 3 and early stage 4. Stage 5-6: lesions emerge in the neocortical high-order association areas (stage5) and first-order association areas and primary fields (stage 6) (Goedert et al., 2013).

β2-Microglobulin

The major histocompatibility complex class I (MHC I) molecule and antigenic peptide are recognized by $CD8^+$ cytotoxic lymphocytes (CTL) during CTL activation and lysis of targets. The heavy chain of the MHCI molecule can interact non-covalently with a number of other molecules to form a CTL activating complex. One of these molecules is β2-microglobulin (β2M), whose role is to serve as a co-receptor for the presentation of the MHC I in nucleated cells for cytotoxic T-cell recognition (Pedersen et al., 1994). $CD8^+$ and β2M, the non-polymorphic ligands of the MHC I heavy chain, have been shown by X ray crystallography to interact with the immunoglobulin-like α3 domain and the α1α2 domains of the MHC I heavy chain in addition to interacting to each other (Saper et al., 1991).

β2-microglobulin is a low molecular weight polypeptide of 11800 Da, synthesized by all nucleated cells, initially as a 119 residue protein and, after processing, secreted as a 99 residue protein. β2M has a β-sandwich fold typical of the immunoglobulin superfamily, and contains seven β-strands (Figure13). Three strands form one side of the sandwich and four strands the other. An internal disulfide bond tethers strands 2 and 6 in the folded protein. Its structure resembles that of the constant domains of IgG and it is found on the cytoplasmic membrane of most cells, where it forms the light chain of histocompatibility antigens (Bjerrum & Plesner, 1985). Free β2M is released into the blood and other body fluids during cell membrane turnover and it is freely filtered by renal glomeruli and then catabolized by the tubules (Peterson et al., 1972). It has been calculated that approximately 150 mg of β2M is metabolized daily by the normal kidney (Vincent et al., 1980), the major site of β2M degradation. In conditions characterized by reduced glomerular filtration rate the serum levels of β2M increase (Wibell et al., 1973). Serum levels are also elevated in diseases associated with increased cell turnover and in several benign conditions such as chronic inflammation, liver disease, renal dysfunction, some acute viral infections, and a number of malignancies, especially hematologic malignancies associated with the B-lymphocyte lineage. In uremia, the increase is massive, which is in contrast to the moderately increased values (two- to

threefold the normal) seen in some other conditions, e.g., lymphoproliferative (Cassuto et al., 1978), autoimmune (Maury et al., 1982), and hepatobiliary diseases (Rashid et al., 1981). Serum β2M level < 4 mcg/mL is a good prognostic factor in patients with multiple mieloma.

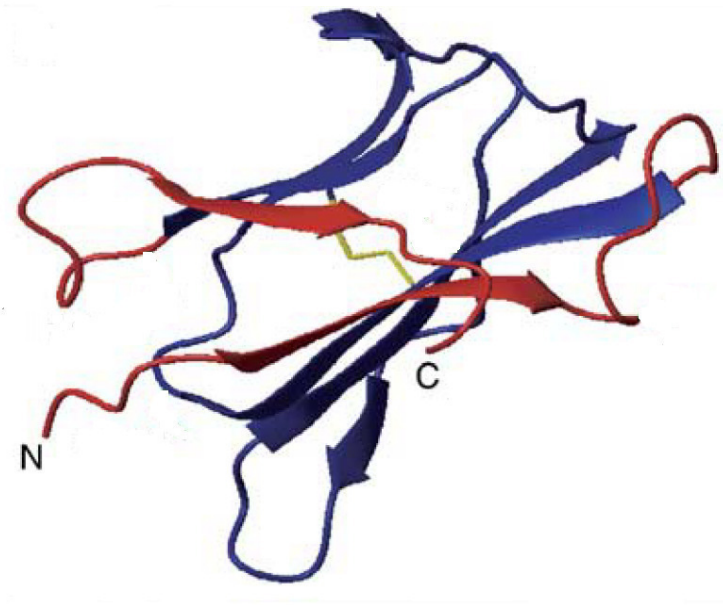

Figure 13 Ribbon structure of β2M. The N- and C-terminal β-strands are shown in red (Bjorkman et al., 1987).

β2-Microglobulin amyloidosis

In 1985 Gejyo *et al*. identified a new type of amyloid fibril protein consisting of β2M. The protein was isolated from amyloid-laden tissue from a patient with chronic renal failure and carpal tunnel syndrome (CTS) who had been on regular hemodialysis (HD) treatment for 13 years. The identification of β2M as an amyloidogenic protein has brought a fundamental contribution to the understanding of the mechanisms of amyloidogenesis in general and has further emphasized the complexity of amyloid disease and the diversity of proteins capable of forming, under certain circumstances, congophilic fibrillar deposits in human tissues.

β2M deposition is associated with the syndrome of arthralgias and arthropathy in long-term dialysis patients, although the precise pathogenic role played by amyloid deposits still needs to be clarified. The chronic arthralgias are usually bilateral and often involve the shoulders initially. Other joints, in particular the knees, wrists and small joints of the

hands, may also be involved. Chronic joint swelling is another important feature of the disease, as may be recurrent haemarthrosis and chronic tenosynovitides of the finger flexors.

CTS is a well-recognized complication in HD patients (Warren & Otieno, 1975) and is clearly related to the duration of HD (Brown & Gower, 1982). A prevalence of 50% has been reported in patients who have received more than 12 years of HD (Schwarz et al., 1984). In HD patients on conventional dialyzers mean serum β2m levels are of the order 30-50 mg/1 (Hurst et al., 1989) (Thielemans et al., 1988) (normal reference range, 0.8-3.0 mg/1). The β2M level appears rather stable in follow-up studies of 2-6 months, but in longer follow-up it tends to increase with the number of years in HD. The serum level of β2M does not discriminate between HD patients who have β2M amyloid and those who do not (Gejyo et al., 1986). In patients on continuous ambulatory peritoneal dialysis (CAPD) serum β2M levels are markedly elevated and are of the same order, although slightly lower, than in HD (Ballardie et al., 1986). The slightly lower levels could be explained by the permeability of the peritoneal membrane to β2M (Thielemans et al., 1988). In fact, the interaction between the blood and the dialysis membranes triggers the activation of mononuclear cells, which stimulate the production of inflammatory cytokines. The activation depends on the material used for dialysis, which is also considered as an index of biocompatibility. Cytokines, such as interleukin-1 (IL-1), tumor necrosis factor-α (TNF-α), and interleukin-6 (IL-6), can induce an inflammatory state of the base during the process of hemodialysis , connected in acute manifestations, such as increased temperature and hypotension (Piazza et al., 2006).

Amyloidogenic properties of β2M have been associated to its secondary structure in particular because it contains two antiparallel beta-pleated sheets. The beta structure has been suggested to be important in the stabilization of the tertiary conformation of heavy chains of class I HLA antigens on the cell surface (Lancet et al., 1979) and is obviously involved in the amyloidogenic properties of β2M. Connors *et al*. demonstrated that amyloid fibrils can be created *in vitro* from intact molecules of β2M (Connors et al., 1985). This is remarkable, since *in vitro* and in vivo creation of amyloid from precursor proteins usually involves limited proteolysis of the precursor (Glenner, 1980). Fragments of β2M may also form amyloid as suggested by the presence of β2M fragments in synovial amyloid in dialysis patients and amyloid kidney stones of uremic patients (Linke et al., 1986).

The current pathogenetic model of β2M amyloidosis has several similarities with the models of the major acquired systemic amyloid diseases, AA and AL amyloidosis (Glenner, 1980). First, there is a circulating precursor which may be either normal or abnormal. In the case of β2m amyloidosis, the precursor is most probably normal β2M, although some evidence suggests the presence of an abnormal β2M fraction in sera from patients on longterm HD. Second, the level of the circulating precursoris markedly elevated. In β2M amyloidosis, the mean serum level of β2M is about 20- to 30-fold the level found under normal conditions. Third, the precursor is elevated for a long period of time. In the case of β2M amyloidosis the duration of the massive elevation is usually ten years or more. Finally, not all patients with prolonged elevation of the amyloid precursors develop amyloidosis. The additional factors required for amyloidogenesis to occur are, however, poorly defined. The role of the mononuclear phagocyte system in amyloid precursor proteins processing is probably important. The possible roles of the amyloid P protein (Woo et al., 1987), a characteristic component of extracerebral amyloid including β2M amyloid (Gorevic et al., 1986), and of amyloid-degrading proteases (Maury, 1988) and amyloid-enhancing factors (Kisilevsky et al., 1986) are yet to be assessed. A number of factors that favour the conversion of β2M fibrils *in vitro* have been identified such as the incubation of highly concentrated β2M for 5-6 days at physiological pH and at a temperature of 20 °C, in addition, the presence of fibrils can act as a trigger for a rapid aggregation of the protein (Esposito et al., 2000). Studies with human neuroblastoma cells, SH-SY5Y, showed instead that, although β2M is potentially neurotoxic, it is unlikely that this protein plays a role in the pathophysiology of cognitive impairment observed in people on hemodialysis because of the protective blood-brain barrier, which keeps low the β2M concentration in the cerebrospinal fluid (Giorgetti et al., 2009).

Although transformation of wild-type β2M into amyloid fibrils is difficult to achieve *in vitro*, many recombinant β2M variants have been investigated, and hypotheses have been developed about the mechanisms underlying fibrillogenesis.

The most important rearrangements of the protein, with respect to its structure in MHC-I, were observed for strands D and E, the interstrand loop D-E, and strand A, including the N-terminal segment. Data showed that these modifications can be considered as the prodromes of the amyloid transition that starts at sheet 1 with the rupture of strand A pairing, and leads to polymerization, through intermolecular pairing at strand D and probably strand C, and precipitation into fibrils. Instead two variants of human β2M

were compared with wild-type protein, namely the mutant R3Aβ2M and the form devoid of the N-terminal tri-peptide (ΔN3β2M), a reduced unfolding free energy was measured compared with wild-type. The results of a systematic investigation on 13 amyloidogenic β2M mutants have been published (Jones et al., 2003). Although no correlation was proposed between the location of the mutations and the extent of destabilization with respect to wild-type sequence, a unique role in amyloid formation was envisaged for the N and C-terminal β-strands of β2M (A and G, respectively) from the increased fibrillogenesis rate at acidic and mildly acidic pH of the variants with mutations in strands A and G. The underlying rationale is based on the loss of local hydrophobic packing by β-strand unpairing, leading to increased population of conformers with exposed assembly-competent surfaces (Corazza et al., 2004).

Asp76Asn Variant β 2 –Microglobulin

Recently the first naturally occurring structural variant, Asp76Asn (D76N), of human β2M was identified in members of a French family showing an autosomal dominant, inheritable systemic amyloidosis with slowly progressive gastrointestinal symptoms and autonomic neuropathy.

In contrast to patients with dialysis-related amyloidosis, all members of this family had normal circulating concentrations of β2M and normal renal function. The pathogenic protein was aggressively fibrillogenic *in vitro*, prompting a re-evaluation of previously hypothesized mechanisms of β2M fibrillogenesis. Extensive amyloid deposits were found in the spleen, liver, heart, salivary glands, and nerves (Valleix et al., 2012). Despite the misfolding propensity of the D76N variant and the essential contribution of β2M to the structure of the HLA class I complex, none of the heterozygotes had clinical evidence of immunodeficiency.

The high-resolution crystal structures of the D76N variant at 1.40 Å, and wild-type β2M (Protein Data Bank code 2YXF) matched closely, with a root mean square difference of 0.59 Å, as calculated over the whole C-alpha backbone (Esposito et al., 2008). The Asp76Asn β2M variant was thermodynamically unstable and remarkably fibrillogenic *in vitro* under physiological conditions. The substitution of asparagine to aspartate at residue 76 has two notable effects. First, the Asn76 amide establishes a new hydrogen bond with Tyr78, which consequently moves about 1.5 Å closer to residue 76. In its new position, Tyr78 provides a hydrogen bond to the amide nitrogen of Thr73. Second,

the theoretical isoelectric point increases from 6.05 to 6.40, which is of particular interest because the negative Asp76 residue in the wild-type protein partly balances the positive charges of the neighbouring Lys41 and Lys75 residues, whereas this region of the protein has a strong positive charge in the D76N variant.

The new hydrogen bonds, Asn76–Tyr78 and Tyr78–Thr73, appear to stabilize the 73–78 region of the polypeptide sequence that connects the E and F strands of the protein (E–F loop) (Figure 14). Indeed, the high B-factors (a measure of the fluctuation of each atom around its position in the crystal) of the E–F loop (165% of the molecularity of native protein folding inferred from the crystal structure) indicate that this is the most flexible part of the structure of wild-type β2M, whereas the equivalent region of the D76N variant is more rigid, with reduced B factors (120% of average) (Valleix et al., 2012).

The D76N substitution allows a fully folded three-dimensional structure almost identical to that of the wild type protein that forms amyloid fibrils in dialysis-related amyloidosis. However, dissection of the mechanism of D76N β2M fibrillogenesis confirmed the previously established paradigm that the amyloidogenicity of monomeric globular proteins is intimately connected to native fold destabilization (Booth et al., 1997).

Importantly, a specific intermediate of the folding pathway of wt β2M that was previously structurally characterized and shown to play a crucial role in priming the amyloid transition (Chiti et al., 2001), is abundantly populated in the D76N variant. It is therefore possible that this specific residue substitution facilitates the molecular mechanism responsible for the inherent amyloidogenicity of wt β2M and thereby enables the variant to cause clinical pathology even at normal plasma concentrations.

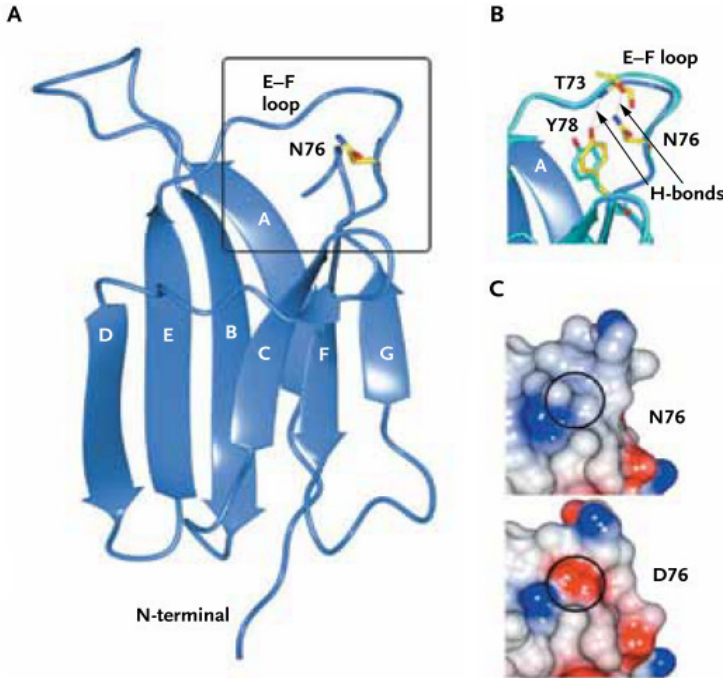

Figure 14 Crystal Structure of D76N Variant β2-Microglobulin. Panel A is a ribbon representation of the D76N variant. Panel B is a close-up view of the E–F loop (residues 70 to 80) shown in Panel A, superimposed on the wild-type β2-microglobulin structure (blue–green). Residues belonging to the D76N variant are yellow, and Tyr78 belonging to wild-type β2-microglobulin is blue–green; hydrogen (H) bonds are shown as dashed lines. Panel C shows the surface electrostatic potential of the E–F loop region in the D76N variant (top) and in wild-type β2-microglobulin (bottom); circles indicate the mutated residue. Blue represents positively charged regions, and red negatively charged regions (Valleix et al., 2012).

Data suggested that the ability of D76N β2M to catalyze fibrillogenesis by wt β2M can be modulated and even blocked by typical chaperones such as crystallin, leading to inhibition of fibrillization that depends on the stoichiometric chaperone/ β2M ratio. A role for extracellular chaperone-like proteins in the inhibition of wt β2M amyloidogenesis has been proposed previously (Ozawa et al., 2011), and it is plausible that the persistent, extremely high concentration of wt β2M in renal failure patients on dialysis may overcome the natural protective role of physiological chaperones that otherwise protect against deposition of this weakly amyloidogenic protein when it circulates at its normal serum concentration.

Extra-Virgin olive oil, a cornerstone of the Mediterranean diet

Olive oil, is one of the hallmarks of the Mediterranean diet (MeDiet). Specifically when olive oil is mentioned in the context of MeDiet, it refers to EVOO. It is a vegetable oil obtained directly from olive fruit using only mechanical extraction (without chemical treatments that can alter the oil quality), with a maximum free acidity in terms of oleic acid of 1g for 100g (Ramirez Tortosa et al., 2006). It needs to be underlined that there is a considerable difference between "olive oil" and "EVOO". The former has a very low concentration of phenolic compounds whereas the latter contains up to 1g/Kg of phenolic compounds (Cheynier et al., 2012). Several studies have shown the effectiveness of EVOO in the prevention of CVD. The proposed mechanism by which EVOO could exert beneficial effects against CVD include the improvement of lipid profile via an increase in HDL with a reduction in LDL, including its susceptibility to oxidation, an improvement in endothelial function, and an improved regulation of blood pressure. Descriptive clinical studies have suggested that EVOO is protective against age-related cognitive decline, AD, metabolic syndrome and diabetes. In the international EVOO conference held in Spain (2008) the beneficial effects against cancer were shown (Lopez-Miranda et al., 2010). For example it was reported by several different studies that approximately 80% of human cancer cases are associated with bad eating habits and lifestyle. However, in countries where the population followed the traditional MeDiet and where EVOO was the principal source of fat, cancer incidence was lower (Trichopoulou et al., 2000) (La Vecchia, 2004) (La Vecchia et al., 1995). It is proposed that EVOO could exert beneficial effects against initiation, promotion and progression of cancer through several mechanisms. Some of these may include alterations in tumour cell composition and structure of cell membranes, changes in eicosanoid biosynthesis or signalling pathways, modulation of gene expression, reduction of cellular oxidative stress and DNA damage, modulation of the immune system and/or hormonal balance in hormone-dependent cancers (Escrich et al., 2006) (Escrich et al., 2007). The most recognized hypothesis is that these protective effects are a result of synergistic and convergent interplay of all oil components triggering a broad range of cell responses that may play a role in cancer prevention; or, if the disease already exists, lead to a reduced biological aggressiveness (Lopez-Miranda et al., 2010).
The biological and therapeutic value of EVOO is related to its composition. It consists of two fractions: the major or saponifiable fraction and the minor or insaponifiable

fraction.

1) Saponifiable fraction. The saponified fraction represents more than 98% of the total oil weight and consists mainly of triacylglycerols, diacylglycerols, monoacylglycerols, free fatty acids and phospholipids. The fatty acids present in this fraction can be divided into two groups: saturated and unsaturated. The most common monounsaturated fatty acid in olive oil is oleic acid, whereas the saturated group includes palmitic and stearic fatty acids. Linoleic acid is the predominant polyunsaturated fatty acid (Sarolic' et al., 2014).

2) Insaponifiable fraction. This fraction represents 1-2% of the EVOO composition. It includes:

hydrocarbons, classified in saturated and polyunsaturated, that represent 50-60% of insaponifiable fraction (De Leonardis et al., 1998);

aliphatic and triterpenic alcohols, 20-35% of this fraction, that influence oil aroma;

polyphenols, 18-37% of the insaponifiable fraction, which include phenolic acids, phenolic alcohols, flavonoids, secoiridoids and lignans. Polyphenols have been recognized to have the following biological effects: antioxidant, anti- inflammatory, anti-allergic, antibacterial and antiviral (Servili & Montedoro, 2002);

tocopherols, 2-3% of the unsaponifiable fraction, known for their antioxidant properties. Among these compounds there is alpha-tocopherol, constituent of vitamin E (about 150-300 mg / kg of oil). It is lipophilic with a strong antioxidant capacity mainly toward the polyunsaturated fatty acids, which are the most likely to oxidize (Baldioli et al., 1996);

pigments, classified in chlorophylls and carotenoids. The carotenoid pigments are responsible for the yellow tint of oil, while chlorophylls are the source of the color green. However, these compounds can undergo oxidation under certain conditions, thus they can be degraded to uncoloured products and promote oxidation of fatty acids (Minguez-Mosquera et al., 1990).

Oleuropein aglycone, typical phenol of extra-virgin olive oil

Oleuropein is a secoiridoid typical of the Oleaceae family. The biosynthesis of oleuropein in Oleaceae is via the mevalonic acid pathway, through branching that results in the formation of oleosides. Secoiridoids are derived from these compounds (Damtoft et al., 1993).

Oleuropein was identified for the first time in olive fruit by Bourquelot and Vintilesco, but elucidation of its chemical structure was described much later (Bourquelot & Vintilesco, 1908). Oleuropein, such as demethyloleuropein and verbascoside, is present in all the constitutive parts of olive fruits such as peel, pulp and seed, but particularly in the pulp. Chemically oleuropein is an ester between HT and elenolic acid. It is important to distinguish two forms of oleuropein; glycated and aglycone (OleA). Glycated oleuropein is characteristic of olive fruit and leaves, whereas OleA is obtained from the deglycosilation operated by β-glycosidase, which is released from olive fruit during crushing (Rigacci & Berti, 2011) (Figure 15).

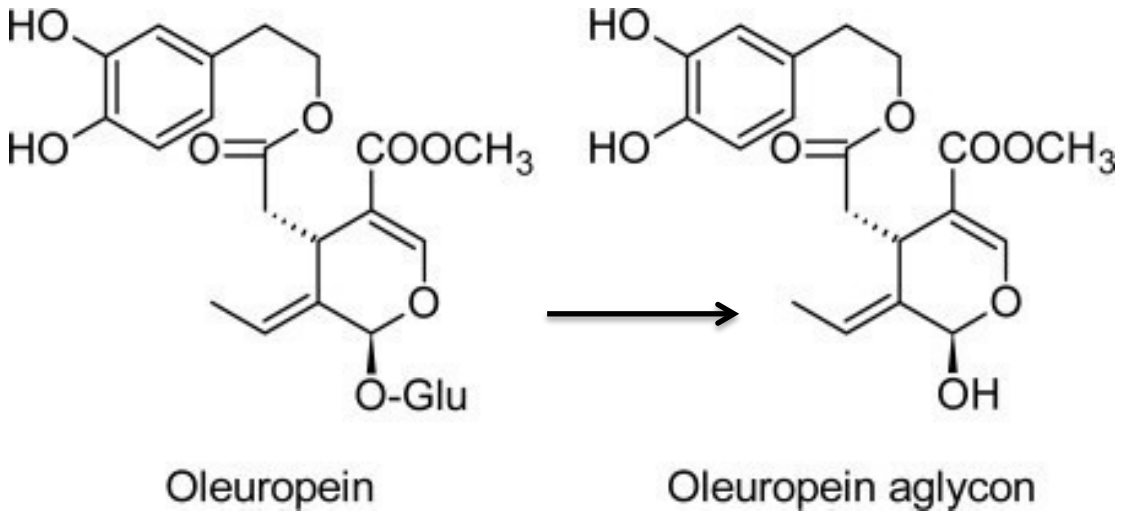

Figure 15 Structure of Oleuropein and Oleuropein aglycone (OleA) (Rigacci & Berti, 2011).

The content of oleuropein in the fruit and OleA in the oil can be affected by several factors: drupe ripeness, cultivation techniques, and the type of oil. The drupe ripeness plays an important role for the oleuropein content as it is higher in the first stage of drupe maturation, and decreases as the fruit ripens. Irrigation also decreases the content of oleuropein in the fruit and the corresponding amount of OleA in the oil. There is also significant difference among the types of olive oil. EVOO, obtained from the first cold extraction, has a higher concentration of OleA as compared to virgin olive oil and olive oil.

Regarding the biological properties of oleuropein (glycated or aglycone), in general oleuropein shows a wide spectrum of activity in numerous contexts including an antioxidant property, cardio-protection, anti-cancer, antimicrobial, antiviral, and inhibition of amyloid toxicity (Rigacci et al., 2011) (Omar, 2010). Recent studies have also highlighted its role as an activator of protective responses in cells, in particular the stimulation of autophagy (Grossi et al., 2013) (Rigacci et al., 2015).

A brief description of its main beneficial properties is given below:

Antioxidant: Oleuropein is a strong antioxidant, demonstrating similar effect to ascorbic acid (vitamin C) and a tocopherol (vitamin E) (Visioli et al., 1998). It causes a dose-dependent inhibition of copper sulphate-induced oxidation of low-density lipoproteins (LDL) (Omar, 2010). De la Puerta et al. (De la Puerta et al., 2001) have shown the ability of oleuropein to scavenge nitric oxide and to cause a parallel increase in the inducible nitric oxide synthase (iNOS) expression. Visioli et al. further reported a scavenging effect of oleuropein against hypochlorous acid (HOCl), oxidative substance produced in vivo by neutrophil myeloperoxidase at the site of inflammation (Visioli et al., 2002). Compared to the glycated form, OleA is more effective against oxidative stress, as its liposolubility permits faster action on penetrating the intracellular context and inhibiting radicals (Rigacci et al., 2011).

Inhibition of amyloid toxicity and neuroprotection: As previously described, the amyloid plaques are characterized by extra-intra cellular deposits of an aggregated proteins. Increasing evidence reported that OleA was able to interfere with the in vitro aggregation of many proteins such as hIAPP (a peptide that aggregates in type II diabetes), Aβ and Tau neutralizing the toxicity of the oligomers. These studies showed that if amylin or Aβ were aggregated in presence of OleA, the result was the production of less toxic molecular species (Rigacci et al., 2011) (Rigacci et al., 2010).

Regarding the peptide Aβ, NMR and Electrospray Ionization Mass Spectrometry (ESI-MS) demonstrated non-covalent interaction between OleA and the peptide. OleA forms a complex with Aβ 1-40 in a 1:1 stoichiometry, with a preference for the apolar region of Aβ (Rigacci et al., 2011). A recent study of Leri et al. further reported a protective effect of OleA in a model of systemic amyloidosis, transthyretin-amyloidosis (TTR-amyloidosis). TTR-amyloidosis is characterized by deposits of insoluble fibrils in the heart, peripheral nerves and other organs. OleA can interfere with TTR-aggregates, similarly to the effect showed on amylin, Aβ and Tau plaques. In the heart TTR-fibrils can bind the glycosaminoglycan GM1 of cardiomyocyte inducing cell damage and

consequent cytotoxicity. In the presence of OleA these aggregates were unable to interact with GM1. The reported data suggested that OleA induced a remodelling of the supramolecular structure of the growing aggregates, reducing TTR aggregates-GM1 interaction, with consequent loss of cytotoxicity (Leri et al., 2016).

Although all these results confirmed the ability of OleA to interfere with amyloid aggregation and propose the use of OleA as preventive therapy, the protective effect of OleA in the presence of already formed toxic plaques is also known. Various mechanisms are under investigation to explain this effect. In vivo studies on TgCRND8 mice, a model of Aβ deposition, fed with OleA for 8 weeks showed improvement in cognitive performance that correlated with improved synaptic function, reduced size and compactness of Aβ plaques, reduced inflammatory response and strong autophagy activation in specific brain areas (Casamenti et al., 2015). These in vivo results were further confirmed by studies in a transgenic C.elegans model, displaying Ab aggregates in muscles that were diminished in worms fed with OleA (Diomede et al., 2013).

Cardioprotective: CVDs are the result of a plethora of pathological conditions such as atherosclerosis, hypertension, hyperlipidemia. Several studies report the beneficial effects of oleuropein, and its metabolite HT against atherosclerosis. Oleuropein can act in different ways to counter atherosclerosis. Some of these mechanisms include: i) inhibition of LDL-oxidation, ii) reduction of monocytoid cell adhesion to stimulated endothelium (Carluccio et al., 2003), iii) inhibition of the stimulated expression of ICAM1 and E-selectin, and, iv) downregulation of inflammatory genes, in particular those encoding for IL-6 and IL-8 cytochines, over-expressed in atherosclerosis (Rigacci & Stefani, 2016). Thrombin-induced platelet aggregation is a pathological condition closely related to CVD. Oleuropein, in particular OleA, can act against platelet aggregation through inhibition of cAMP phosphodiesterase, which leads to an increase in cAMP concentration. As an anti-hypertensive agent, OleA inhibits both angiotensin converting enzyme (ACE) and neprilysin (NEP). The role of ACE enzyme is the conversion of angiotensin I to angiotensin II (AngII). Ang II constricts blood vessels, producing high blood pressure. On the other hand, NEP is an enzyme highly expressed in the kidney and lung tissues that degrades signalling peptides such as encephalins, substance P, endothelin and atrial natriuretic peptide. In vitro studies have shown the effectiveness of OleA (extracted by Ligustrum vulgare) against both ACE and NEP with IC50 20mM for ACE and 35 mM for NEP. Notably, under the same conditions oleuropein glycate was not shown to be effective. Moreover, hyperlipidemia is a risk

factor for cardiovascular diseases. Oleuropein, both glycated and aglycone, is effective on lipid metabolism, lowering LDL plasma levels and total cholesterol, and increasing high-density lipoproteins (HDL) levels (Rigacci et al., 2011).

Anticancer: Some studies showed anti-cancer properties of oleuropein and OleA. Corona et al. have shown that olive oil extract (where OleA was the most abundant phenol) was able to block cell cycle in G2/M phase in colon adenocarcinoma cells (Caco2). This G2/M block was mediated by the ability of OleA and other polyphenols present in the extract to inhibit p38 and CREB phosphorylation, which then led to a downstream reduction in COX-2 expression (Corona et al., 2007). Barbaro et al. reported anti-proliferative and proapoptotic effects of oleuropein glycate in breast adenocarcinoma, colorectal adenocarcinoma, glioblastoma, lung carcinoma, prostate cancer, melanoma, renal cell adenocarcinoma (Barbaro et al., 2014). A dose-dependent antiproliferative effect of OleA was reported in breast cancer. In this study, HER2 oncogene, overexpressed in human breast cancer, was proposed as specific target of OleA (Menendez et al., 2008). Beneficial effects against cancer can also depend on antioxidant (protection of cells against oxidative stress characteristic of oncogenesis) and anti-angiogenic effects (prevention of tumour progression). Tumours release vascular endothelial growth factor (VEGF), a factor that promotes the formation of new vessels resulting in angiogenesis. In the absence of VEGF, the vessels cannot develop and the tumour is no longer able to obtain necessary nutrients or oxygen for growth. VEGF is therefore an important target for cancer therapy. In addition to VEGF, other factors such as metalloproteinases are closely linked to growth, invasion, metastasis and angiogenesis of cancer. Kimura et al. have shown inhibition of VEGF, as well as the metalloproteinases MMP-2, MMP-9 and MMP-13 by OleA in a model of chronic UVB-induced skin damage and carcinogenesis (Barbaro et al., 2014).

Antimicrobial: Oleuropein has strong antimicrobial activity against Gram negative and Gram positive bacteria and mycoplasma. The mechanism of antimicrobial activity is not completely understood, even if some studies suggest that the catecholic portion plays an important role. There are three proposed mechanisms: i) damaging of the bacterial membrane and/or disrupting cell peptidoglycans, ii) interference with the synthesis of amino acids necessary for the growth of microrganism, and, iii) stimulation of the immune system that leads to phagocytosis of microbes. Saija and Uccella (Saija & Uccella, 2011) reported a greater efficacy of OleA compared to the glycated form. The

glycoside group in fact could reduce the ability of the phenol to penetrate the cell membrane and get to the target site (Omar, 2010).

Antiviral: Oleuropein has antiviral activities against herpes mononucleosis, hepatitis virus, rotavirus, bovine rhinovirus, canine parvovirus, feline leukemia virus, respiratory syncytial virus and para-influenza type 3 virus (Omar, 2010). The protective effect against the human immunodeficiency virus was demonstrated; an action likely mediated via the inhibition of HIV 1 integrase activity (Lee-Huang et al., 2007).

Autophagy activation: Autophagy is a cellular pathway involved in degradation of altered proteins and organelles. Several pathological conditions such as neurodegenerative diseases, infectious diseases, and cancer are characterized by dysfunction in autophagy. Restoring defective autophagy in these conditions has been shown to be a promising therapeutic strategy. Grossi and colleagues highlighted the effect of OleA as autophagy activator in vitro and in vivo while investigating its protective effect in neurodegenerative disorders. In TgCRND8 mice, OleA administration (50 mg OLE /kg of diet for 8 weeks) induced autophagic response, promoting autophagosome-lysosome fusion, the last step of the autophagy machinery, which leads to the clearance of misfolded proteins (Grossi et al., 2013). In light of these findings, the aim of this thesis was to discriminate the cellular and molecular mechanisms underlying OleA-induced autophagy (Rigacci et al., 2015).

Autophagy

Autophagy, which literally means “self-eating”, represents a non-selective degradation system, regulating the turnover of several cellular constituents, included damaged organelles, soluble or aggregated proteins amongst others (Rubinsztein, 2006). The interest in autophagy was instigated when genetic studies in yeasts identified a series of autophagy-related (ATG) genes (Klionsky et al., 2003). Several of the autophagy specific genes are highly conserved emphasizing the importance of this process in all organisms (Nakatogawa et al., 2009). Three defined types of autophagy, which include macro-autophagy, micro-autophagy, and chaperone-mediated autophagy, are known. They differ in how the material to be degraded is transported into the lysosomal lumen; in the type of material to be degraded; and, in the cellular regulation (Glick et al., 2010) (Figure 16). In general the term autophagy is classically referring to macroautophagy.

A brief description of the main types of autophagy is given below:

Macroautophagy: the macroautophagy pathway was first described by Christian De Duve in 1963 (De Duve, 1963). Macroautophagy is considered the main type of autophagy and has been more extensively studied than microautophagy and chaperone-mediated autophagy. It is important in physiological conditions, but is also activated by stress and nutrient starvation. This process includes three different steps: i) phagophore formation, ii) closure of phagophore and formation of an "autophagosome", and, iii) autophagosome-lysosome fusion.

In the first step the phagophore or pre-autophagosome, a double membrane structure, sequesters cytoplasm constituents, including mutated proteins and damaged organelles. Despite that this step is well characterized the origin of the autophagic sequestering cisterna remains unknown. Two hypotheses have been formulated regarding the origin of the phagophore. One line of thought is de novo synthesis or utilization of pre-existing cytoplasmic membranes (endoplasmic reticulum, mitochondrial membrane, plasma membrane and Golgi cisterns) (Vilchez et al., 2014). In the second step, the phagophore is sealed and forms an autophagosome. The autophagosomes then fuse with lysosomes or alternatively with endosomes, forming an amphisome, before fusing with lysosomes.

Amphisomes can be ultrastructurally recognized as organelles containing both cytoplasmatic components and endocytic markers. They are delimited by a single or double membrane with an acidic interior compartment allowing for autophagocytosed cytoplasm to become denaturated. Amphisomes are distinguished from autophagosomes by endocitic markers, but the distinction between amphisomes and lysosomes is more problematic since the endosomal fusion can bring some lysosomal enzymes inside the amphisome. Once autophagosomes or amphisomes fuse with lysosomes, the sequestered material is degraded or recycled (Mizushima et al., 2011) (Vilchez et al., 2014).

Microautophagy: microautophagy consists of the incorporation and degradation of entire cytosolic regions by lysosome itself, without the involvement of autophagosomes (Glick et al., 2010). This type of autophagy is important for the degradation of proteins as well as entire organelles. In yeasts, a specific form of microautophagy, the "micropexophagy", was described. It is involved in the selective degradation of peroxisomes (Klionsky et al., 2007). Microautophagy is active in basal conditions, but unresponsive to stimuli such as nutrient deprivation, glucagon or amino acids, which are shown to activate other types of autophagy (Cuervo, 2004).

Chaperone mediated autophagy (CMA). In chaperone-mediated autophagy (CMA), chaperone proteins (such as Hsc-70, heat-shock protein 70) and co-chaperones recognize the proteins containing a particular pentapeptide consensus motif (KERFQ) to form a complex. Targeted proteins associated with chaperones are then translocated across the lysosomal membrane where they are recognized by lysosome-associated membrane protein 2 (LAMP-2A), resulting in their unfolding and degradation (Glick et al., 2010). This type of autophagy is very selective and is especially activated in stressful conditions, such as prolonged nutrient deprivation or exposure to toxic compounds (Cuervo & Dice, 1998) (Dice, 200).

Both macroautophagy and CMA can act during nutrient starvation. Macroautophagy represents the first response aimed to degrade indiscriminately cytosolic components to obtain energy. However if the starvation is prolonged then to prevent the cell from 'eating itself', the activity of macroautophagy begins to decline and the CMA becomes the new supplier of amino acids for the synthesis of new proteins, allowing selective degradation of substrates. Interestingly, recent studies reported CMA has tissue and cell-specific effects. In fact, starvation activated preferentially CMA in the liver, the heart, and the kidney (Cuervo, 2004), and among the cells there were differences in the induction of CMA. Although the CMA induced by starvation is less present in the brain, cultured astrocytes showed high levels of CMA after serum deprivation (Martin et al., 2002).

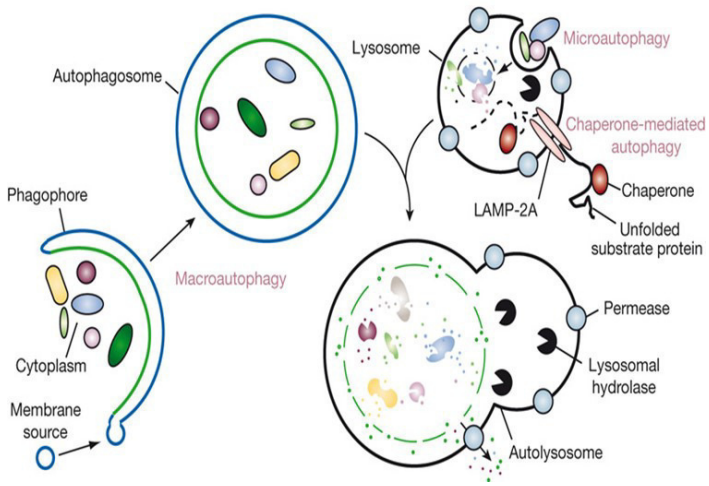

Figure 16 Types of autophagy. Microautophagy: sequestering of cytosolic constituents by lysosomes through invaginations in their membrane. Macroautophagy requires three steps: i) cytosolic substrates are sequestered within a unique double-membrane vesicle

called “pre- autophagosome” or “phagophore” ii) closure of phagophore forms an“autophagosome”. iii) fusion of autophagosome-endosome (not shown) or autophagosome-lysosome and formation of the “autolysosome”. The material is degradated into the autolysosome and the recycled macromolecules are released back into the cytosol. Chaperone mediated autophagy: proteins marked with the KFERQ motif are recognized and complexed by chaperone proteins (such as Hsp70) The complex substrate-chaperone moves toward lysosomes and the proteins are translocated by Lamp2 into the lumen for degradation (Mizushima et al., 2008).

Macroautophagy (hereafter referred to as autophagy) is a highly conserved process shared by all organisms which can be triggered in different ways and requires the participation of over 20 ATG proteins in yeast (Mizushima et al., 2011).

The discovery of the genes that regulate autophagy in the yeast Saccharomyces cerevisiae has permitted a step forward for the understanding of the molecular mechanisms of autophagy. The process of autophagy is under control of four main protein systems: 1) ULK complex 2) Class III phosphatidylinositol 3-kinase 3) Ubiquitin-like conjugation systems (Atg5–Atg12/ Atg8- PE) 4) SNAREs and other fusion proteins.

The ULK complex is required for the early stages of autophagy. It includes ULK1, Atg13 and Atg 17. ULK1, known as Atg1 in yeasts, interacts with autophagy-proteins such as Atg13, Atg17, Atg29 and Atg31 in a nutrient status and TOR kinase activity dependent manner. In particular, the interaction with Atg13-Atg17 is essential for Atg1 activity and autophagy induction. When there is availability of nutrients, the kinase mTOR phosphorylates and deactivates Atg13, resulting in the repression of autophagy. Under starvation periods mTOR is inactive, Atg13 phosphorylation is suppressed and Atg13 is activated. Activated Atg13 induces the recruitment of Atg1, Atg17 and other Atg proteins to the pre-autophagosome structure (PAS) (Jung et al., 2010).

The role of class III phosphoinositide 3-kinase (PI3K-III), also called “Vps34” (vesicular protein sorting 34), and its binding with Beclin-1 (Atg6) in phagophore formation and autophagy is not entirely known in mammalian systems. PI3K-III is unique amongst PI3-kinases in only using phosphatidylinositol (PI) as substrate to generate phosphatidyl inositol triphosphate (PI3P), which is essential for phagophore elongation and recruitment of other Atg proteins. The PI3K-Beclin1 interaction promotes the catalytic activity of PI3K (Glick et al., 2010). Beclin1, and PI3K, can

interact with other proteins. Beclin1 protein contains three prominent domains: “BH3 domain”, “CCD domain” and “ECD” domain. The BH3 domain promotes the interaction with Bcl-2, an antiapoptotic protein, and several studies reported that this interaction had an autophagy-inhibitory effect. Through the CCD domain Beclin1 can interact with UVRAG, Atg14L (also named Barkor) and RUBICON. PI3K binds Beclin1 at its ECD (McKnight & Zhenyu, 2013). A study of Russell et al. reported that ULK1 activated Beclin1 through phosphorylation. ULK1 is recruited to the PI3K-Beclin-1 complex via binding to ATG14L. After recruitment, it can phosphorylate Beclin-1, activate PI3K and promote PI3P production at the nascent autophagosome (Russell et al., 2013).

Two convergent-systems are required for the second stage of autophagy: maturation of phagophore and autophagosome formation. These systems recall some features of the ubiquitination of proteins in the ubiquitin-proteasome system.

The first conjugation system (Atg5-Atg12). It involves the Atg proteins 5, 7, 10, 12. Atg7 and Atg10 are similar to the E1 and E2 enzymes in the ubiquitin pathway. The final complex formed consists of Atg5–Atg12 non-covalently associated with Atg16 (Meijer & Codogno , 2004)

The second conjugation system (Atg8-PE). It is characterized by the conjugation of the protein LC3 (Atg8) with the phospholipid phosphatidylethanolamine (PE). The interaction LC3-PE is dependent on Atg7 and Atg3 activity. LC3 (19 kDa) is a full-length cytosolic protein that is proteolytically cleaved by Atg4 to generate LC3B-I upon the induction of autophagy. The carboxyterminal glycine of LC3B-I exposed by Atg-4 mediated cleavage is then activated by Atg7, an E1-like protein and LC3B-I activated is subsequently transferred to Atg3, an E2-like protein. At this point phosphatidylethanolamine (PE) can bind activated LC3-I generating the processed LC3-II (17Kda). Recruitment of LC3-II into the phagophore is dependent on Atg5– Atg12, and LC3-II is found on both the internal and external surfaces of the autophagosome. It is considered one of the main markers of autophagy induction. LC3-II, acts as a ‘receptor’ at the phagophore and autophagosome membranes where it interacts with scaffolding proteins such as p62 in addition to several other molecules (eg protein aggregates, damaged mitochondria) to promote their selective uptake and degradation. p62/SQSTM1 is a protein involved in both UPS and autophagy degradation systems. It promotes the turnover of poly-ubiquitinated protein aggregates, to which it is linked through the UBA domain. The binding site for LC3 is called LIR domain and is formed

by 8 aminoacids. The LC3-p62 link encourages the recruitment to autophagic vacuoles of damaged organelles or mutates proteins. P62 is an essential protein, and its mutation is linked to Paget's disease, a pathology characterized by the abnormal turnover of bone (Glick et al., 2010). NBR1 is a protein similar to p62, and could compensate a possible loss of p62 and as the latter has UBA and LIR domains and is degraded by autophagolysosomes. However, NBR1 contains a FW domain, a four tryptophan residues domain, not present in p62. The FW domain plays an important role in activation, control and differentiation of T cells and in inflammatory processes. The loss of this domain induces alterations in p62 expression and hyperactivation of the p38 MAPK (Johansen & Lamark, 2011).

The last step of autophagy requires the fusion between the autophagosome and lysosome medited by SNAREs.

Microtubules and actin filaments have been implicated in the transport of autophagosomes towards the lysosomes, and the movements along the microtubules are driven by kinesin and dynein. While microtubules are formed by dimers of a and b tubulins, the actin filaments are comprised of polymerized actin monomers. Rab GTPase is an important player in the trafficking of autophagosomes, connecting autophagosomes or endosomes to microtubule proteins through the interaction with the protein RILP (Rab-interacting lysosomal protein). Rab-GTPase is also involved in the recruitment of the protein FYCO1 (FYVE and coiled-coil domain containing 1) on the autophagosome membrane. FYCO1 in turn connects kinesins to autophagosomes. FYCO1 also contains an LC3-interacting motif promoting LC3-II recruitment to autophagosomes (Ganley, 2013). With regards to the autophagosome-lysosome fusion, a recent study demonstred that HDAC6 (histone deacetylase 6) recruiting cortactin, a protein responsible of actin polymerization, could be involved in the mechanism of fusion and degradation of protein aggregates (Lee et al., 2010).

In addition during this step, Rab GTPases, membrane-tethering complexes and SNAREs proteins are recruited. Rab proteins, localized on both membranes, bind tethering complexes (HOPS complex, TECPR1 complex) that act as bridges approaching the compartments involved in the fusion. The tethering complex in turn activates SNAREs proteins (Vam3, Vam7, Vti1 e Ykt6), which drive the fusion of lipid bilayers between autophagosome and lysosome. SNAREs localized on the opposing membrane interact with each other forming complexes essential for their activity.

Lysosomal-associated membrane protein-2 (LAMP-2) is a component of the lysosomal membrane, also involved in the autophagosome-lysosome fusion. Given its pivotal role, mutations of LAMP-2 are associated with accumulation of autophagosomes and Danon disease, a disorder characterized by skeletal myopathy and cardiomyopathy, as well as mental retardation (Ganley, 2013).

Finally the cargo is degraded by the lysosomal enzymes cathepsins D, B and L. The cathepsins are a class of proteases able to degrade modified proteins. Many cathepsins involved in autophagy machinery are characterized by the presence of cysteine residues in their structures. Catepsin D is often studied as a late marker of autophagy (Eskelinen, 2005).

As described above, the autophagy pathway requires different steps and several drugs have been reported as activators or inhibitors acting on specific steps of the autophagy machinery (Figure 17). Among these, drugs such as BCL-2 homology 3 (BH3) mimetics disrupt the inhibitory interaction between Beclin 1 and Bcl-2/Bcl-X(L), thus activating autophagy. In contrast, inhibition of Beclin 1 protein by Spautin-1 or PI3K by 3- methyladenine (3-MA) can inhibit autophagy. Some drugs can inhibit the later stages of autophagy. These include chloroquine (CQ), which inhibits the acidification inside the lysosome; bafilomycin A1, which inhibits the vacuolar ATPase (V-ATPase) located in the lysosomal membrane; and, pepstatin A or cystatin B that inhibit the lysosomal proteases.

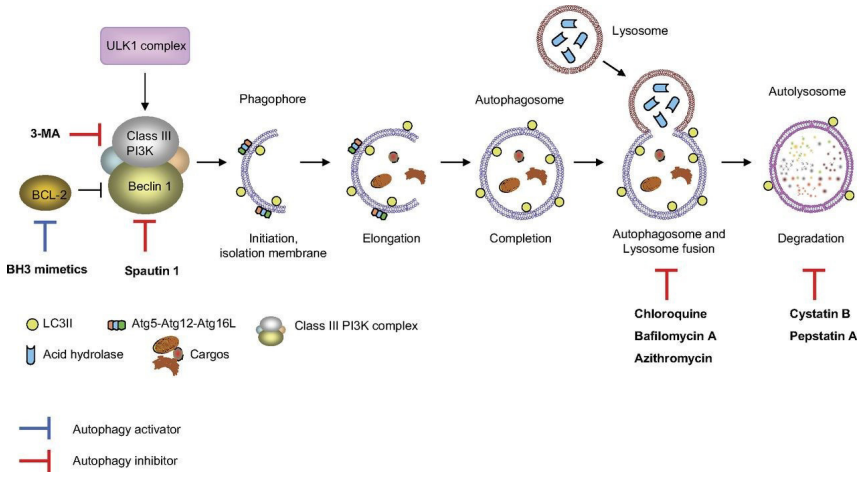

Figure 17 Molecular mechanisms of macroautophagy. Macroautophagy starts with the formation of a double-membrane structure “phagophore” of undefined origin. The protein complexes involved in this step are represented by ULK1 and Class III

phosphoinositide 3-kinase (PI3K-III). Atg5-Atg12-Atg16L complex and LC3-II phosphatidylethanolamine (PE) conjugate promote the phagophore elongation and substrate sequestering. The closure of phagophore forms autophagosome. In this step LC3-II is found on both the internal and external surfaces of the autophagosomes. SNAREs proteins mediate the fusion autophasgosomes-lysosomes and the cargos are degraded by lysosomal hydrolases. Some drugs can interfere at different levels with autophagic machinery, activating or inhibiting macroautophagy (Nakahira & Choi, 2013).

Signalling pathways of autophagy

Autophagy is a well-regulated process. A variety of extracellular (starvation, hormones or pharmacological treatments) and intracellular stimuli (accumulation of misfolded proteins, pathogens invasion) can modulate the machinery controlling autophagy (Yang et al., 2005). In most cases these stimuli, although different from each other, converge to a common target upstream of the molecular machinery, the kinase mTOR, which is involved in the formation of the autophagosomes (Meijer & Codogno , 2004).

mTOR is a target of rapamycin, a macrolide-antibiotic with antifungal and immunosuppressive properties. Rapamycin, inhibiting mTOR, has an autophagy activating effect. In mammalian cells mTOR interacts with regulatory proteins to form two different complexes: mTORC1 and mTORC2 (Alayev et al., 2014).

mTORC1 is particularly sensitive to the antibiotic rapamycin, whereas mTORC2 is sensitive to rapamycin and rapalogs (analogues of rapamycin) only after prolonged exposure. The best characterized substrates of mTORC1 kinase activity are eukaryotic initiation factor 4E-binding proteins 1, 2 and 3 (4E-BP1, 2 and 3) and the p70 S6 kinases (S6K1 and S6K2). mTORC1 phosphorylates p70-S6K on at least two residues, promoting its efficiency in stimulating protein synthesis through the activation of the ribosomal S6 protein and other components of transcription apparatus. Phosphorylation of 4E-BP1 on four Ser/Thr residues induces the dissociation of 4E-BP1 from eIF4E (Eukaryotic translation initiation factor 4E). This event causes the repression of 4E-BP1 and the activation of eIF4E, ultimately promoting eIF4E mediated growth and cell proliferation.

mTORC2 can target the serine/threonine Akt, phosphorylating it on serine S473. The phosphorylation of this residue leads to full activation of Akt and Akt-mediated inhibition of autophagy (Dunlop & Tee , 2009).

Although the mTOR-dependent autophagy is predominant, mTOR-independent autophagy is also present. Lithium, carbamazepine and valproate are so-called "mood-stabilizing medications" used in the treatment of mental disorders and can induce autophagy independently from mTOR signalling (Rubinsztein et al., 2011).

The serine/threonine kinase mTOR is an important regulator of autophagy, acting as a sensor for amino acids and ATP levels and integrating hormonal stimuli via the class I PI-3K/PKB pathway (Dennis et al., 2001) (Marygold & Leevers , 2002) (Rohde et al., 2001) (Figure 18).

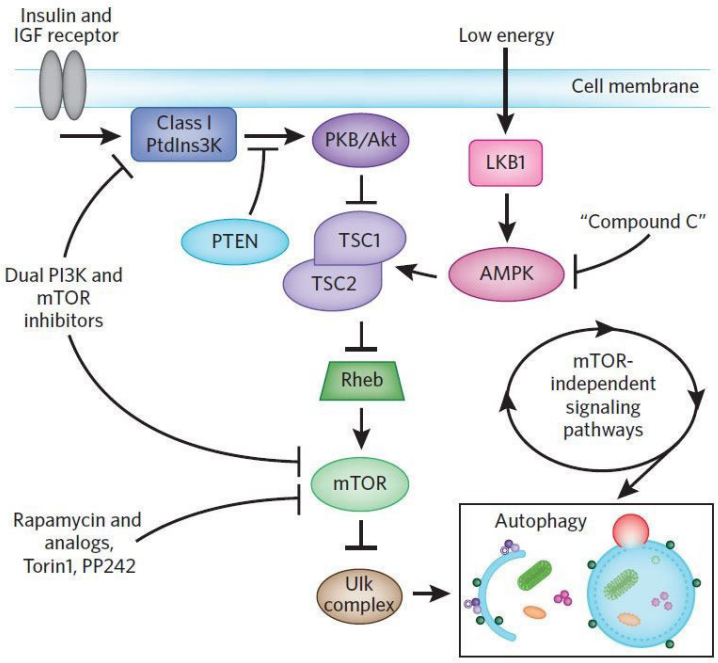

Figure 18 Schematic representation of the mTOR signalling pathway. In mTOR dependent signalling, autophagy is inhibited by the serine/threonine kinase mTOR. Different signals such as amino acids, insulin and ATP converge to the kinase mTOR. mTOR is inhibited by rapamycin (and its analogs), Torin1 and PP242, which induce autophagy. AMPK activation also causes inhibition of mTOR signalling, resulting in autophagy stimulation. Dual PI3K and mTOR inhibitors induce robust autophagy activation compared to single mTOR inhibitor (Fleming et al., 2011).

Mortimore and Schworer (Mortimore & Schworer, 1977) showed for the first time that amino acids, the final products of autophagic degradation, had an inhibitory effect on autophagy in rat liver cells. The inhibitory effects were observed on the formation of autophagosome, a step regulated by mTOR (Mortimore & Kadowaki , 1994) (Seglen & Bohley , 1992). Other studies showed the interference of amino acids in different steps of autophagy. For example, studies on isolated rat hepatocytes showed that high concentrations of leucine together with glutamine or histidine were particularly effective in inhibiting autophagic sequestration of cytosolic substrates. Asparagine, if used at high concentrations, interfered with the fusion between autophagosomes and lysosomes. An effect on the lysosome activity was also reported for leucine. The latter increased the lysosomal pH at high concentrations; presumably through direct inhibition of the lysosomal proton pump (Codogno & Meijer , 2003). The link between mTOR and amino acids in the control of autophagy was showed in rat hepatocytes, with the discovery that the inhibitory effect of amino acids on autophagy could be reverted by rapamycin (Blommaart et al., 1995).

Although it is generally accepted that amino acids activate mTOR, how the amino acids signal their presence to the cell is not clear. Initially it was thought that amino acids bound a plasma membrane localized receptor and this signal was transmitted inside the cell. According to studies, amino acid starvation is sensed by the degree of amino acid charging of tRNA. In fact, it was observed in yeasts, that free tRNA, which did not bind amino acids, prevented the phosphorylation of p70S6K protein mediated by mTOR. Despite these controversial findings for amino acid signalling, the fact that the inhibition of the transport of amino acids markedly inhibited the phosphorylation of p70S6K protein system demonstrated that the amino acids exerted their effects upon entering the cell (Van Sluijters et al., 2000). Along the same lines, insulin was shown to have an inhibitory effect on autophagy signalling, independent from amino acid signalling. In fact the administration of amino acids, leucine in particular, resulted in phosphorylation of ribosomal protein S6K and 4E-BP1 in the absence of insulin or other growth factors. Both are targets of mTOR. Furthermore amino acids and insulin can also act synergistically on mTOR signalling to inhibit autophagy. According to this, leucine can activate glutamate dehydrogenase, that promotes insulin production in β-cells and the insulin signalling (Yang et al., 2005).

ATP/ADP levels. Autophagy is also regulated by ATP levels. A decrease in cellular ATP levels is sensed by the AMP-dependent protein kinase (AMPK). The activation of

AMPK occurs through phosphorylation by LKB1 in response to an increase in the AMP/ATP ratio and by calmodulin-dependent protein kinase kinase-beta (CaMKKb, activated by cytosolic calcium) (Cai et al., 2012). Activated AMPK phosphorylates TSC1/2 complex, which inhibits mTOR activity through Rheb (Inoki et al., 2003). When mTORC1 is inactive, dephosphorylation of ULK1/2 activates its kinase activity, phosphorylating Atg13, FIP200 and ULK1/2 itself and promoting autophagy (Jung et al., 2010). Other studies have reported a direct effect of pAMPK on ULK1 phosphorylation thereby affecting the initial step of autophagy (Cai et al., 2012).

In response to excess of nutrients, insulin is produced. Insulin binds a specific receptor on plasma membrane, IR receptor. The binding hormone-receptor induces autophosphorylation that in turn phosphorylates the insulin receptor substrate IRS that activates PI3K (Fulop et al., 2003). Activated PI3K phosphorylates the lipid phosphatidylinositol present on the internal surface of the cell membrane, producing PtdIns (3,4,5)P3 which in turn activate protein kinaseB (AKT/PKB) and other enzymes. This is followed by the activation of mTOR and autophagy inhibition. The phosphatase PTEN and the hormone glucagone are among the known signals that induce autophagy . PtdIns(3,4,5)P3 can also be hydrolysed by phosphatase PTEN resulting in a stimulatory effect on autophagy. Glucagone, released in nutrient starvation, activates instead autophagy through PI3K inhibition (Meijer & Codogno , 2004) (Yang et al., 2005).

Autophagy and diseases

Autophagy can play a protective or deleterious role in many pathological conditions, depending on the context. Defective autophagy can contribute to the pathogenesis of several diseases, such as infection and inflammatory diseases, lysosomal storage disorders, cancer, obesity, cardiovascular and, neurodegenerative diseases (Figure19).

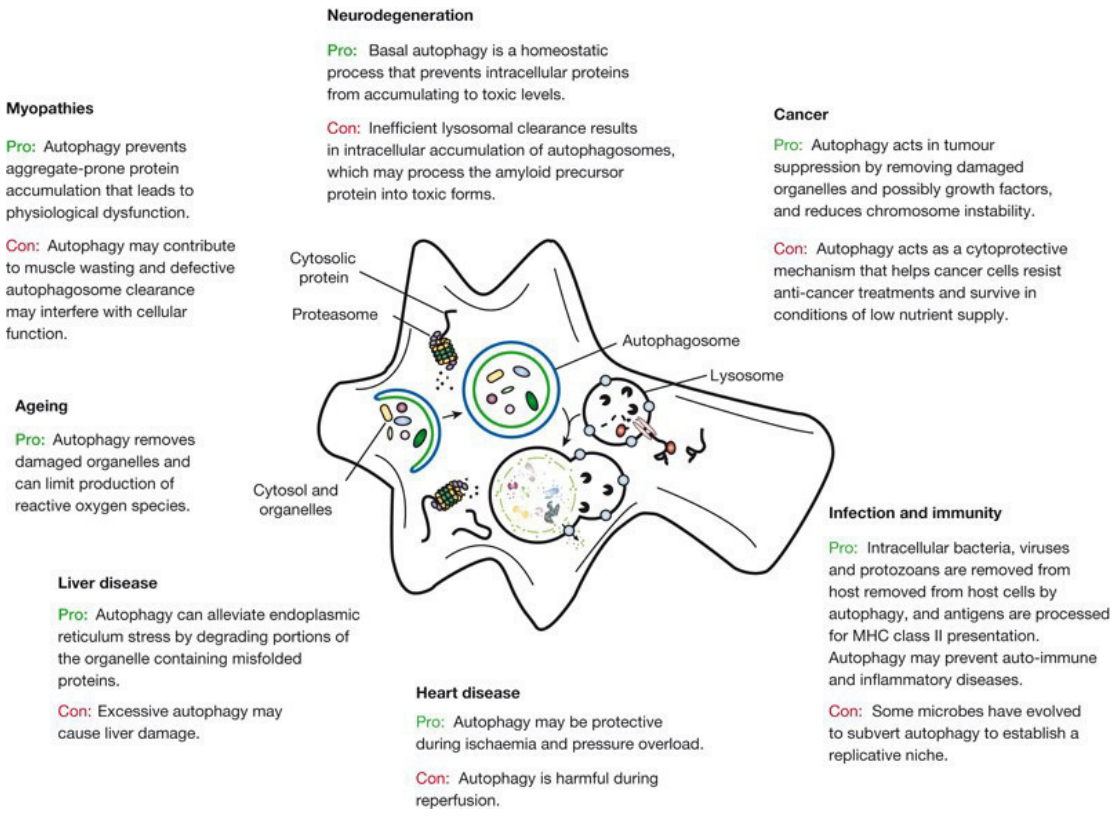

Figure 19 Role of autophagy in human diseases. In basal conditions autophagy is considered protective for cell homeostasis. Due to its crucial role, dysregulation in autophagy is associated to several pathological conditions The type and progression of diseases have to be considered to determine whether autophagy inhibition or stimulation may be beneficial (Mizushima et al., 2008).

Aim of the study

My work, during these three years of PhD, focused on two projects. As it is possible to understand from the topics discussed in the introduction, two different phenomena were evaluated in the presence of different aggregated proteins precisely the α-Syn and the first genetic variant of β2-Microglobulin, named D76N β2M.
In the case of α-Syn, we have observed that the presence of polyphenol OleA is able to interfere with the amyloid aggregation process, while as regards the D76N β2M we have discovered to be able to activate the phenomenon of autophagy.
Therefore this thesis has two goals:

1) To study the effect of OleA on α-Syn aggregation into amyloid fibrils.

The use of natural or synthetic small molecules seems to be an attracting way to counteract amyloidogenesis. In particular, plant compounds, such as polyphenols and curcuminoids, have been reported to interfere with the amyloid aggregation of several proteins/peptides of neuropathological interest, including α-Syn, Aβ and Tau (Masuda et al., 2006).

Recently, it has been reported that OleA, the main polyphenol in olive leaves and drupes (Rodríguez-Morató et al., 2015), interferes with the aggregation *in vitro* of several peptides/proteins associated with amyloid diseases including amylin (Rigacci et al., 2010), Aβ peptides (Rigacci et al., 2011), Tau (Daccache et al., 2011), Transthyretin (Leri et al., 2016) and beta2-microglobulin (Leri et al., 2018). It has been proposed that OleA can be beneficial against several amyloid diseases, either systemic (type-2 diabetes) (Rigacci & Stefani, 2016) or neurodegenerative (Casamenti & Stefani, 2017). However, no data are presently available on the interference of OleA with α-Syn aggregation and its possible protection against the toxicity of α-Syn aggregates.
So the first aim of this study was investigate on how OleA interferes with the path of α-Syn aggregation and modifies the biophysical properties of preformed α-Syn assemblies. We also evaluated the influence of OleA on the cytotoxicity of variously α-Syn aggregates and analysed the structural and biological features of the so-generated oligomeric species. Finally, we isolated and characterized an oligomeric species of α-Syn grown in the presence of OleA.

2) To describe the molecular mechanisms of autophagy induction by D76N β2M.

Autophagy is a key process involved in cell homeostasis of proteins (proteostasis), lipids and organelles and contributes to clear materials of endogenous or exogenous origin.

Usually, autophagy is induced in response to cellular stress such as starvation, and protects cells by eliminating dysfunctional and aged cellular organelles, principally mitochondria (mitophagy) and deposit of toxic aggregated proteins (O'Keefe & Denton, 2018). Autophagy efficiency declines with age, with consequent accumulation of harmful protein aggregates and damaged mitochondria, which leads to increased ROS production and cell stress which favour inflammation and cell death (Cuervo, 2008). For this reason autophagy is increasingly considered as a promising target to treat a number of pathologies, particularly those associated with neurodegeneration (Bové et al., 2011) as well as ageing (Rubinsztein et al., 2011).

Recent studies have shown that the main mechanism by which amyloid aggregates induce cytotoxicity is through interaction with cell membranes. The interaction between the cell membrane and the aggregates determines a destabilization of the lipid double layer which sees its permeability modified and compromised the functioning of specific membrane proteins and signaling pathways.

Furthermore, the presence of toxic aggregates inside the cell and on the external surface can induce cellular phenomena such as apoptosis and autophagy.

Colocalization and FRET experiments showed that the interaction with the cell membrane of aged D76N aggregates occurred at the raft level and involved the GM1 ganglioside, a key raft component, particularly its sialic acid moiety. This suggested that such interaction was mediated predominantly by electrostatic interactions (Leri et al., 2016).

Confirmed the interaction of the aggregates of D76N β2M the second goal of this thesis is to demonstrate the activation of autophagy and the related signaling pathways.

Materials and Methods

Before starting to describe the techniques used for the study of the effects of the OleA on the aggregation and toxicity of the α-Syn, it is important to specify that the techniques of expression and purification by RP-HPLC of the protein, structural and chemical characterization, TEM and DLS analysis, Limited proteolysis and finally the fingerprinting analysis of off-pathway oligomers have been performed in collaboration with the Department of Pharmaceutical Sciences, CRIBI Biotechnology Centre of the University of Padova.

Oleuropein deglycosylation

Oleuropein glycated was purchased from Extrasynthase, Genay Cedex, France. OleA was obtained by oleuropein deglycosylation according to Konno et al. (Konno et al., 1999), with minor modifications. Briefly, oleuropein glycated was solubilized at a 10 mM concentration in 0.1 M sodium phosphate buffer pH 7.0, and incubated with 9.0 I.U./mL of β-glucosidase overnight at room temperature in the dark. The aglycone was precipitated by centrifuging the reaction mixture at 13200 × g for 10 minutes (min). The complete oleuropein deglycosylation was confirmed by assaying the glucose released in the supernatant with the Glucose (HK) Assay Kit (Sigma-Aldrich). The glucose determination is based on two enzymatic reactions:

1) Glucose + ATP $\xrightarrow{\text{Hexokinase}}$ Glucose-6P +ADP

2) Glucose 6-Phosphate + NAD $\xrightarrow{\text{G6PD}}$ 6- Phosphogluconate + NADH

In the first reaction the hexokinase catalyses the phosphorylation of glucose into glucose-6-phosphate. Glucose-6-phosphate (G6P) is then oxidized in the second reaction to 6-phospho-gluconate in the presence of oxidized nicotinamide adenine dinucleotide (NAD) through the glucose-6-phosphate dehydrogenase (G6PDH) enzyme. During this reaction, an equimolar amount of NAD is reduced to NADH. The increase in absorbance at 340 nm of NADH is directly proportional to glucose concentration, which is equimolar to OleA. The determination of the amount of OleA allowed its solubilisation in DMSO at a final concentration of 50mM. This stock solution was kept in the dark at -20°C until further use. OleA working solution was obtained by diluting

the stock solution into buffer.

Expression, purification and aggregation experiments

α-Syn was expressed in Escherichia coli BL21(DE3) cell line transfected with the pET28b/α-syn plasmid. The recombinant protein was expressed and purified according to De Franceschi et al procedure (De Franceschi et al., 2009) and further purified by RP-HPLC. The identity and purity of the eluted material were assessed by mass spectrometry.

To induce α-Syn aggregation, 70 μM protein samples were filtered with a 0.22 μm pore-size filter (Millipore, Bedford, MA, USA) and incubated at 37 °C in PBS (8.0 mM Na2HPO4, 137 mM NaCl, 2.0 mM KH2PO4, 2.7 mM KCl, pH 7.4) for up to 7 days under shaking at 500 rpm with a thermo-mixer (Compact, Eppendorf, Hamburg, DE) in the absence or in the presence of OleA (210–700 μM, corresponding to a α-Syn:OleA molar ratio of 1:3 or 1:10, respectively). Protein aggregation in sample aliquots collected at the indicated incubation times was checked by Thioflavin T (ThT) binding assay, 1-anilinonaphtalene-8-sulfonate (ANS) fluorescence, transmission electron microscopy (TEM), limited proteolysis, gel filtration (GF) chromatography and reverse phase (RP)-HPLC. The interference of OleA in ThT and ANS analysis was assayed by performing controls experiments where the polyphenol was added in pre-made α-Syn aggregates (48 h and 168 h) either immediately before or after the addition of ThT or ANS solution. Oligomer-enriched or fibril-enriched sample were prepared by incubating α-Syn for hours (h), 48 h or up to 168 h, respectively.

D76N β2M was expressed and purified as Valleix's group reported (Valleix et al., 2012) (Mangione et al., 2013). The aggregation reaction was initiated starting from the freeze-dried protein. Briefly, the protein was dissolved in PBS (Sigma-Aldrich, St. Louis, MO, USA). At time 0 of the aggregation reaction, the protein solution was centrifuged for 5 min. at 13,200 9 g and filtrated through 0.02 μm nanofilters (Whatman Inc., Amersharm, UK) to eliminate possible aggregation seeds. The resulting supernatant was diluted to a protein concentration of 20 μM. The latter was determined by measuring the absorption at 280 nm, using a molar extinction coefficient of 19,940 per M/cm, a 1.0-mm path-length cell and a Jasco V-630 UV visible spectrophotometer (Tokyo, Japan). A 300 μL of the obtained solution was incubated in a 1.5 ml eppendorf tube lying in horizontal position, under vigorous shaking, 900rpm, at 37°C. Oligomer-enriched or fibril-

enriched sample were prepared by incubating D76N β2M 24 h (β2 24h) or up to 144 h (β2 144h), respectively.

Disaggregation experiments

For disaggregation experiments, 48 h-aged oligomers were incubated with OleA (1:10) at 37 °C under shaking at 500 rpm, for 24 h (α-Syn 48 h + OleA 24 h) or 5d (α-Syn 48 h + OleA 5d); 168 h-aged fibrils were incubated with OleA for 8 h (α-Syn 168 h + OleA 8 h) or for 5d (α-Syn 168 h + OleA 5d). All aggregate concentrations were expressed as monomer protein concentration.

Structural characterization

Protein concentrations were determined by absorption measurements at 280 nm using a double-beam Perkin Elmer (Norwalk, CT) Lambda-20 spectrophotometer. The molar absorptivity at 280 nm for α-Syn was 5960 cm−1 M−1, as evaluated from its amino acid composition by the method of Gill and von Hippel (Gill & von Hippel, 1989). Circular dichroism (CD) spectra were recorded by a Jasco (Tokyo, Japan) J-710 spectropolarimeter, using a 1.0-mm path-length quartz cell and a protein concentration of 7.0 μM. The mean residue ellipticity [θ] (degcm2 dmol−1) was calculated according to the formula [θ] = (θobs/10)(MRW/lc), where θobs is the observed ellipticity in deg, MRW is the mean residue molecular weight of the protein, l is the optical path-length (as cm) and c is protein concentration (as mg/ml). The spectra were recorded in PBS, pH 7.4. Fluorescence measurements were performed using a Jasco (Tokyo, Japan) FP-6500 spectrofluorimeter and a 0.1-cm path length cuvette. The ThT binding assay was performed accordingly to LeVine (Le Vine , 1999) using a 25 μM ThT solution in 25 mM sodium phosphate buffer, pH 6.0. Aliquots (30 μl) of protein samples were collected at the indicated times and diluted into the ThT buffer. Fluorescence emission measurements were performed at 25 °C at an excitation wavelength of 440 nm by recording the ThT fluorescence emission in the 455–600 nm interval. For ANS binding experiments, a 350 nm excitation wavelength was used and the emission spectra were scanned in the 380–600 nm interval (Hawe et al., 2008). All spectra were recorded at 25 °C using a 50 μM ANS solution and a 2.5 μM protein solution. ANS-binding experiments were carried out in 50 mM Tris-HCl buffer, pH 7.4. ANS concentration was determined using a molar absorption coefficient of 4950 M−1 cm−1 at 350 nm. To

evaluate the possible interference of OleA with the ThT and ANS fluorescence assay, two different controls were performed by monitoring the emission fluorescence spectra intensity of α-Syn aggregates before and after OleA addition: i) OleA was added together to the probe or ii) OleA was added after the probe and the fluorescence spectra were re-acquired immediately.

TEM and DLS analysis

Size and morphology of α-Syn aggregates were investigated by transmission electron microscopy (TEM) and dynamic light scattering (DLS). Negative staining was obtained by placing a drop of the sample solution on a Butvar-coated copper grid (400-square mesh) (TAAB-Laboratories Equipment Ltd, Berks, UK). Then, the sample was dried and negatively stained with a drop of uranyl acetate solution (1.0%, w/v). TEM pictures were taken on a Tecnai G2 12 Twin instrument (FEI Company, Hillsboro, OR) at an excitation voltage of 100 kV. Size distribution of protein samples was calculated on the basis of 382 particles manually extracted from the micrographs using ImageJ software. Only clearly defined spherical and isolated particles were selected. Measurements were obtained with a standard deviation of 5.04. Size distributions were also evaluated by DLS experiments carried out in duplicate, at 25 °C in PBS, pH 7.4, using a Zetasizer Nano-ZS instrument (Malvern Instrument, UK), the oligomer sample was concentrated using the Amicon 3000 MCWO and then centrifuged at 12000 rpm for 10 minutes.
Twelve runs were collected during each measurement.

TEM analysis was carried out on D76N β2M as reported by Leri M. et al. (Leri et al., 2016) 5.0 mL aliquots of D76N b2M were withdrawn from the aggregation mixture at different time intervals, loaded onto a formvar/carbon-coated 400 mesh nickel grids (Agar Scientific, Stansted, UK) and negatively stained with 2.0% (w/v) uranyl acetate (Sigma-Aldrich, Saint Louis, MO, USA). The grid was air-dried and examined using a JEM 1010 transmission electron microscope at 80 kV excitation voltage.

Chemical characterization

Gel filtration (GF) chromatography was performed by a Superdex 75 10/300GL c column (Amersham Biosciences, Uppsala, Sweden), using an ÄKTA FPLC system (Amersham Biosciences, Uppsala, Sweden). Sample aliquots (200 μL) were taken from

the aggregation mixture, filtered (0.22 μm filters), loaded onto the column and eluted at 0.5 ml/min in 20 mM Tris-HCl, 0.15 M NaCl, pH 7.4. The effluent was monitored by recording the absorbance at 214 nm. Column calibration was performed using the following standards: blue dextran (void volume); albumin, 67 kDa; ovalbumin, 45 kDa; α-lactalbumin, 14.4 kDa and aprotinin, 6.5 kDa. The RP-HPLC analyses were carried out on an Agilent 1200 chromatographer (Santa Clara, CA) using a Jupiter C18 column (4.6 × 250 mm; Phenomenex, CA, USA), eluted with the following acetoni- trile/0.085% TFA- water/0.1% TFA gradient: 5–25%, 5 min, 25–28%, 13 min, 28–39%, 3 min, 39–43%, 21 min. The effluent was monitored by recording the absorbance at 226 nm. The identity of the eluted material was assessed by mass spectrometry, carried out with an electrospray ionization (ESI) mass spectrometer equipped with a Q-Tof analyzer (Micro) (Waters, Manchester, UK) or a QTof Xevo G2S (Waters, Manchster, UK). Measurements were carried out at 1.5–1.8 kV capillary voltage and 30–40 V cone voltage.

Limited proteolysis

Limited proteolysis experiments of α-Syn and α-Syn /OleA (1:3, 1:10) samples were carried out in PBS, pH 7.4, at room temperature using proteinase K at E/S ratio of 1:1000 (by weight) at 70 μM α-Syn concentration. The reactions were quenched after 5 min by acidification with TFA in water (4.0%, v/v) and analysed by RP-HPLC, as described above.

Fingerprinting analysis of off-pathway oligomers

The α-Syn aggregated species were purified by harvesting the material eluted from RP-HPLC at RT 51.2 min at the conditions described above. The protein samples were dried in Savant and solubilised in 6.0 M guanidine (Gnd)-HCl/20 mM Tris-HCl, pH 8.5. Then, the samples were diluted 1:10 and trypsin was added to an 1:25 enzyme to substrate (E/S) ratio. After 15 h of incubation at 37 °C, the proteolysis mixture was analysed with RP-HPLC by the same column and gradient used for purification and the peptide species were identified by ESI-MS. For proteinase K proteolysis, the sample was further diluted reaching a final concentration of 1.0 M Gnd-HCl before adding the enzyme (E/S 1:1000). The reactions were carried out for 5 or 70 min at 37 °C.

Immortalised cell line and cell treatment

SY-SY5Y were cultured in 1:1 mixture of DMEM and HAM medium, supplemented with 10% fetal calf serum (FCS, Sigma-Aldrich, Steinheim, Germany), 3.0 mM glutamine, 100 units/ml penicillin and 100 mg/ml streptomycin in both studies. The cells were maintained in a humidified incubator at 37°C with 5% CO2. All materials used for cell culture were from Sigma.

Cytotoxicity assay: MTT test

MTT is a cell viability test using 3-(4,5,dimethylthiazol-2-yl)-2,5 diphenil tetrazolium-bromide (MTT), a compound yellowish in solution. The MTT substrate is prepared in a physiologically balanced solution, added to cells in culture, usually at a final concentration 0.5mg/ml, and incubated for 1 to 4 h. Mitocondrial dehydrogenases of viable cells cleave the tetrazolium ring converting MTT into purple colored formazan cristals which are insoluble in aqueous solution (Figure 20). The formazan crystals are then solubilized in DMSO and the resulting purple solution is measured spectrophotometrically. The quantity of formazan (presumably directly proportional to the number of viable cells) is measured by recording changes in absorbance at 570 nm. The exact mechanism responsible of MTT reduction into formazan is not well understood, but probably NADH or similar reducing molecules that transfer electrons to MTT are involved (Marshall et al, 1995). SH-SY5Y cells were plated and incubated for 24 h at a density of 10000 cells/ well on 96-well plates in 100 µl culture medium. The day after the medium was replaced with fresh complete medium (HAM F12, 10% FBS, 10%Horse Serum,1% penicillin/streptomycin) and then, the cells were treated.

In the α-Syn study the cells were treated for 48 h with 5.0 µM α-Syn aggregates grown in the absence or in the presence of OleA (1:10); while, to evaluate the cytotoxicity of the different forms of D76N β2M aggregates, the cells were treated with the sonicated (β2 24hS) and not sonicated (β2 24h) oligomers for different times.

At the end of exposure to the aggregates, the cells were incubated for 2h with 100µl DMEM without phenol red, containing 0.5mg/ml MTT. Then, 100µl of cell lysis buffer (20% SDS, 50% N,N-dimethylformamide, pH 4,7) was added to each well and the samples were incubated at 37 °C to allow complete cell lysis and to solubilize the

formazan crystals precipitated. The blue formazan absorbance was recorded at 595 nm with an automatic plate reader (Bio-Rad, Hercules, California). Final absorption values were calculated by averaging three independent measurements of each sample after subtraction of the average of the blank solution (100 µl of MTT solution and 100 µl of lysis buffer). All data were expressed as mean ± standard deviation.

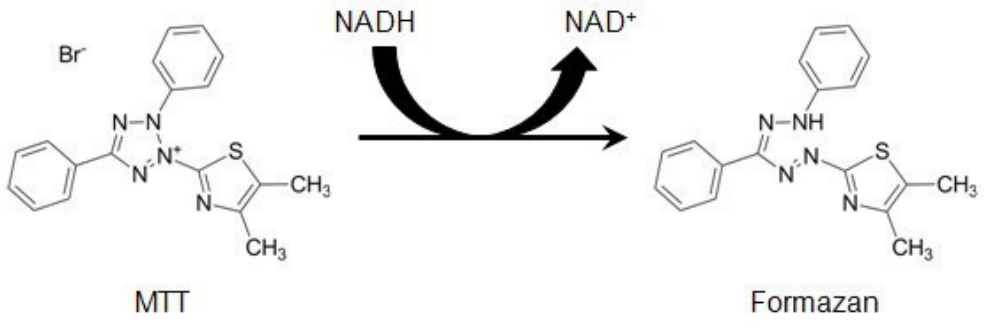

Figure 20 Conversion of MTT in colored formazan product (Riss et al., 2013).

Reactive oxygen species

The intracellular reactive oxygen species (ROS) were determined using the fluorescent probe 2',7'-dichlorofluorescein diacetate, acetyl ester (CM-H2 DCFDA; Sigma-Aldrich). CM-H2 DCFDA is a cell-permeant indicator for ROS that becomes fluorescent upon removal of the acetate groups by intracellular esterases and subsequent oxidation. The latter modification can be detected by monitoring the increase in fluorescence at 538 nm. The SH-SY5Y cells were plated at a density of 10,000 cells per well on 96-well plates and the following day the cells were exposed for 48 h to 5.0 µM α-Syn aggregates in the α-Syn study and treated with the D76N β2M aggregates at a final concentration of 5.0 µM during the experiment for D76N β2M project. At the end of the both treatments 10 mM DCFDA in DMEM without phenol red was added. After 30 min, the fluorescence values at 538 nm were detected with the use of a Fluoroskan Ascent FL (Thermo-Fisher, Illkinch, France).

Confocal immunofluorescence

Subconfluent SH-SY5Y cells grown on glass coverslips were treated for 48 h with α-Syn aggregates at a 5.0 μM final concentration and then washed with PBS. The same was done during the D76N β2M study: SH-SY5Y cells were treated for different times (30 min, 1h, 3h and 5h) with D76N β2M oligomers and sonicated D76N β2M oligomers, at 5.0 μM final concentration and after incubation, the cells were washed with PBS.

Labelling at the cell surface monosialotetrahexosylganglioside (GM1) was obtained by incubating the cells with 10 ng/ml CTX-B Alexa488 in complete medium for 30 min at room temperature. Then, the cells were fixed in 2.0% buffered paraformaldehyde for 10 min, permeabilized by a cold 1:1 acetone/ethanol solution for 4 min at room temperature and blocked with PBS containing 0.5% BSA and 0.2% gelatine for 30 min. After blockage, the cells were incubated for 1 h at room temperature with a rabbit polyclonal anti- α-Syn antibody (Abcam, Cambridge UK) diluted 1:500 and with a rabbit polyclonal antibody raised against D76N β2-m (Abcam, Cambridge, UK) diluted 1:600, respectively, in blocking solution and then washed with PBS for 30 min under stirring. The immunoreaction was revealed by Alexa 568-conjugated anti-rabbit Abs (Molecular Probes, Eugene, Oregon, USA) diluted 1:100 in PBS. Finally, the cells were washed twice in PBS and once in water to remove non-specifically bound antibodies. Cell fluorescence was imaged using a confocal TCS SP5 scanning microscope (Leica) equipped with a HeNe/Ar laser source for fluorescence measurements. Sample observations were performed by a Leica Plan Apo X63 oil immersion objective suited with optics for differential interference contrast acquisition. FRET analysis was carried out by the FRET sensitized emission (SE) method which is one of the most used and simple methods for the evaluation of FRET efficiencies (Jares-EriJman & Jovin, 2006). The method involves measuring the acceptor fluorescence emission when only the donor has been excited (I_{AD}) in sequence with the emission detection of the directly excited acceptor (I_{AA}). The ratio of these two signals is approximately proportional to the FRET efficiency: $E \propto SE/I_{AA} \approx I_{AD}/I_{AA}$ (van Rheenen et al., 2004).

The last approximation holds when the spectral bleed-through contributions are negligible. These noise components are mainly of two types: the donor emission detected in the acceptor channel and the acceptor emission caused by a direct excitation. Confocal 3D Z-stacks images of I_{AD} and I_{AA} were then taken by sequential acquisitions

of the Alexa Fluor 568 fluorescence once excited by the laser lines at 458 nm and 543 nm respectively. FRET efficiency was calculated by using equation, indicated above, for each one of the Z-stacks and then Z-projected onto a single 'extended focus' pseudocolor image (Nosi et al., 2012).

Analysis of autophagic vacuoles

The Cyto-ID® Autophagy Detection Kit (Enzo Life Sciences) which uses a novel dye that selectively labels autophagic vacuoles in living cells was used to monitor autophagy induction by fluorescence microscopy, according to the manufacturer instructions. The cells were plated for 24h in 24-well plates containing coverslips and then treated with 5 μM different aggregated species of D76N β2M for 5h. After incubation with D76N β2M, the medium was removed and the cells were washed twice with 100 μl of PBS and then with 100 μl of 1 × Assay-Buffer provided with Dectection Kit containing 10% FCS. After washing, the cells were incubated for 30 min at 37 °C with 100 μl of Dual detection reagent (prepared by diluting Cyto-ID Green Detection Reagent 330 times in a mixture of 1× Assay Buffer plus FCS), protected from light. Finally, the cells were washed three times with the same solution (1 × Assay Buffer-FCS 10%) and the coverslips were placed on microscope slides. The stained cells were analyzed by using a confocal Leica.

Western blotting

After treatment, SH-SY5Y cells were lysed in LEAMLI buffer. Before immunoblotting, protein concentration was determined with a BCA detection kit (Pierce, USA) and adjusted to equal concentrations across different samples. The samples were added with β-mercaptoethanol and bromophenol blue, boiled for 10 min and clarified at 10000 × g for 10min.

The extracted protein was placed in each well with 20 μg samples and separated by SDS-PAGE gels (BioRad), then transferred onto a PVDF membrane. The membrane was then blocked with 5% bovine serum albumin (BSA) at room temperature and incubated with appropriate primary antibodies: rabbit monoclonal anti-beclin1 antibody (1:1000, Cell Signaling), rabbit monoclonal anti-LC3-II A/B antibody (1:1000, Cell Signaling), rabbit monoclonal anti-Akt (1:5000 abcam), rabbit monoclonal anti-p-Akt (1:5000 abcam), the phosphorilazed form, rabbit monoclonal anti-p-GSK-3β (1:1000

Cell Signaling), rabbit monoclonal anti-S6 (1:1000 Cell Signaling), rabbit monoclonal anti-p-S6 (1:2000 Cell Signaling), mouse monoclonal anti-Erk (1:2000 Cell Signaling), rabbit monoclonal anti-p-Erk (1: 1000 Cell Signaling) overnight at 4°C.

The day after, the membrane was washed with Tris-Buffered-Saline with Tween (TBST) and then the blots were incubated for 1h with specific secondary antibodies (1:10000, goat anti-rabbit antibody and goat anti-mouse antibody, Molecular Probes, Life Technologies); the immunoreactive bands were detected with the Electrochemiluminescence (ECL) reagent, analised by Amersham Imager 600 imagers (GE Healthcare, UK) and quantificated by densitometric analysis using Image J software. Statistical analysis of the bands was performed on results from at least three independent experiments and are expressed as mean± standard deviation.

Data analysis and statistics

Statistical analysis was performed using Student's t-test. The results were compared using Student's t-test between two groups, *$P < 0.05$; **$P < 0.01$; ***$P < 0.001$ versus untreated cells and °$P < 0.05$; °°$P < 0.01$; °°°$P < 0.001$ versus cells treated with aggregates grown in the absence of OleA.

Results

Interaction between OleA and monomeric α-Syn

The effect of OleA on the secondary structure of α-Syn was evaluated by far-UV CD spectroscopy (Figure 21b, inset). We found that at neutral pH the protein displays a far-UV CD spectrum typical of a substantially unfolded polypeptide chain, with an intense minimum near 198 nm and the absence of characteristic bands in the 208–230 nm region (Figure 21b, red dashed line). In the presence of OleA at two different α-Syn/OleA molar ratios (1:3 or 1:10), no changes in the shape or intensity of the spectra recorded just after sample preparation were detected, supporting the lack of any direct conformational modification. For simplicity, Figure 21b, inset, reports only the spectrum relative to the 1:10 α-Syn/OleA ratio (black continuous line). To confirm this, we also analysed α-Syn in the absence and in the presence of OleA (1:10) by gel filtration (GF) (Figure 21b) and RP-HPLC (Figure 21c). To avoid technical problems, the samples for GF analysis were filtered (0.22 μm filters) before loading; to simplify the figure, the profiles obtained in the presence of 1:3 α-Syn/ OleA ratio are not shown. The GF profiles of α-Syn in the absence or in the presence of OleA are similar and show a major species eluting at ~9.4 ml, corresponding to monomeric α-Syn. In the presence of OleA a minor high MW species (~1%) at shorter elution volume was also seen (Figure 21b). No variation in the retention time (RT 35.5 min) of α-Syn when eluted in the presence of OleA was seen in RP-HPLC; however, we noticed the presence of a new peak at RT 51.2 min (Figure 21c, highlighted with two stars), indicating increased hydrophobicity, likely due to some chemical modifications or change in the aggregation state of this species. These two main fractions were collected and analyzed in more detail.

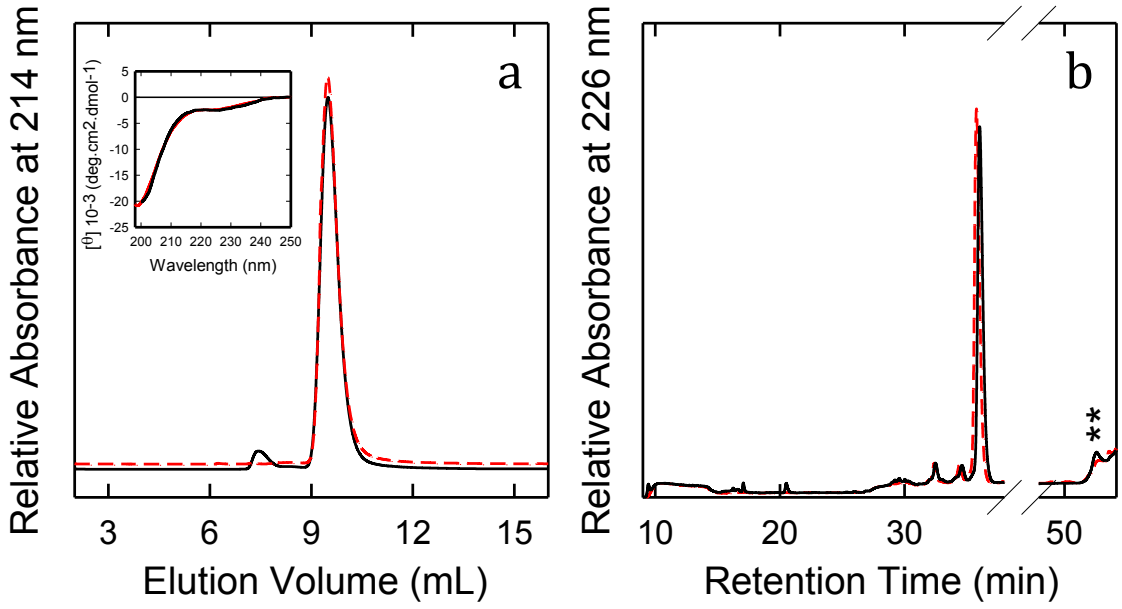

Figure 21 (a,inset) Far-UV CD spectra of α-Syn in the absence (red line) and in the presence of OleA (Syn/OleA 1:10) (black line). Spectra were taken at 25 °C in PBS (pH 7.4). (a) Gel filtration and (b) RP-HPLC chromatograms of α-Syn in the absence (red dashed line) and in the presence of 1:10 OleA (black line). In (b) the peak relative to RT 51.2 is highlighted with two stars.

Mass spectrometry analysis indicated the presence of α-Syn species in both fractions (Table 3). α-Syn appeared chemically modified in very low percentage (~5.0%) by the presence of some covalent adducts resulting in mass increases of 205 and 223 Da. These adducts could result from the reaction of α-Syn with demethylated and dehydrated forms of the elenolic acid arising from OleA degradation (Gutierrez-Rosales et al., 2010). The presence of these modifications in both monomeric and late-eluting α-Syn allows to exclude they are the cause of the RP-HPLC shift.

RT[a] (min)	Found mass[b] (Da)	Theoretical mass[c] (Da)	Protein species
35.5	14461.5 (± 0.1) 14477.2 (± 0.8) 14682.8 (± 0.8)	14460.5 14476.5 14683.2	SynSyn + 1ox Syn + 223
51.2	14462.1 (± 1.5) 14478.5 (± 1.8) 14665.2 (± 0.5) 14683.2 (± 0.1)	14460.5 14476.5 14665.2 14683.2	SynSyn + 1ox Syn + 205 Syn + 223

Table 3 Chemical characterization of the main protein species in the mixture formed by

α-Syn and OleA in the 1:10 ratio eluted from the RP-HPLC column (Figure 21c). The term ox indicates an oxidized derivative (+16 Da). [a]Proteins are listed in order of retention time (RT). [b]Experimental molecular masses determined by ESI-QTOF-MS. [c]Molecular masses calculated from α-Syn amino acid sequence.

OleA interferes with α-Syn aggregation into amyloid fibrils

When incubated in vitro at 37 °C and pH 7.4 for 168 h, α-Syn aggregates into fibrils (Uversky, 2007). The amyloid fibril formation kinetics was monitored by following the increase of ThT fluorescence emission at 485 nm during the aggregation process. According to previous data (Uversky et al., 2001), we found an initial lag phase followed by an exponential growth phase and a final plateau, consistent with a nucleation-dependent mechanism (Figure 22a). TEM imaging showed that the 48 h sample was populated with oligomers and pre-fibrillar aggregates (Figure 22c), while fibrils with typical amyloid morphology became the major aggregated species after 168 h of incubation (Figure 22f). Then, we investigated the effect of OleA on the kinetics of fibril formation by using a α-Syn /OleA ratio of 1:3. We found that the curve maintained a sigmoid trend, yet in the presence of OleA (Figure 22a), and some amyloid fibrils were still detectable in the sample (Figure 22 d,g).

When we used a 1:10 α-Syn/OleA ratio, the ThT fluorescence intensity was scarcely increased (Figure 22a) but other types of aggregates populated the sample, as seen by TEM imaging (Figure 22 e,h), suggesting some interference of the polyphenol with the aggregation process.

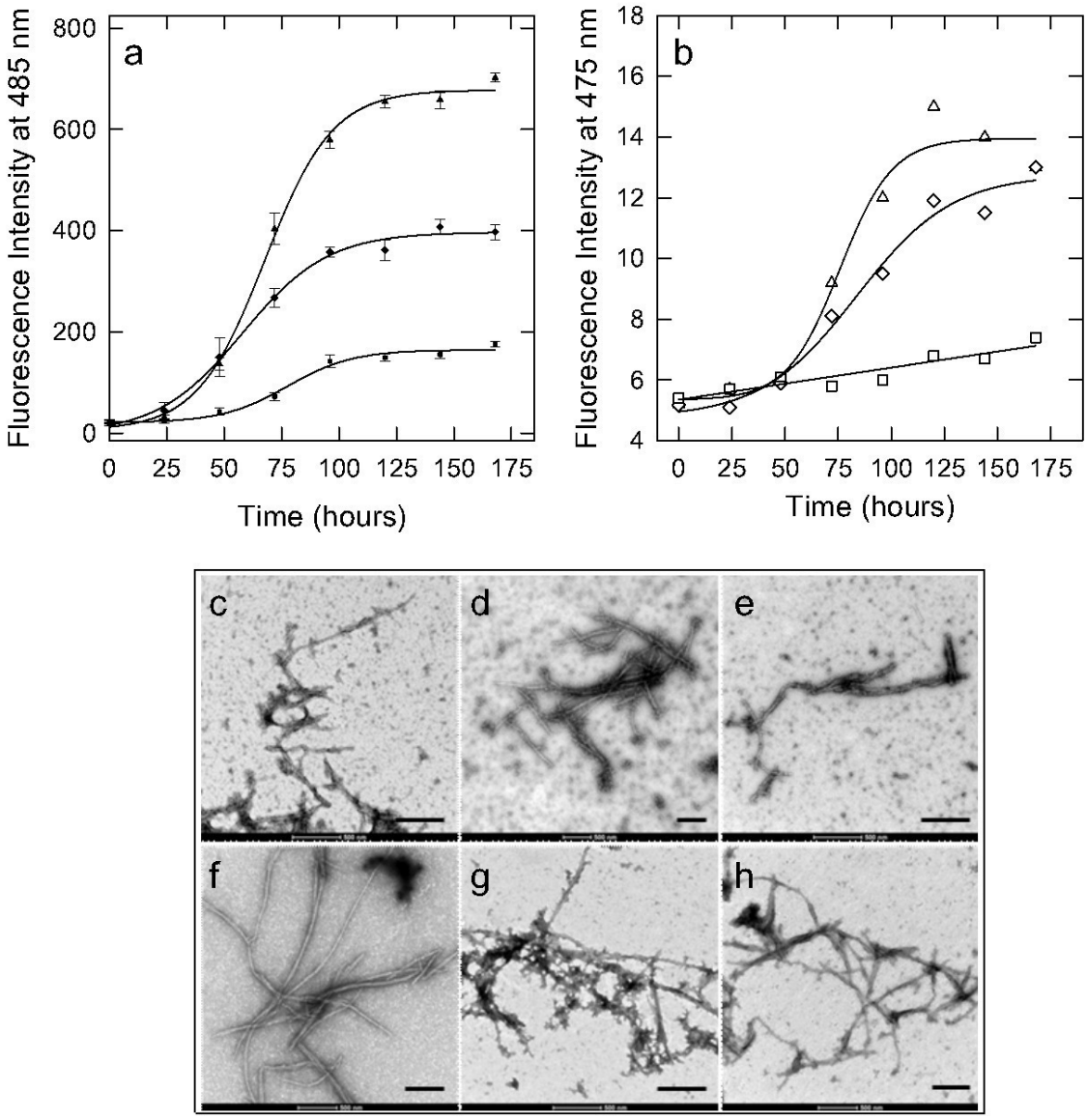

Figure 22 Effect of OleA on α-Syn aggregation probed by ThT (a), ANS (b) fluorescence spectroscopy and TEM (c–h). Syn aggregation kinetics (triangle), α-Syn aggregation in the presence of 1:3 (diamond) or 1:10 (square) OleA. For the ThT assay, aliquots (30 µl) of the protein solution, incubated for the indicated times, were added to a 25 µM solution (470 µl) of ThT in 25 mM phosphate buffer, pH 6.0. Excitation wavelength: 440 nm, fluorescence emission: 485 nm. For the ANS assay, excitation wavelength: 350 nm, fluorescence emission: 475 nm at 25 °C. TEM pictures taken from α-Syn aggregation mixture after 48 h and 168 h of incubation in the absence (c,f) or in the presence of a 1:3 (d,g) or 1:10 (e,h) α-Syn/OleA ratio. Scale bar in every picture corresponds to 500 nm.

α-Syn aggregation was further characterized in terms of hydrophobic exposure, monitored as ANS binding, by recording the increase of fluorescence emission at 475 nm by ANS added to sample aliquots withdrawn from the aggregation mixture at different incubation times (Figure 22b). The experimental data points fit an irregular sigmoidal curve recalling, in part, the trend observed in the ThT experiment. When the aggregation was carried out at α-Syn/OleA 1:10, we found a moderate increase of fluorescence intensity during the process. Overall, these data confirm that OleA interferes with the aggregation process of α-Syn.

Mapping α-synuclein conformation during aggregation in the presence of OleA by limited proteolysis

The propensity of α-Syn to be hydrolysed by proteinase K at different stages of amyloid aggregation was investigated by highlighting the sites of proteolysis in the absence or in the presence of OleA. Proteinase K was chosen because of its broad specificity (Ebeling et al., 1974); accordingly, its cleavage sites are not expected to be dictated by the amino acid sequence, rather, they depend on the conformational and dynamical features of the polypeptide chain (Fontana et al., 2004) (Polverino de Laureto et al., 2003). An E/S ratio of 1:1000 was used in the experiment and the proteolysis mixtures were analysed by RP-HPLC after 5 min incubation of α-Syn with the protease (Figure 23). As expected from its natively unfolded character, monomeric α-Syn was highly susceptible to the proteolytic attack and many fragments were seen in the chromatogram after 5 min. incubation (Figure 23a). When α-Syn was kept for 48 h in aggregation buffer, a slightly reduced susceptibility to proteolysis was evident (Figure 23b); moreover, at longer incubation times, α-Syn became progressively more resistant to proteolysis, in parallel with the increase of fibril content in the aggregation mixture, as previously observed for other proteins (Polverino de Laureto et al., 2003) (Figure 23c). Then, the proteolysis experiment was carried out on the α-Syn/OleA 1:3 or 1:10 samples. We found that at time 0 all proteolytic mixtures showed a similar pattern (Figure 23 a,d,g). As the aggregation time increased, α-Syn appeared apparently less resistant to proteolysis (Figure 23 e,f,h,i); in fact, the peak relative to the intact protein (RT 35.5 min) was slightly less intense than that obtained in the absence of OleA (highlighted with a star in the figure). It is worth noting the presence of the peak at RT 51.2 min (highlighted with two stars in figure 23). This species increased as far as the aggregation time was prolonged (from T 0 to T 168 h,) and OleA concentration in the sample was increased

(Figure 23 d–f,g–i).

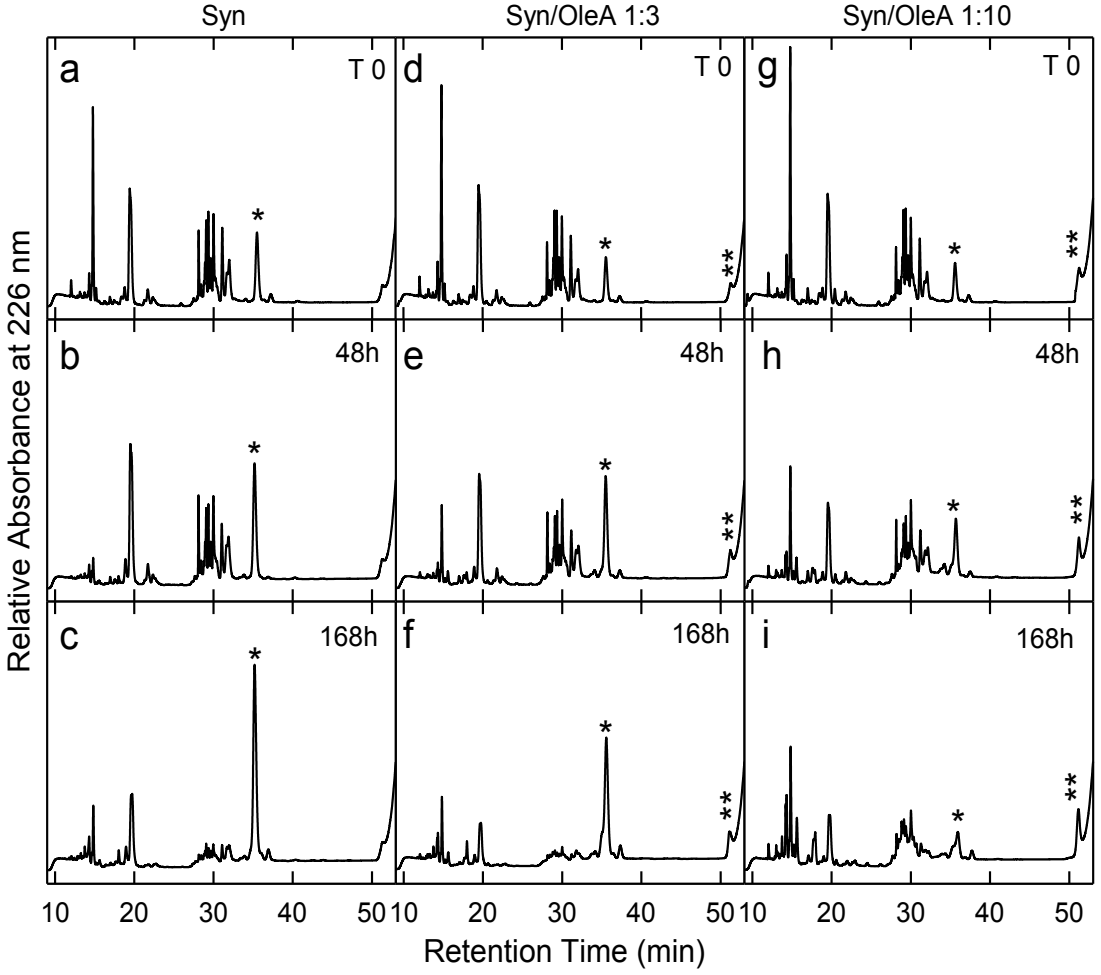

Figure 23 α-Syn aggregation in the absence or in the presence of OleA 1:3 and 1:10 ratio investigated by limited proteolysis. During aggregation, proteinase K was added at an E/S ratio of 1:1000 (by weight) to aliquots (40 µl) taken from the mixture at different time intervals (0, 48, 168 h). Proteolysis was allowed to take place at 22 °C for 5 min and then quenched by addition of 4.0% TFA in water. The proteolysis samples were analysed by RP-HPLC using a Jupiter C18 column (4.6 × 250 mm) and eluted with a gradient of acetonitrile/0.085% TFA vs water/0.1% TFA from 5.0% to 25% in 5 min, from 25% to 28% in 13 min, from 28% to 39% in 3 min, from 39% to 43% in 21 min. The peaks relative to intact α-Syn and to the oligomeric species are highlighted.

Overall, the proteolysis data indicate that the presence of OleA in the aggregation mixture of α-Syn increases the monomeric α-Syn sensitivity to proteolysis. Moreover, OleA favours the growth of other types of aggregated species, that elute late in RP-HPLC and exhibit increased resistance to proteolysis. To better describe this finding, the α-Syn species were classified as PK-sensitive, PK-resistant and PK-resistant off-pathway oligomers (Figure 24). The first fraction contained the soluble components of the aggregation mixture; the PK-resistant α-Syn contained the pre-fibrillar and fibrillar species in equilibrium with the soluble ones; the PK-resistant off-pathway oligomers fraction contained the protease-resistant molecular species eluting at RT 51.2 min. At the beginning of the aggregation (Figure 24a), the most populated fraction was the PK-sensitive one. As expected, as far as aggregation proceeds, the PK-resistant population increased, at the expense of the PK-sensitive fraction that decreased inversely (Figure 24b,c).

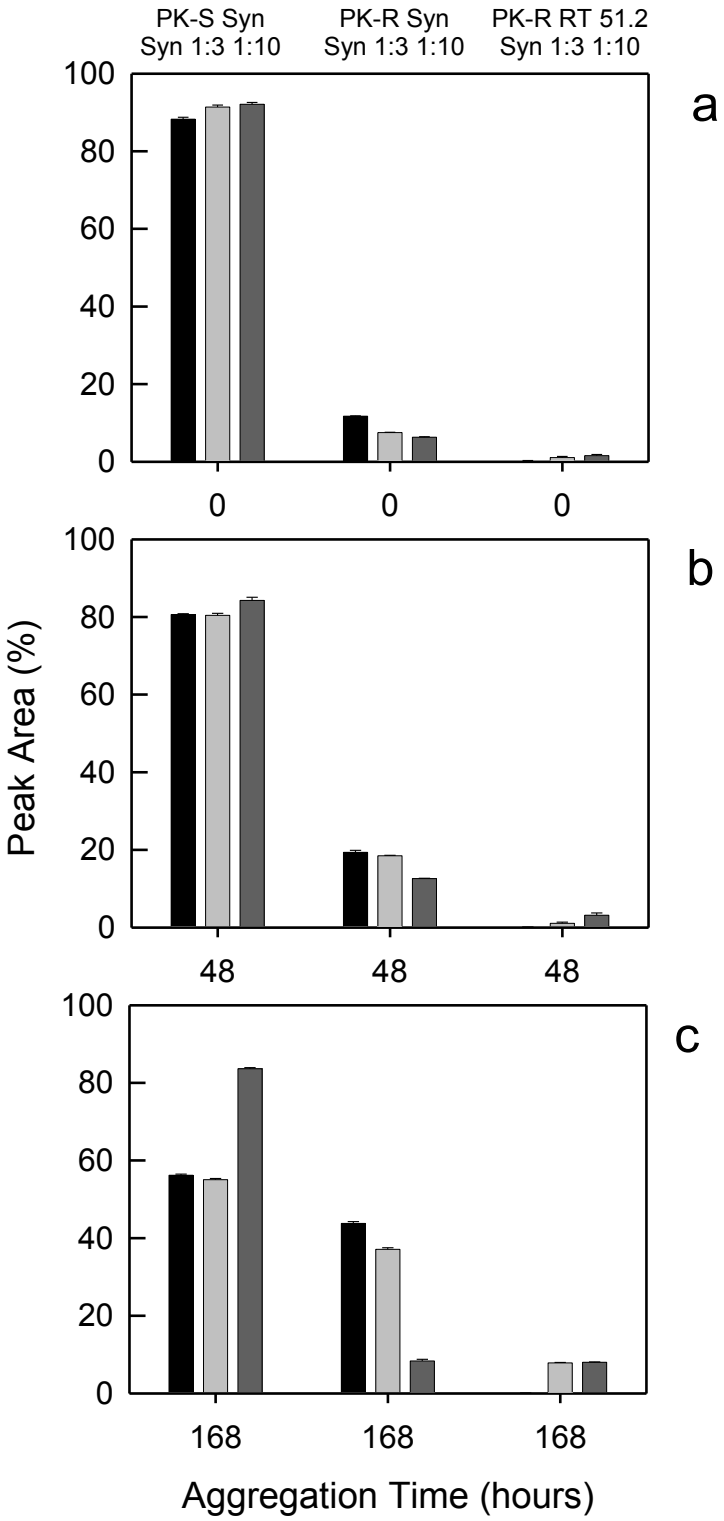

Figure 24 Quantification of the different population of α-Syn coexisting in the aggregation mixture in the absence or in the presence of OleA, calculated by the limited proteolysis experiments shown in figure 23. The extent of each population was evaluated from the area of the chromatographic peaks relative to the purification of the

proteolysis mixtures of α-Syn with proteinase K (PK) during aggregation. Peaks areas relative to proteolysis (a) at 0 h; (b) at 48 h; (c) at 168 h of α-Syn incubation. PK-S α-Syn consists of the fragments produced by PK-proteolysis; PK-R α-Syn represents undigested α-Syn and PK-R RT 51.2 represents undigested off-pathway oligomers.

Characterization of the off-pathway species arising during α-Syn aggregation in the presence of OleA

Next, we look at the fraction eluted at RT 51.2 min by RP-HPLC under aggregation conditions in the presence of OleA. This species was collected and concentrated for further characterization. Figure 25a reports the GF chromatogram relative to the α-Syn/OleA (1:10) mixture after 168 h of aggregation. Two main fractions (7.4 ml; 9.4 ml) were detected. The species eluting at 7.4 ml and increasing over time (cfr. Figure 21b) was related to that eluting at 51.2 min in RP-HPLC, when an aliquot of the corresponding GF fraction was reloaded onto the RP-HPLC column (not shown). Its UV-vis spectrum (Figure 25a, inset, continuous line) showed a profile characterized by two main signals at 340 nm and 280 nm, indicative of the presence of both OleA and α-Syn. The fraction at 9.4 ml, eluted as monomeric α-Syn, also contained OleA, whose absorbance bands were detectable in the UV-vis spectrum (Figure 25a, inset, dashed line). The same mixture (α-Syn /OleA, 1:10 ratio; 168 h) was also analysed by RP-HPLC by recording the effluent at 340 nm (Figure 25b) to monitor OleA absorbance. The chromatogram relative to the analysis of the freshly prepared α-Syn /OleA mixture is also reported as a reference (dashed line). The chromatograms were characterized by two main peaks at RT 20.5 min and RT 51.2 min, respectively. These fractions were analysed by MS, confirming the presence of OleA in both and the absence of protein material in the peak at 20.5 min (not shown). The intensity of the peaks at 20.5 min and 51.2 min reciprocally changed during incubation. At the beginning, the signal relative to OleA was higher and decreased with time, probably due to the formation of the OleA-α-Syn complex eluting at 51.2 min. When imaged by negative stain TEM, the latter sample showed a morphology consistent with an oligomeric structure (Figure 25c, inset). These oligomers appeared as not fully homogenous spheroidal particles with an average diameter of 22.5 nm (12.5 nm the smaller species, 42.3 nm the larger ones). By DLS analysis, the average hydrodynamic diameter was of ~43 nm (Figure 25c).

The far-UV CD spectrum of the RT 51.2 sample is reported in Figure 25d. The shape of

the spectrum and the presence of two minima at ~203 and ~220 nm indicate that oligomer structure is not disordered, when compared to that resulting from the CD spectrum of monomeric α-Syn (Figure 21c). The spectra also showed that different conformers, partially folded and unfolded, did exist at equilibrium. Further characterization is required to better define the secondary structure content of these species.

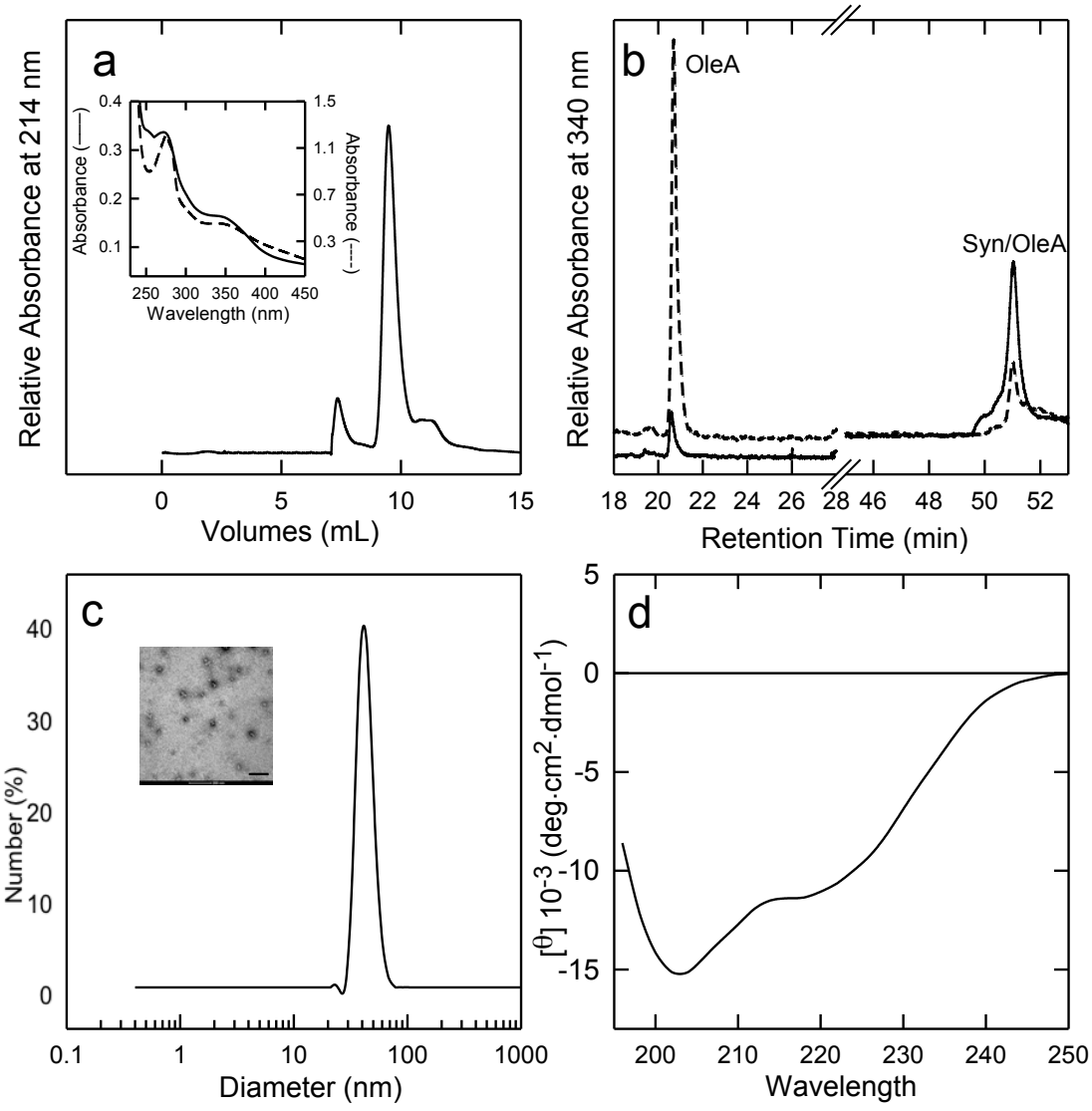

Figure 25 Characterization of α-Syn off-pathway oligomers (RT 51.2) grown in the presence of OleA. (a) Gel filtration chromatography of the α-Syn/OleA (1:10) mixture after 168 h of incubation Inset: UV-vis spectra of the fractions at 7.4 (−) mL (continued line) and 9.4 (−) mL (dashed line) of elution volume in GF. (b) RP-HPLC chromatogram at 340 nm of the α-Syn/ OleA (ratio 1:10) mixture at time 0 (dashed line) and 168 h (continuous line) of incubation. (c) DLS and TEM (inset) analysis of the purified oligomers. (d) Far-UV CD of the purified oligomers. The oligomers were

purified by RP-HPLC and concentrated until organic solvent and TFA removal, but never dried to avoid morphological changes. Other experimental details are reported in the methods section. The scale bar in the TEM image correspond to 200 nm.

Then, we mapped the overall structure of the oligomeric species at RT 51.2 min by finger printing analysis using trypsin after partial destabilization of the complex by Gnd-HCl (Figure 26). Indeed, these oligomers were quite resistant to proteolysis, probably because of some protection by OleA or by OleA-induced conformational modifications (cfr. Figure 23). By performing exhaustive fragmentation by trypsin (15 h), only a few peptide species were found in the proteolysis mixture of the RT 51.2 species (Figure 26a), when compared with same analysis carried out with monomeric α-Syn (Figure 26b). In particular, the large fragments corresponding to the sequences 59–140 and 46–102 remained undigested even after 15 h (Figure 26a) of incubation in the proteolysis mixture, suggesting that these species are rigid, structured or protected. To explain the presence of these peptide species, a pattern of fragmentation can be hypothesized and it is conceivable that RT 51.2 was cleaved, initially, at the level of the 45–46 peptide bond, thus generating the 1–45 and 46–140 fragments. The N-terminal species 1–45 was not visible, since it was further fragmented into smaller fragments. The C-terminal 46–140 was further cleaved at the level of the 102–103 peptide bond, producing the quite resistant 46–102 fragment and the 103–140 fragment, that was further degraded in smaller species. On the other hand, the 59–140 fragment was also seen in the chromatogram. This species could arise from the cleavage of the 58–59 peptide bond in the 46–140 fragment. Then, the 59–140 species underwent further fragmentation generating the 59–102 species. In conclusion, the 46–102, and in minor extent the 59–140, are the most resistant, upon prolonged trypsin treatment and after oligomer destabilization by Gnd-HCl.

A better structural characterization of the off-pathway oligomers (RT 51.2) was obtained by carrying out the mapping by PK with (Figure 26d,f) or without (Figure 26c,e) destabilization by Gnd-HCl. Indeed, the rationale of this approach was based on the general observation that, in the absence of the denaturant, the substrate of the protease is the most flexible species in equilibrium with a more structured one, not accessible by PK. Gnd-HCl addition destabilized the PK-resistant species, making it more susceptible to proteolysis. Moreover, in this case, the proteolysis reactions were

carried out for 5- and 70-min, to identify the first proteolytic events (Figure 26c,d) and those occurring subsequently on a perturbed substrate, in order to recognise the proteolysis resistant species accumulating in the mixture (Figure 26e,f). In the absence of Gnd-HCl, the RT 51.2 species was only partially fragmented by the protease, as indicated by the fact that its peak was still visible even after 70 min of reaction (Figure 26e) and that any peculiar fragment did not accumulate in the mixture.

However, following partial destabilization of the complex, this species was almost exhaustively digested upon incubation up to 70 min (Figure 26f). Moreover, in the presence of Gnd-HCl, after 5 min some species seemed to accumulate and two main cleavages did occur (Figure 26d). The two N-terminal fragments (1–56 and 1–72) were scarcely represented in comparison to the C-terminal ones (57–140 and 73–140) since the former were probably cleaved into smaller hydrophilic fragments. After longer incubation with the enzyme (Figure 26f, 70 min), further cleavages took place on the C-terminal species, which generated mainly the 57–89, 73–89 and 90–140 fragments, that remained undigested even after 70 min of incubation with PK (Figure 26f).

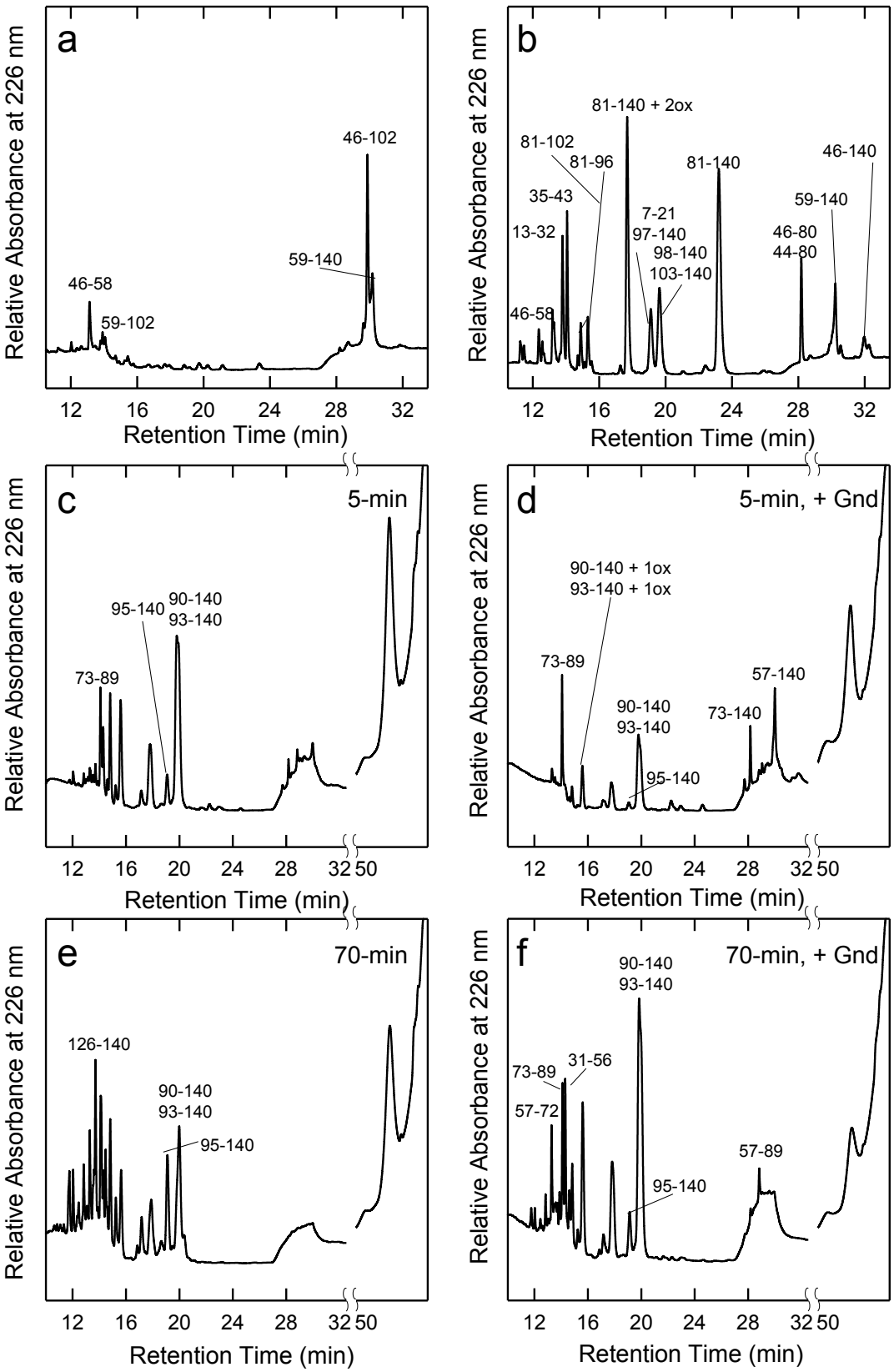

Figure 26 Mapping of (a) α-Syn off-pathway oligomers (RT 51.2) and (b) α-Syn monomers by trypsin proteolysis. The chromatograms refer to incubation with PK of the RT 51.2 sample for 5-min (c,d) or 70 min (e,f). In (d) and (f), the proteolysis was

carried out on samples partially destabilized in Gnd-HCl. The numbers close to the peaks indicate the identified fragments. The term ox refers to the presence of oxidation in the peptides.

These data confirm those obtained by trypsin and suggest the coexistence of two different population of off-pathway oligomers: one more susceptible to proteolysis, undergoing fragmentation in the absence of denaturant, and another, more resistant, that is cleaved only after denaturation. Moreover, from a comparison between the two proteoytic patterns, those encompassing residues 46–102, 57–89, 59–140 and 90–140 appear to be the more protected regions, belonging to the NAC and C-terminal regions of the α-Syn sequence.

α-Syn aggregates grown in the presence of OleA show reduced cytotoxicity

Once described at the molecular level the interference of OleA with α-Syn aggregation, we investigated whether OleA also affected aggregate cytotoxicity. A first experiment was designed to determine the cytotoxicity of α-Syn aggregates at different fibrillation times. To this purpose, we used human neuroblastoma, SH-SY5Y, cells exposed for 24 or 48 h to α-Syn solutions enriched of protein in different conformations: monomer, oligomers or fibrils, obtained by incubating the protein for 0, 48 or 168 h in aggregation conditions, respectively. Oligomers and fibrils were dose-dependently cytotoxic to cells exposed for 48 h, as shown by the MTT assay (Figure 27). Under these conditions, the solution enriched in α-Syn fibrils (Syn 168 h) was the most cytotoxic sample, followed by the solution enriched in oligomers (Syn 48 h); some cytotoxicity, not dose-dependent, was also seen in the case of the monomeric protein before aggregation started (Syn) (Figure 27).

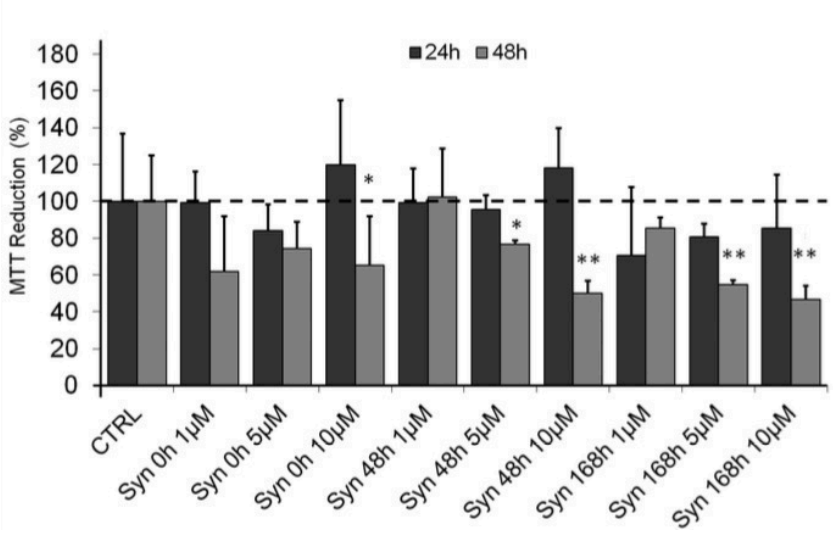

Figure 27 Cytotoxicity of α-Syn aggregates at different fibrillation time-points. SH-SY5Y cells were treated for 24 or 48 h with α-Syn as monomer, oligomer or fibril, obtained, respectively, after 0h, 24-48 h or 168 h of aggregation. Oligomers and fibrils showed a dose dependent cytotoxic effect after 48 h of cell incubation. Error bars indicate the standard deviation of independent experiments carried out in triplicate.

Based on these data, we decided to expose the cells for 48 h to the three different α-Syn solutions (5.0 µM) enriched in monomers, oligomers or fibrils, in the absence or in the presence of 1:10 α-Syn/OleA. The MTT assay showed a significant decrease of toxicity when the cells were treated with samples aggregated for 48 or 168 h in the presence of OleA (Syn 48 h/OleA, Syn 168 h/OleA) (Figure 28a). Cell survival after exposure to the Syn 48 h/OleA was around 100% ± 10.6 while cell survival was around 80% ± 3.1 in the presence of the Syn 168 h/OleA indicating that OleA was only partially effective in protecting cells against fibril cytotoxicity. Furthermore, the evaluation, by MTT assay, of the toxic power of the species eluted in RP-HPLC at RT 51.2 min showed that this sample was completely harmless even when tested purified at the final concentration of 5.0 µM (Figure 28a).

In consideration of the key role performed by oxidative stress in the pathogenesis of PD, we also sought to assess the redox status of the variously treated cells by using the ROS-sensitive fluorescent probe CM-H2 DCFDA. We found that the different α-Syn aggregates stimulated some ROS production in SH-SY5Y cells that was particularly evident when the cells were exposed for 48 h to α-Syn fibrils (Syn 168 h) (Figure 28b). However, cell exposure to the different aggregates of α-Syn grown in the presence of 1:10 α-Syn/OleA did not result in any statistically significant increase of ROS levels

(Figure 28b). These data led us to conclude that the presence of OleA during α-Syn aggregation decreases the ability of the resulting aggregates to raise ROS production thus making non-toxic the oligomers whereas the toxicity of the fibrillar sample was not completely abolished. OleA effect on preformed α-Syn oligomers and fibrils.

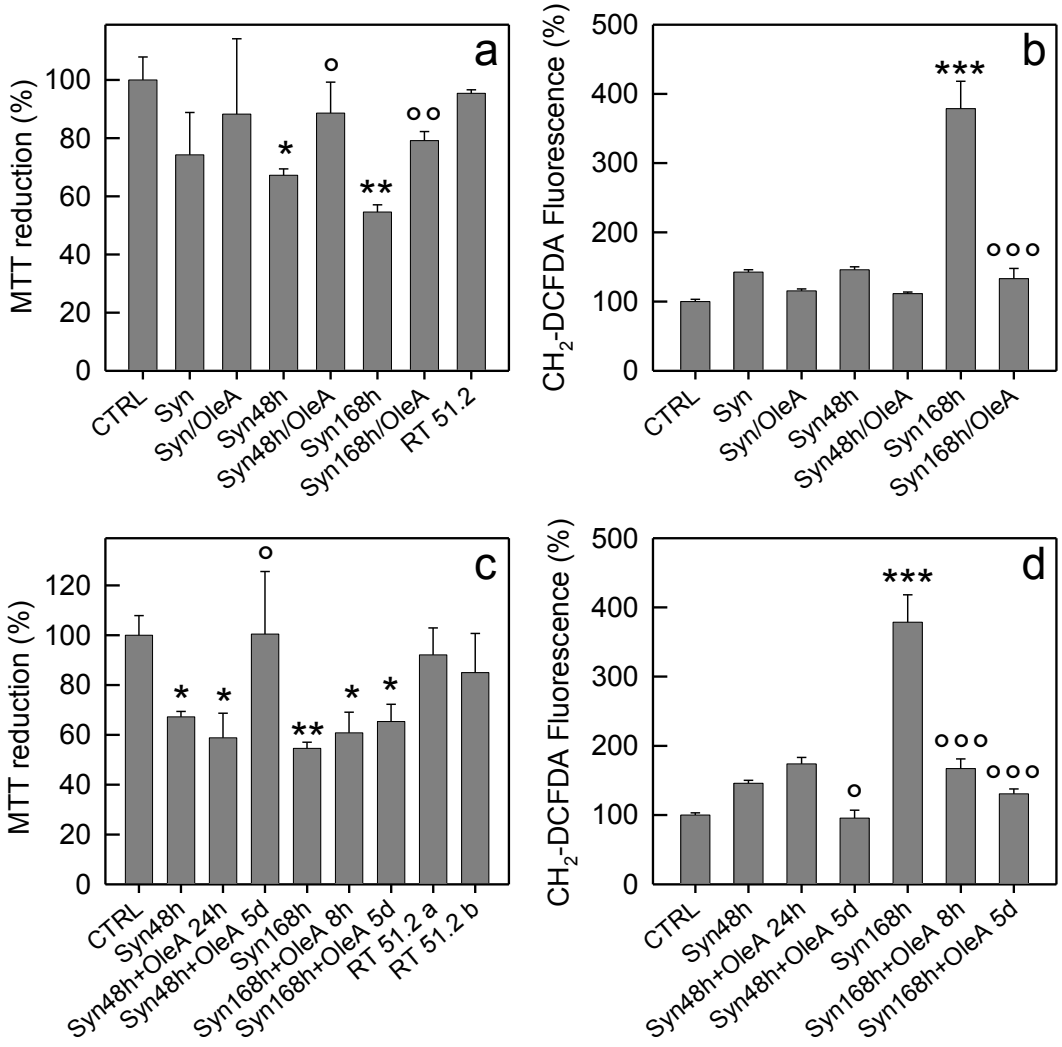

Figure 28 Cell viability and ROS levels. (a,b) SH-SY5Y cells treated for 48 h with a 5.0 μM α-Syn solution obtained at different times of aggregation (0, 48 and 168 h) enriched in monomeric (Syn), oligomeric (Syn 48 h) or fibrillar (Syn 168 h) species, respectively. Each sample was obtained in the absence or in the presence of OleA (Syn:OleA, 1:10). (a) Cell viability assessed by the MTT reduction assay and (b) by ROS production. For the MTT assay, the RT 51.2 species purified by RP-HPLC was also tested. (c,d) OleA modulates the toxicity of preformed α-Syn assemblies. (c) MTT assay and (d) ROS endogenous levels in SH-SY5Y cells exposed for 48 h to 5.0 μM Syn enriched in oligomers (Syn 48 h) or fibrils (Syn 168 h). The oligomeric samples were also analysed

following addition of OleA after further incubation of 24 h or 5 d (Syn 48 h + OleA 24 h) and (Syn 48 h + OleA 5d). The fibrillar species were analysed after 8 h or 5 d of incubation in the presence of OleA (Syn 168 h + OleA 8 h) and (Syn 168 h + OleA 5d). The RT 51.2 samples purified by RP-HPLC from the mixture corresponding to (Syn 48 h + OleA 24 h) sample (RT 51.2a) and from that corresponding to (Syn 168 h + OleA 8 h) sample (RT 51.2b) were also tested by the MTT assay. Error bars indicate the standard deviation of independent experiments carried out in triplicate.

Once established that OleA interferes with α-Syn aggregation yielding substantially non-toxic aggregates, we analysed the effect of OleA on preformed α-Syn oligomers and fibrils to assess whether it favoured fibrils disassembly with leakage of toxic oligomers. OleA (1:10 ratio) was added to preformed solutions enriched in oligomeric species (48 h) or fibrils (168 h). The disaggregation activity by OleA was followed by fluorescence spectroscopy, limited proteolysis and MTT assay. The ThT spectra (Figure 29a) were obtained from α-Syn oligomers (48 h) after further 24 h of incubation in the presence (48 h + OleA 24 h) or in the absence (72 h) of OleA in comparison with α-Syn oligomers (the starting point) (48 h). As expected, in the absence of OleA, the aggregation process proceeded towards fibrils formation with substantial increase of ThT intensity (as indicated by the arrow). The 48 h + OleA 24 h sample showed a decrease of ThT fluorescence, indicative of a stop or a slowdown of the formation of α-Syn aggregates. The same experimental scheme was followed with α-Syn fibrils samples (168 h). In this case, ThT fluorescence spectra were recorded after further 8 h of incubation with (168 h + OleA 8 h) or without OleA (176 h). We did not find any remarkable reduction of ThT fluorescence in the (168 h + OleA 8 h) sample, which indicated a negligible effect of OleA on preformed fibrils.

The same samples were also subjected to limited proteolysis (Figure 29c–h). As expected, the sample aged for 72 h in the absence of OleA (Figure 29d) showed a slightly increased resistance to proteolysis in comparison to the sample aged for 48 h (Figure 29c) and small fragments eluting at short RT appeared in the chromatogram. In the proteolytic pattern obtained from samples treated with OleA for 24 h (48 h + OleA 24 h), the low intensity of the peak relative to intact α-Syn (RT 35.5 min) suggested that the monomeric α-Syn still present in the mixture was fragmented and resulted, under these conditions, more susceptible to proteolysis (Figure 29e). In the meantime, the species at RT 51.2 min, previously found to increase as far as the aggregation time was

prolonged, appeared in the chromatogram. In synthesis, monomeric α-Syn underwent formation of a species more susceptible to proteolysis (the peak of intact α-Syn was decreased) and a protease-resistant one (RT 51.2).

The proteolytic patterns relative to the aggregation mixture at 168 h and 176 h, in the absence of OleA, are quite similar since no critical events occurred in this time (Figure 29f,g).

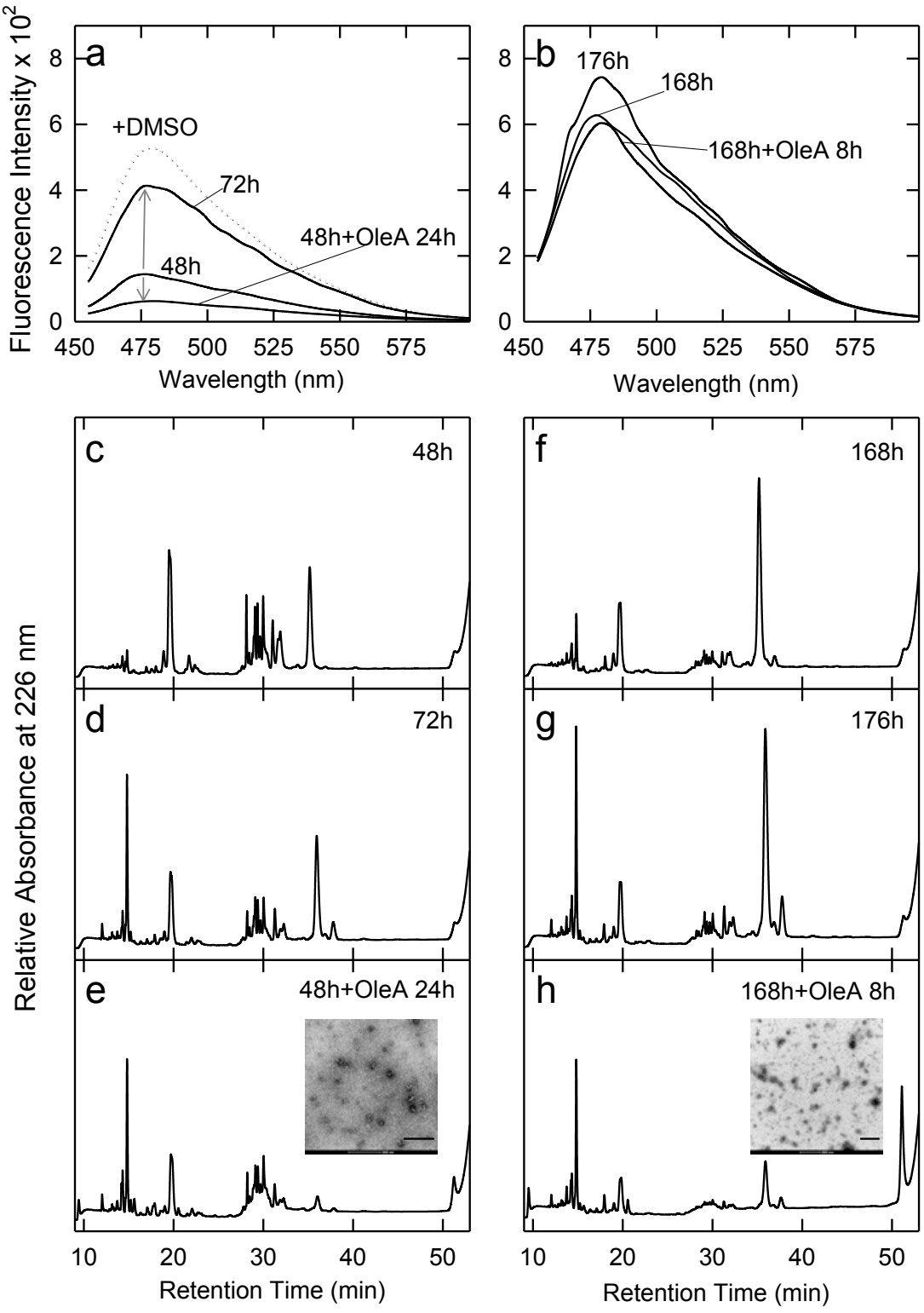

Figure 29 OleA-induced α-Syn disaggregation probed by (a,b) ThT fluorescence and (c–h) limited proteolysis. During aggregation, aliquots were collected from the mixture at 48 h and 168 h, then OleA was added to a 1:10 final Syn:OleA ratio. ThT spectra in (a) refer to α-Syn samples corresponding to 48 h of aggregation (48 h) and to further 24 h of incubation in the absence (72 h) or in the presence (48 h + OleA 24 h) of OleA. The

ThT spectra in (b) were recorded at 168 h and after additional 8 h of incubation without (176 h) or with (168 h + OleA 8 h) OleA. (c-h) RP-HPLC analysis of the proteolysis mixture of α-Syn samples during aggregation (c) at 48 h, (d) after further 24 h of incubation in buffer without polyphenol (72 h), (e) in the presence of OleA. The same scheme was followed for α-Syn samples collected from the aggregation mixture at 168 h of incubation (f), after further 8 h of incubation in the absence (g) or in the presence (h) of OleA. (e,h, inset), TEM images taken from samples corresponding to the peaks eluting at RT 51.2 min; scale bar: 200 nm.

However, upon addition of OleA (Figure 29h), the proteolytic pattern was completely different and the RT 51.2 species arose in higher percentage (Figure 30).

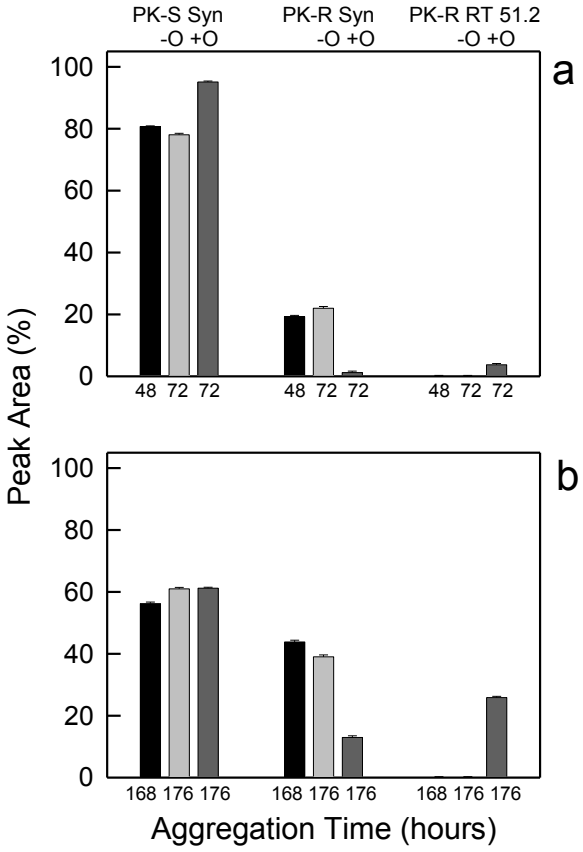

Figure 30 Quantification of the different population of aggregated α-Syn arising during disaggregation following addition of OleA, calculated by the limited proteolysis experiments shown in Fig. c-h. The amount of each population was evaluated from the area of the chromatographic peaks relative to the purification of the mixtures of α-Syn arising from PK proteolysis during disaggregation. (a) Peak areas obtained from the

purification of the proteolytic oligomeric-enriched mixture (48h), and the same mixture after further 24h incubation in the presence (+O) or in the absence (-O) of OleA. (b) Proteolysis of the fibril-enriched mixture (168h) and the same mixture after further 8h-incubation in the presence (+O) or in the absence (-O) of OleA. PK-S α-Syn represents α-Syn fragments; PK-R α-Syn represents undigested α-Syn and PK-R RT 51.2 represents undigested late-eluting aggregates.

Also in this case, the proteolysis data can be explained with the co-existence, in the mixture, of species characterized by different susceptibility to proteolysis. The species eluting at RT 51.2 min, an aggregated and highly hydrophobic one induced by the presence of OleA either during aggregation or at the end of the latter, was accumulating in the mixture and represented a PK- resistant fraction.

We also investigated whether OleA modified the toxicity of α-Syn preformed oligomers and fibrils. To this aim, we compared the (Syn 48 h + OleA 24 h) and (Syn 168 h + OleA 8 h) cytotoxicity to SH-SY5Y cells with that displayed by the same samples without the polyphenol by using the MTT and ROS assay. In addition, α-Syn oligomers and fibrils were incubated in the presence of OleA for an extra time (5 days), to assess whether OleA had some effects under extreme experimental conditions. Figure 28 c,d show that the (Syn 48 h + OleA 24 h) sample maintained its potential toxicity; however, a prolonged OleA treatment (Syn 48 h + OleA 5d) made it harmless to cells (Figure 28c) that also displayed reduced endogenous ROS levels (Figure 28d). As far as the effect of OleA on preformed fibrils is concerned, we observed a very slight decrease of fibril cytotoxicity in both samples (Syn 168 h + OleA 8 h) and (Syn 168 h + OleA 5d) (Figure 28c). In spite of an evident cell sufferance, the fibrils treated with OleA for short and long incubation times, induced a significant decrease in ROS intracellular levels (Figure 28d). We also evaluated the toxicity of the RT 51.2 samples after its purification by RP-HPLC from the mixture corresponding to the Syn 48 h + OleA 24 h sample (RT 51.2a) and from that corresponding to the Syn 168 h + OleA 8 h sample (RT 51.2b). The MTT assay confirmed that this sample was completely innocuous to SH-SY5Y cells (Figure 28c).

OleA interferes with the interaction of α-Syn aggregates with the cell membrane

Finally, we investigated whether OleA interfered with the ability of α-Syn aggregates to interact with the cell membrane. In fact, recent data have widely reported that amyloid aggregates are able to bind to lipid bilayers and that aggregate interaction with the cell membranes is a crucial step of amyloid cytotoxicity (Canale et al., 2018) (Walsh et al., 2014). In particular, it has been reported that exogenous oligomers and fibrils bind to the cell membrane and accumulate in lipid rafts, liquid ordered membrane microdomains rich in functional proteins (receptors, carriers, signalling molecules), sphingosine, cholesterol and ganglioside GM1 (Wakabayashi & Matsuzaki, 2009) (Leri et al., 2016). In this context, α-Syn oligomers have been reported to display membrane disrupting power on anionic lipid bilayers and to alter the permeability and the integrity of the cell membrane (van Maarschalkerweerd et al., 2014).

To assess whether α-Syn amyloid species grown in the presence of OleA modified their propensity to interact with the cell membrane, we performed a sensitized FRET analysis between Alexa-488 GM1 fluorescence and Alexa-546 immunofluorescence on α-Syn aggregates. We found that both α-Syn oligomers and fibrils interacted with the cell membrane at the lipid raft level, as shown by the aggregate-GM1 colocalization (Figure 31a,c) and by FRET efficiency (Figure 31b,d). Such interaction was drastically reduced when the cells were treated with α-Syn aggregates grown in the presence of OleA (Figure 31e,f,g,h). Then, SH-SY5Y cells were treated for 48 h with preformed α-Syn assemblies exposed for short (Syn 48h+OleA 24h, Syn 168h+OleA 8h) or long (Syn 48h+OleA 5d, Syn 168 h + OleA 5d) time to OleA before supplementation to the cell medium. Confocal images and FRET analysis revealed that short treatment of the aggregates with the polyphenol did not alter significantly the ability of the Syn 48 h and Syn 168 h samples to interact with the membrane at the level of the GM1 component of lipid raft domains (Figure 31 i,l,m,n), whereas a prolonged exposure reduced significantly oligomers, but not fibrils, interaction with the cells (Figure 31 o,p,q,r), in agreement with the results of the toxicity experiments reported in the preceding section.

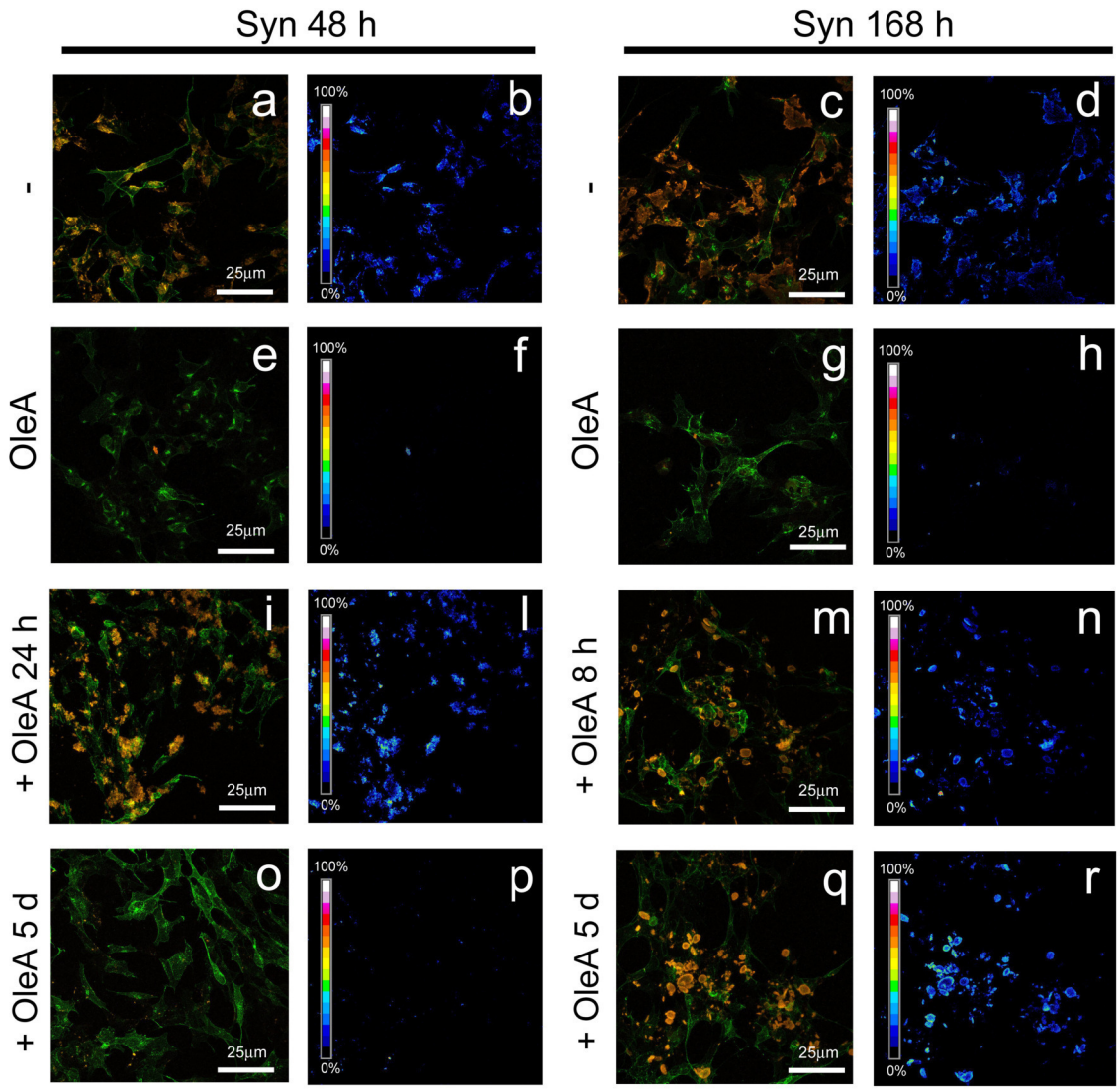

Figure 31 The complex OleA-α-Syn does not bind to the plasma membrane. (a,e and c,g) Z-projection of α-Syn samples grown in the presence (Syn 48/OleA, Syn 168/OleA) or in the absence of OleA (Syn 48 h, Syn 168 h) by immunostaining (red) and GM1 staining (green) on SHSY5Y cell membrane. (b,f and d,h) FRET analysis between GM1 staining and aggregate immunostaining. OleA affects preformed α-Syn assemblies and their membrane interaction. (i,o, and m,q) Z-projection of preformed α-Syn assemblies (oligomers and fibrils) treated with OleA for two different times (Syn 48h+OleA 24h and Syn 48h+OleA 5d) and (Syn 168h+OleA 8h and Syn 168 h + OleA 5d) by immunostaining (red) and GM1 staining (green) on SH-SY5Y cell membrane. (l,p, and n,r) FRET analysis between GM1 staining and aggregate immunostaining.

D76N β2M sonicated oligomers induce citoxicity and ROS production

We investigated whether the D76N β2M oligomers were toxic and, if so, whether toxicity was associated to membrane binding and/or aggregate internalization. The cytotoxicity in our cell model was studied using human SH-SY5Y neuroblastoma cells previously shown to be sensitive to the toxicity of 20 μM β2M aggregates (Leri et al., 2016).

To this aim, human SH-SY5Y cells were exposed for different times to 5 μM D76N β2M sonicated (β2 24hS) and not sonicated oligomers (β2 24h) grown for 24h under our aggregation conditions; then, aggregate cytotoxicity was evaluated by the MTT assay. Significant toxicity values started to appear at very early time in cells exposed to sonicated oligomers (β2 24hS) and decrease in cells exposed to samples for long time. If at the beginning the cells appear to be suffering, over time a recovery perhaps due to a cell response such as the autophagic process was observed. The non-sonicated oligomers MTT assay, instead, show how this species is not toxic for cells or has a significant toxicity only in the long term treatment (Figure 32 a,b).

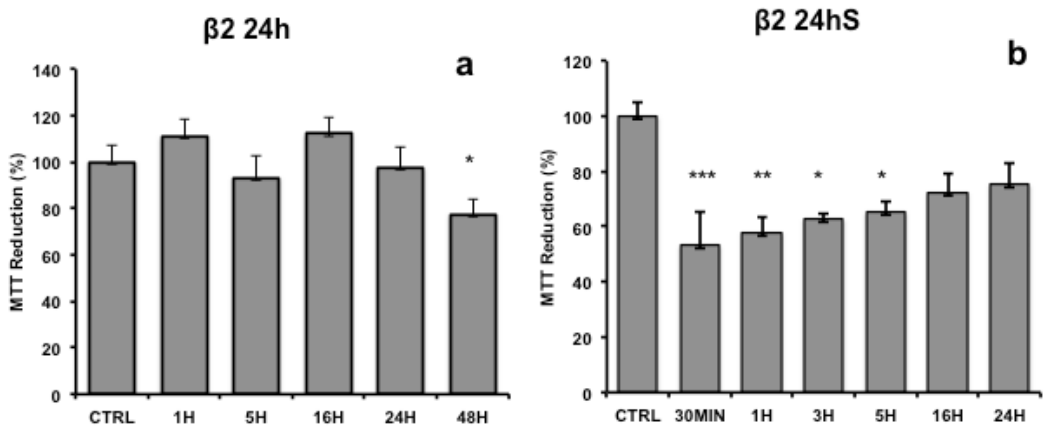

Figure 32 Cytotoxicity differences between D76N β2M sonicated (β2 24hS) and not sonicated oligomers (β2 24h). (a) Only after a very long time of treatment, 48h, D76N β2M not sonicated oligomers (β2 24h) show about 20% of cytotoxicity. (b) MTT assay on SH-SY5Y cells exposed for different time intervals (30', 1h, 3h, 5h, 16h and 24h) to β2 24hS showed how aggregates induced cellular toxicity is higher when cells are treated for short periods of time. Error bars indicate the standard deviation of independent experiments carried out in triplicate.

Next, we measured the amount of ROS levels in SH-SY5Y cells treated with D76N

β2M oligomers for different time periods. Figure 33 shows that ROS levels increased significantly from 24 to 48h of treatment in cells exposed to not sonicated D76N β2M oligomers (β2 24h) while in the samples treated with sonicated D76N β2M oligomers (β2 24hS) ROS level increased both at early and at longer times in agreement with the MTT results.

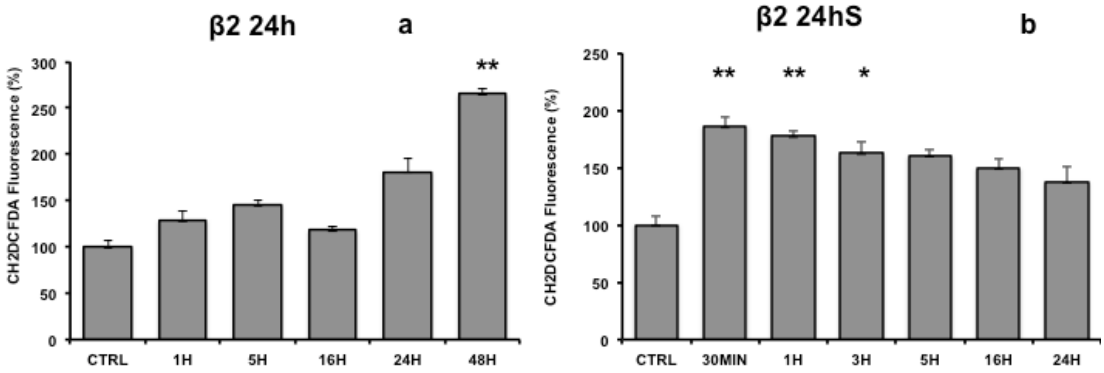

Figure 33 ROS production. (a) ROS production in SH-SY5Y cells exposed for different time to 5.0 μM of D76N β2M not sonicated oligomers (β2 24h). (b) treatments with D76N b2M sonicated (β2 24hS) for long times lead to an increase in employee time. Error bars indicate the standard deviation of independent experiments carried out in triplicate.

Different morphology of β2 and sonicated β2 oligomers

The morphological differences between the sonicated (β2 24hS) and non-sonicated (β2 24h) D76N β2M oligomers, well observable at the TEM, could be responsible for the greater ability to induce cytotoxicity and ROS production.

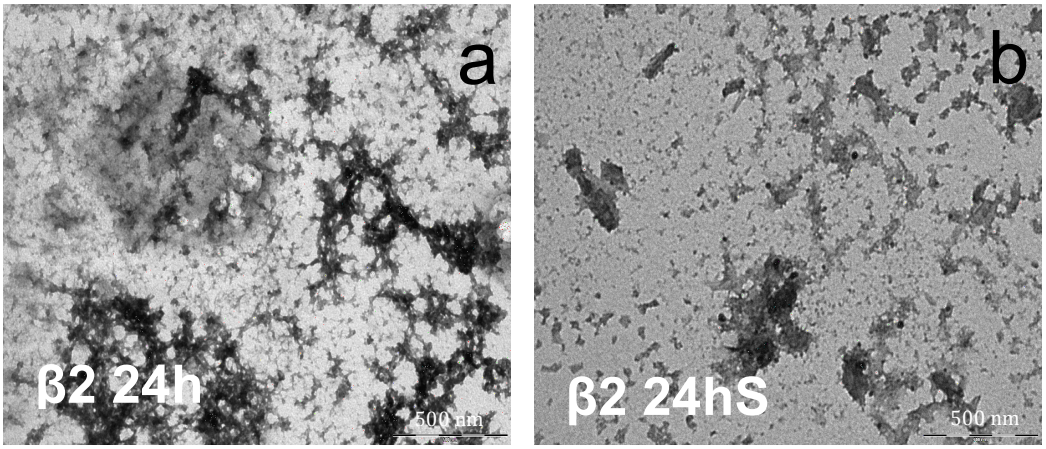

Figure 34 TEM images show the morphological differences between β2M 24h and β2M 24hS aggregates. (a) TEM images of samples containing D76N β2M after 24h of aggregation time (β2 24h). The protein forms fibrils densely packed and embedded in a diffuse background of small rod-like aggregates. (b) TEM images of samples containing D76N β2M aggregated for 24h and then sonicated (β2 24hS). The protein results fragmented into very small fibrillar structures.

Autophagy activation induced by sonicated oligomers of D76N β2M

To investigate whether D76N β2M was involved in the autophagic signalling pathway activation, the cells were incubated with the different species (the native form - β2 pH7, the oligomeric species - β2 24h and β2 24hS, and finally the fibrils conformation - β2 144h) of aggregate for 5h. Then autophagy induction was evaluated by Cyto-ID® Autophagy Detection Kit (Enzo Life Sciences). At these conditions, the cells displayed a significant increase in autophagic vacuoles staining (Figure 35), in the sample treated with sonicated oligomers (β2 24hS) suggesting that autophagy activation results from sonicated oligomers after 5h of treatment. This analysis seems to confirm the hypothesis that sonicated oligomers of D76N β2M are able to trigger an answer to the stress that bring the cell back to a state of equilibrium.

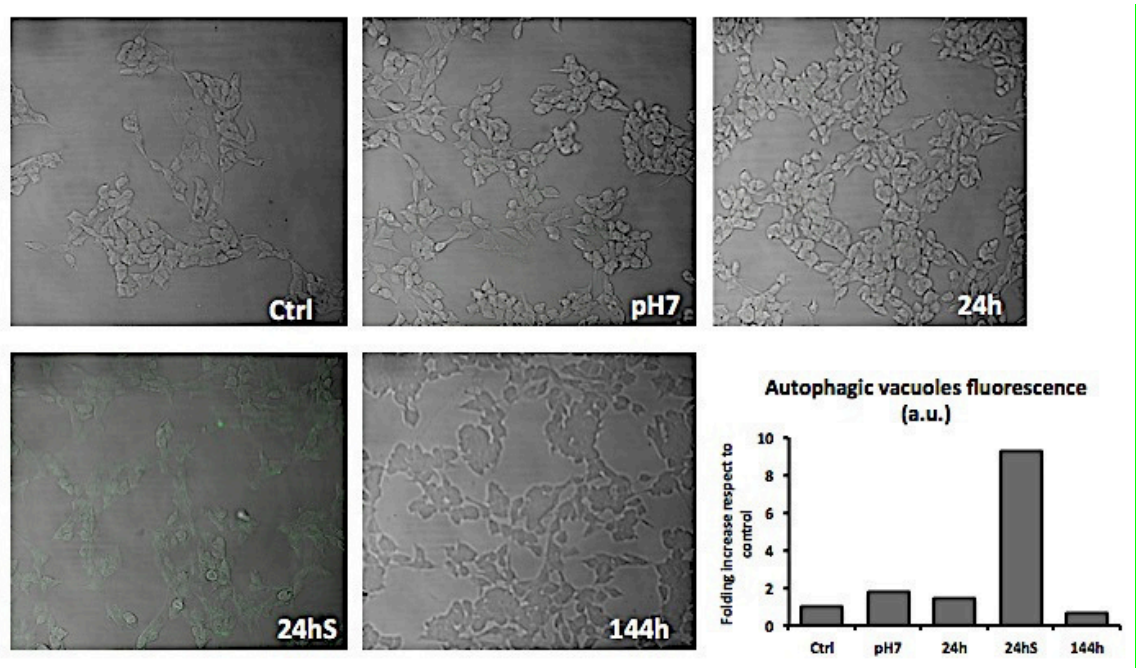

Figure 35 Autophagic vacuoles fluorescence analysis. The green fluorescence observed only in the sample of cells treated with β2 24hS oligomers indicates that at 5h treatment the cells respond to the cytotoxic stress induced by the oligomers, by autophagy activation. The lower bar graph shows the quantification of the Cyto-ID® fluorescence observed at the confocal microscope and indicates that autophagy is activated in the presence of sonicated oligomers (β2 24hS).

Further evidence of how the D76N β2M protein was involved in the process of autophagy and in particular the sonicated oligomeric form (β2 24hS) was the western blot analysis, the result of which showed the LC3 protein, in particular the conjugated form (LC3II) which is the most widely used marker of autophagosomes, increases in SH-SY5Y cells treated for 5h with sonicated oligomers of D76N β2M (β2 24hS) as shown in the figure 36a. To confirm the chosen timing of the 5 hours used for the experiments just described, figure 36b shows how even in cells treated only with D76N β2M sonicated oligomers (β2 24hS) for different times, the 5h are the timing at which LC3II increases more.

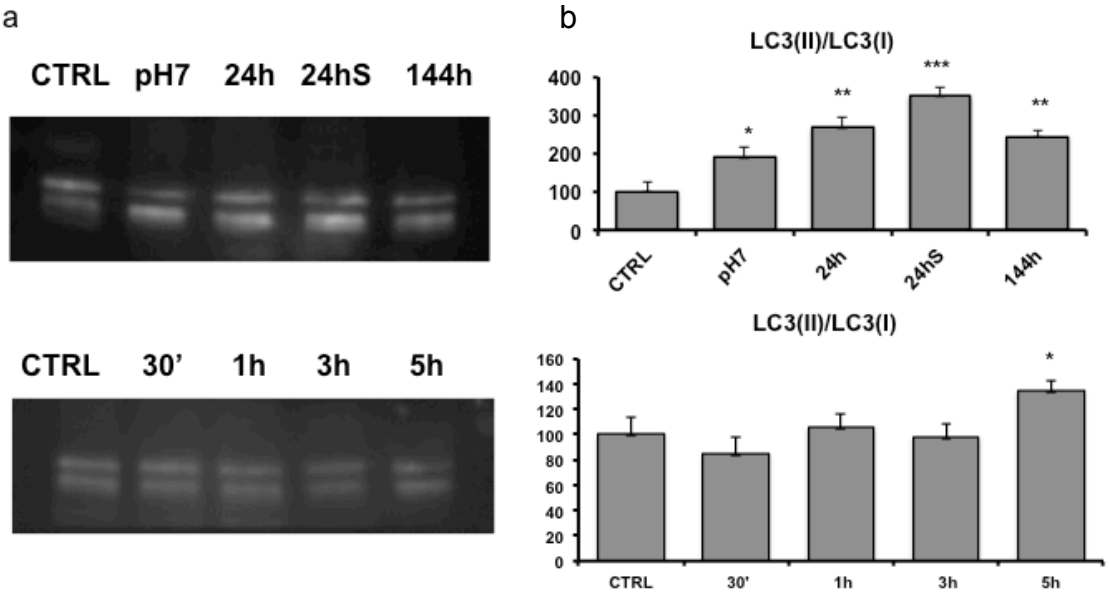

Figure 36 Sonicated oligomers of D76N β2M (β2 24hS) induce an increase in LC3II protein expression in SH-SY5Y cells. (a) Representative Western blots bands of LC3 protein. (b) Quantification of signals from a densitometry analysis of at least three independent experiments. Error bars indicate the standard deviation of independent experiments carried out in triplicate.

Description of the autophagy signaling pathway induced by D76N β2M sonicated oligomers

On the basis of these data, we explored the pathway involved of AKT, ERK and GSK-3β which indicate an inhibition of the complex mTOR to confirm the previous results. The involvement of the proteins just mentioned, in the autophagy pathway, is clearly shown in the figure 37.

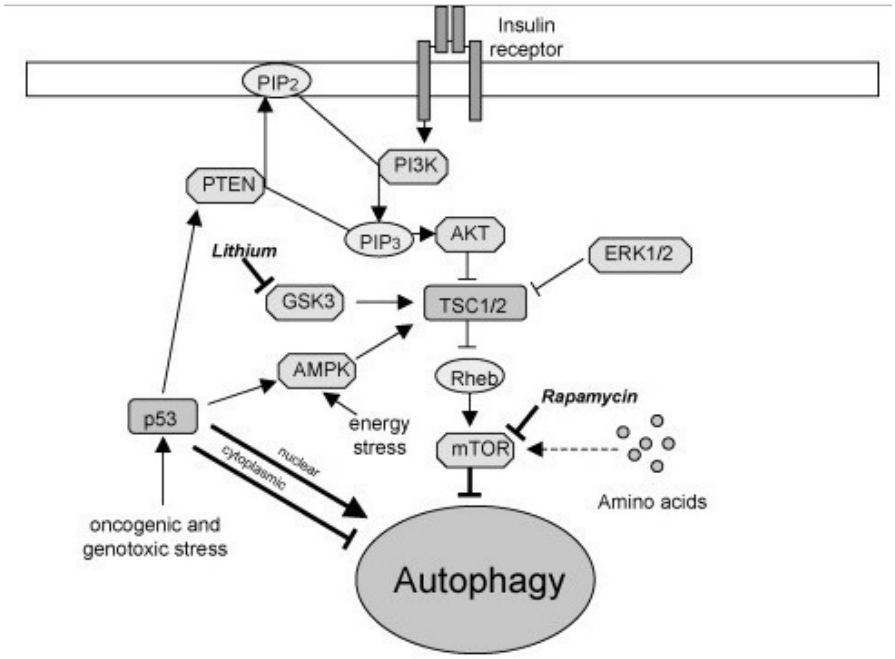

Figure 37. Schematic diagram of possible autophagy signalling pathways showing the targets evaluated by Western Blot analysis.

The Western Blot analysis reveals that the protein expression of phospho-AKT (P-AKT) and phospho-ERK (P-ERK) which result in an activation of their kinase activity decrease after 3 and 5h in SH-SY5Y cells treated with sonicated oligomers of D76N β2M (β2 24hS) (Figure 38), this result indicates an inhibition of the mTOR complex in the signalling of autophagy.

The reduction of the phosphorylated form of AKT and ERK causes the TSC1/2 complex to not activate the Rheb protein which is responsible for the activation of the mTOR complex. It follows, as anticipated, the activation of the autophagy process. Regarding GSK-3β protein, this one can be phosphorylated at serine 21 in GSK-3β or serine 9 in GSK-3β, resulting in inhibition of GSK-3β kinase activity (Fang et al., 2000).

For our analysis of Western Blot we used an antibody against GSK-3β phosphorylated form in serin 9. The values of the latter in the samples treated with D76N β2M sonicated oligomers (β2 24hS) decrease after 5h indicating a hyper-activation which determines the increase of the activity of the TSC1/2 complex which inhibits the Rheb protein. This inhibition causes the mTOR complex to not activate and the autophagic process can begin (Figure 38).

Based on the results just described we decided to investigate a marker that was after of the mTOR complex and we discovered a decrease in the values of phosphorylated form of S6 a substrate of the complex mTOR which has the task of inhibiting the autophagic process (Figure 38) in particular after 5h of treatment with D76N β2M 24hS in agreement with the Cyto-ID® Autophagy analysis.

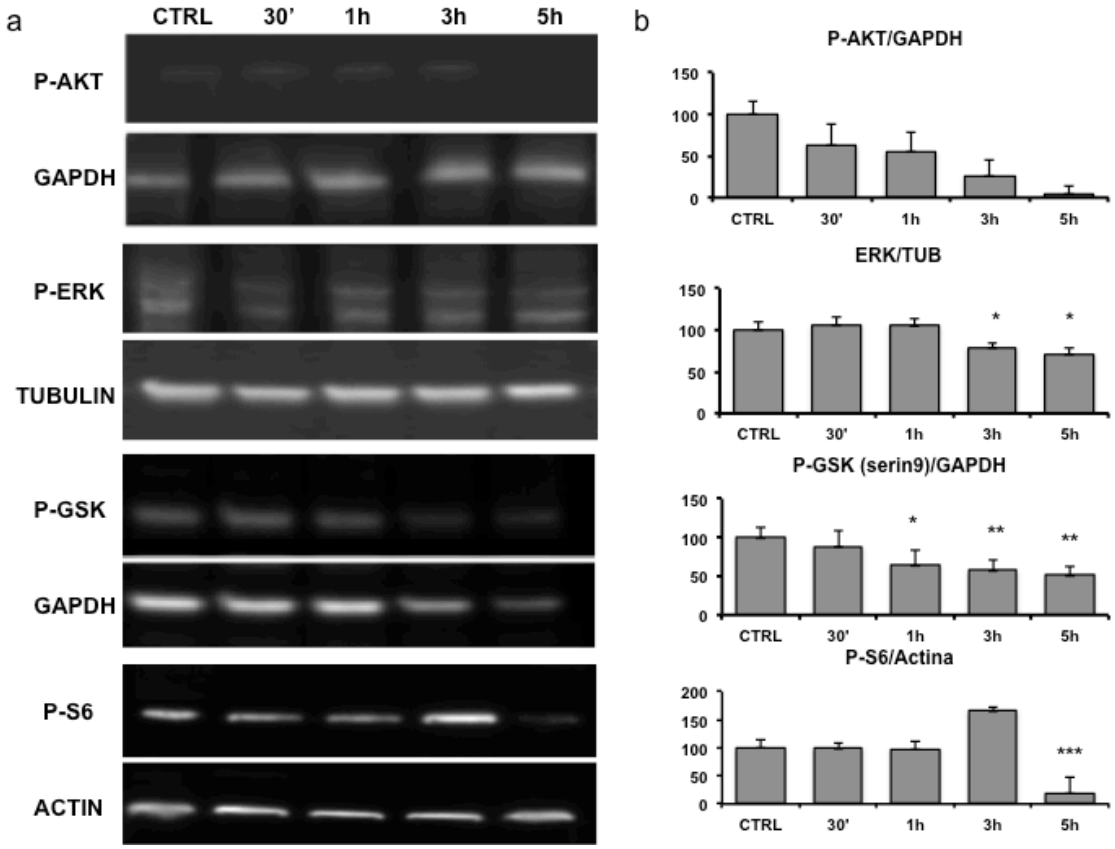

Figure 38 Western blotting analysis of the status of autophagy markers in SH-SY5Y cells after D76N β2M 24hS treatment for different times (30', 1h, 3h, 5h) (a) Representative Western blots bands of AKT, ERK, GSK and S6 phosphorilation form. (b) Quantification of signals from a densitometry analysis of at least three independent experiments. Error bars indicate the standard deviation of independent experiments.

These data further support the idea that autophagy is activated by the treatment with D76N β2M 24hS.

The interaction of the D76N β2M sonicated oligomers with the cell membrane favors the aggregation of the former

Despite of the identification of the above described signalling pathway it remains to be discovered from where this signaling cascade starts.

We have already known that the mechanism of amyloid aggregate cytotoxicity requires the primary interaction between the aggregates and the cell membrane. For this reason we evaluated the aggregate-membrane interaction, precisely the interaction between the protein and GM1, the monosialoganglioside which is a major raft marker.

To further elucidate whether our D76N β2M 24hS aggregates interacted with the cell membrane at GM1-rich sites, we carried out confocal fluorescence microscopy experiments as described in Materials and Methods (Figure 39). When the cells were exposed to the D76N β2M 24hS oligomers, we detect that at short times, of about 30 min and 1h (Figure 39), the red of the protein appears widespread on the cell, at 3 and 5 h (Figure 39) of treatment we can observe red agglomerates over the cells.

These data confirm that D76N β2M 24hS aggregates bind at the cell surface. They also suggest that the interaction involves GM1 and occurs preferentially at its negatively charged moiety, highlighting the importance of electrostatic binding. Finally, the confocal images show how the membrane has as an aggregating effect on sonicated oligomers that increase their size over time. In fact, recent data indicate GM1 can also mediate the interaction of amyloid assemblies with the plasma membrane, notably by means of its negatively charged sialic acid component (Sartiani et al., 2016).

Based on these data, to make sure that the diffused red was really protein we performed a TEM morphological analysis (Figure 34) which showed how the D76N β2M 24hS oligomers are very small, especially compared to the non-sonicated species D76N β2M 24h.

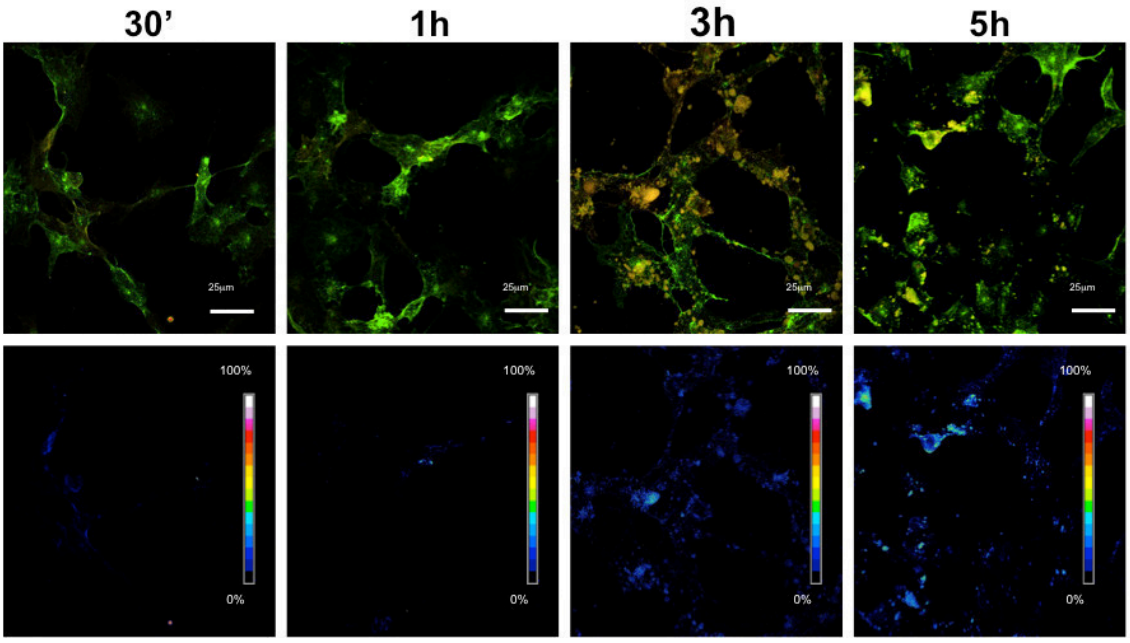

Figure 39 D76N β2M sonicated oligomers induced FRET (a) Immunolocalization of D76N β2M aggregates onto the plasma membrane. SH-SY5Y cells exposed for different times (30', 1h, 3h, 5h) to 5.0 µM D76N β2M 24hS oligomers. The cells were stained with Alexa 488-conjugated CTX-B (green fluorescence); protein aggregates were stained with anti-β2M antibodies followed by treatment with Alexa 568-conjugated anti-rabbit secondary antibodies (red fluorescence). In short time the protein signal is weak and homogeneously spread on the cells. With the passage of time the aggregates seem to become more evident, and more specifically located on the cell membrane. (b) FRET efficiency is shown in SH-SY5Y cells treated with D76N β2M 24hS oligomers after 3 and 5h. We can observe an increase in the FRET signal over time.

Discussion

Current therapeutic interventions for neurodegeneration include three different strategies. First, preventing the toxic protein aggregate build-up. Second, dissolving the already culminated toxic protein aggregates inside the neurons. Various groups identified small molecules and peptides that can bring about disintegration of the aggregate. This has been a widely used strategy for many years as a promising anti-neurodegeneration therapeutic. For example, for AD, few small molecule candidates that dissolve the amyloid plaques are currently in the clinical trials in USA and Europe. The third and recent approach is to promote cellular pathways to capture and degrade the protein aggregates by either ubiquitin proteasome (UPS) or autophagy systems (Suresh et al., 2018).

Our study on the interference of the OleA on the α-Syn aggregation process falls into the first type of possible therapy for neurodegenerative diseases. We show that OleA interferes with α-Syn fibrillation in a dose-dependent manner, with the optimal 1:10 α-Syn/OleA ratio; the inhibition is due, apparently, to OleA interaction with α-Syn monomeric and oligomeric species, an effect similar to that reported for other polyphenols (Hong et al., 2008) (Lorenzen et al., 2014). We also report that OleA reduces the toxicity of α-Syn amyloid aggregates, favouring the growth of harmless off-pathway oligomers. In fact, α-Syn aggregates grown in the absence or in the presence of OleA, displayed a very different ability to interact with the plasma membrane and to induce sufferance and oxidative stress in exposed cells. Moreover, the ability of α-Syn to self-propagate and spread progressively between interconnected brain regions via a cell-to-cell transmission in PD model and patients has been recently reported and is increasingly accepted as a central mechanism in the development of the disease (Sano et al., 2018) (Danzer et al., 2009). In view of this notion, several new therapeutic strategies to combat PD are aimed at inhibiting not only α-Syn misfolding and aggregation, but also the prion-like interneuronal transport of aggregation seeds (Lashuel et al., 2013). In this context, our findings showing a decreased interaction of the OleA/α-Syn complex with GM1-enriched sites at the cell membrane and the OleA interaction with preformed α-Syn aggregates (notably oligomers and prefibrillar assemblies), converting them into stable and inert species are of interest. Overall, these data suggest that the polyphenol, besides interfering with the aggregation path, also hinders the association of α-Syn and/or its aggregates with the cell membrane, presumably, by generating new species with different surface properties. Our findings are of importance in the evaluation of the

potential use of OleA in PD treatment, suggesting that OleA could be beneficial not only by interfering with toxic aggregation of α-Syn and by favouring aggregate disassembly in non-toxic species, but also by hampering their self-propagation.

To better elucidate the mechanism of OleA effects at the molecular level, we investigated the modifications of the structure and cytotoxicity of α-Syn in different aggregated states arising in the presence of OleA. α-Syn-OleA interaction was probed by several biophysical and biochemical techniques. We found that OleA does not modify the secondary structure of monomeric α-Syn and its chromatographic behaviour (retention time in RP and elution volume in GF). On the other hand, the immediate appearance, in the protein/OleA mixture, of a late eluting species in RP (51.2 min), yet earlier than monomeric α-Syn in GF, clearly indicates that the polyphenol exerts an instantaneous effect on α-Syn, inducing the formation of a new species (see Figures 25 and 26, for its characterization). The abundance of this species appeared to be dependent on incubation time and OleA concentration, however it did not evolve into fibrils; overall, the structural features of this species allow to classify it as a population of off-pathway oligomers (Breydo & Uversky, 2015) (Bemporad & Chiti, 2012).
Interestingly, when OleA was added to the aggregation mixture during the elongation phase, the growing aggregates (oligomers and protofibrils) were apparently solubilised into species recalling the off-pathway oligomers formed when OleA was present since the beginning of aggregation. The harmless off-pathway oligomers appeared characterized by a heterogeneous morphology, even though mainly spheroidal. Their secondary structure was substantially random, yet in the presence of a minor content of beta-sheet. Of note, the proteolysis mapping experiments on off-pathway oligomers showed that the NAC and C-terminal regions of α-Syn are most persistent in solution and suggested a high affinity of OleA for specific regions of α-Syn. In fact, OleA stabilized the NAC and C-terminal region and hindered the long-range interactions favouring amyloid aggregation.
The limited proteolysis data provided important information on α-Syn dynamics and structural rearrangement during the aggregation process in the presence or in the absence of OleA. Actually, α-Syn displayed increased resistance to proteolysis as far as the aggregation process proceeded; this is not surprising, when one considers that, as reported for other amyloid forming proteins, during aggregation the α-Syn polypeptide chain is progressively embedded into the highly ordered, compact fibrillar structure

(Polverino de Laureto et al., 2003).

In the presence of OleA, α-Syn exhibited a reduced tendency to aggregate and a concomitant increased sensitivity to proteolysis, whereas, the off-pathway oligomeric species eluting at RT 51.2 min were proteolysis-resistant. To better describe this finding, the α-Syn species were classified as PK-sensitive, PK-resistant and PK-resistant off-pathway oligomers (Figure 24). These data confirm that the oligomeric species in the mixture do interact with OleA, giving rise to off-pathway oligomers (PK-resistant RT 51.2) and to a stabilized form of monomeric α-Syn (PK-sensitive). Moreover, the species populating this sample showed a membrane activity and cytotoxicity that decreased as far as the incubation with the polyphenol was prolonged. In parallel, we observed a concomitant decrease in ROS levels, one of the events associated to amyloid toxicity, which, in this case, was assigned to OleA re-modelling of the growing assemblies, that, eventually, showed different surface properties. In the case of pre-formed fibrils, the ThT data showed a modest effect of OleA. However, the limited proteolysis experiments suggest that the polyphenol induces the formation of the PK-resistant species eluted at RT 51.2 with reduction of PK-resistant α-Syn, whereas monomeric PK-sensitive α-Syn was scarcely affected (Figure 24b). Furthermore, the toxicity of pre-formed fibrils treated with the polyphenol was not significantly affected even after a prolonged treatment (5 days), yet in the presence of a significant reduction of oxidative stress. The reduced cellular levels of ROS could result from the radical scavenging properties of OleA in accordance with previous studies describing the role of the antioxidant properties of this polyphenol in the prevention of amyloid assembly cytotoxicity (Rizzo et al., 2017). However, in this case, aggregate toxicity persisted because OleA failed to reduce the membrane activity of the pre-formed fibrils treated with the polyphenol.

In conclusion, our data support the existence of parallel mechanisms of action of OleA. We hypothesized that OleA interacts differently with the previously reported interconverting conformers of monomeric α-Syn in solution (Esteban-Martín et al., 2013), stabilizing the best-fitting conformation. Moreover, OleA might select the most prone-to-aggregation conformation, confining it into a non-toxic off-pathway oligomer. This view can be supported by the faster conversion of the aggregation-prone monomeric α-Syn into off-pathway oligomers in the presence of OleA, during the early elongation phase; the latter normally is populated by aggregation-prone monomeric α-Syn and early on-pathway oligomers, that become solubilised and stabilized in the

presence of OleA. At the plateau phase, the effect of OleA on pre-formed fibrils is different, since OleA did not solubilize the fibrils but converted them into smaller assemblies that eluted in RP-HPLC as the off-pathway oligomers grown from aggregation prone α-Syn. In addition, at molecular level, OleA stabilized the NAC and C-terminal regions of α-Syn, preventing the long-range and hydrophobic interactions that favour amyloid aggregation (Dedmon et al., 2005).

Taken together, our data support the potentiality of polyphenols and similar compounds as neuroprotective agents extending the beneficial properties of olive polyphenols or their molecular scaffolds as promising candidates for long-term nutraceutical treatment of PD. The latter could reduce and delay aging-associated neurodegeneration in sporadic PD limiting the need of the symptomatic pharmacological treatment, the only one presently available, in the expectation that new therapies, such as cell therapy, will improve their efficacy in large number of patients. Moreover, our analysis of the structural and biological features of the α-Syn oligomeric species grown at different aggregation conditions provides an useful contribution to better understand, at the molecular level, their neurotoxicity in neurodegeneration, as issue of particular relevance in PD pathogenesis.

Our work on D76N β2M, instead, belong to that group of therapies that try to identify a pathway able to induce the autophagic process in order to promote the clearance of the aggregated proteins. Numerous groups have demonstrated that neurodegeneration could be ameliorated by up-regulating the activities of cellular clearance systems such as proteasome or autophagy through small molecules or peptides. Many small molecule screens have been reported that have identified the druggable candidate(s) (target proteins or pathways).

Our cytotoxicity results showed that despite the different treatment times SH-SY5Y cells treated with D76N β2M non-sonicated oligomers (β2 24h) did not show any real toxicity, on the contrary, the cells treated with D76N β2M sonicated oligomers (β2 24hS) showed a time dependent cytotoxicity (Figure 32). Having evaluated times between 30 min and 24h we took as revering treatment time an intermediate value of 5h.

Consistent with the MTT assay results, the data obtained from the ROS analysis shows slightly higher levels of ROS than those found in the untreated sample in cells treated

with β2 24h, while the levels increase, always in a time-dependent manner, in the treated samples with β2 24hS for longer (Figure 33).

Based on these data we evaluated the possibility of activating the autophagy process. We show that in the presence of D76N β2M sonicated oligomers, therefore morphologically different, precisely, smaller than those not sonicated, is observed the presence of autophagosomes, a spherical structure with double layer membranes which delivers cytoplasmic components to the lysosomes, by Cyto-ID® analysis. Further the autophagosome formation, after 5h of treatment, is confirmed in the presence of the D76N β2M sonicated oligomeric species by the Western Blot analysis which show the expression of conjugated form of the LC3 protein (LC3II) presents on the autophagosome surface (Figure 35 and 36).

Once the autophagic process was established, we tried to identify the signaling cascade responsible for activating autophagy. We focused on the markers that in literature are the ones most cited to be involved in the autophagy pathway like ERK (extracellular signal–regulated kinases), a protein belonging to the MAPK kinase family in mammals (Martinez-Lopez et al., 2013), AKT, also known as Protein kinase B (PKB), a serine/threonine kinase protein of 57-kDa (Memmott & Dennis, 2009) involved in the PI3K/AKT/mTOR pathway, GSK-3β (glycogen synthase kinase 3) (Gowrikumar et al., 2014) and S6 molecule, a substrate of p70 which is a direct substrate of mTOR (Sun et al., 2018).

Indeed, our Western Blot results have identified a signalling pathway involving phosphorilased form of ERK, AKT and GSK-3β which are before the mTOR complex which, as we have already specified in the previous chapters, is the key molecule for the activation of autophagy. To confirm the inhibition of mTOR we dimostrated the reduction of the expression of the phosphorylation of the S6 which is after the key complex of mTOR.

Despite the pathway described above, we have not yet been able to identify where this signalling cascade begins at the level of the cell membrane. Previous studies, carried out in our laboratory, have identified the lipids rich in GM1 as membrane areas where the interaction between cell and protein aggregates is strong. The D76N β2M fibrils (144h) bound to the cell membrane without penetrating inside the cells and that their cytotoxicity was associated to some modification of membrane permeability, suggesting that our fibrillar aggregates did heavily dismantle the phospholipid bilayer of the

exposed cells (Leri et al., 2016). Co-localization and FRET experiments showed that the interaction with the cell membrane of aged D76N aggregates occurred at the raft level and involved the GM1 ganglioside, a key raft component, particularly its sialic acid moiety.

On the basis of these data and further confocal microscopy analysis we had identified a receptor that appeared to be co-localizing with the D76N β2M sonicated oligomers. This receptor known by the name of GPR37 is a seven-pass transmembran G protein-coupled receptor (GPCR) which is highly expressed in the nervous system and is partitioned in GM1 ganglioside containing lipid rafts in the plasma membrane of live cells. Unfortunately, various analyses of both western blot and confocal immunofluorescence have not confirmed this theory. Not much of this receptor is known, in fact it is called an orphan receptor (Mattila et al., 2016).

Signalling pathways do not act in isolation, but crosstalk (i.e., interact) with each other, forming complex signalling networks (Rozengurt, 2007). Multiple lines of evidence support the notion that crosstalk between hepta-helical G protein-coupled receptor (GPCR) and the insulin/insulin-like growth factor 1 (IGF-1) receptor signalling systems plays a critical role in the regulation of multiple physiological functions (Rozengurt et al., 2010). For this reason we focused on the possible involvement of IGF-1R but, also in this case, after Western Blot and immunofluorescence experiments the results have not been satisfactory so we are still looking for a possible responsible at the level of the cell membrane. We have to keep working on identifying which receptor on the cell membrane is involved in the interaction with the D76N β2M sonicated oligomers and in the initiation of the autophagic process.

Clearly this study is still evolving but the precise autophagy pathway identified remains the focus of the project and the key point from which to continue with the experiments, infact autophagy-related proteins and enzymes in neurodegenerative disorders, as already mentioned, may open the avenues for potential targets for discovering effective therapies.

Following these encouraging results, this thesis sought to investigate the molecular and cellular mechanisms, involved in the interference of OleA on the α-Syn aggregation process and in the capacity of D76N β2M sonicated oligomers to induce the autophagy activation using human neuroblastoma SH-SY5Y cells, to find a possible therapy for the

treatment of Synucleinopathies of which the most famous and important is PD and the β2-Microglobulin amyloidosis.

References

Alarcón, J.M. et al., 2006. on channel formation by Alzheimer's disease amyloid beta-peptide (Abeta40) in unilamellar liposomes is determined by anionic phospholipids. *peptides*, 27, pp.95-104.

Alayev , A. et al., 2014. Phosphoproteomics reveals resveratrol-dependent inhibition of Akt/mTORC1/S6K1 signaling. *J Proteome Res* , 13, pp.5734-42.

Anderson, R.G., 1998. The caveolae membrane system. *Annu. Rev. Biochem.* , 67, pp.199-225.

Andringa, G. et al., 2004. Tissue transglutaminase catalyzes the formation of alpha-synuclein crosslinks in Parkinson's disease. *FASEB J.*, 18, pp.932-34.

Appel-Cresswell, S. et al., 2013. Alpha-synuclein p.H50Q, a novel pathogenic mutation for Parkinson's disease. *Mov Disord.*, 28, pp.811-13.

Arispe, N., Pollard, H.B. & Rojas, E., 1993. Giant multilevel cation channels formed by Alzheimer disease amyloid beta-protein [A beta P-(1-40)] in bilayer membranes. *Proc Natl Acad Sci U S A.* , 90, pp.10573-10577.

Baldioli, M., Servili, M., Perretti, G. & Montedoro, G.F., 1996. Antioxidant activity of tocopherols and phenolic compounds of virgin olive oil. *J. Am. Oil Chem. Soc.* , 73, pp.1589-1593.

Ballardie, F.W., Kerr, D.N.S., Tennent, G. & Pepys, M.B., 1986. Haemodialysis versus CAPD: equal predisposition to amyloidosis?. *Lancet* , 1, pp.795-796.

Barbaro, B. et al., 2014. Effects of the Olive-Derived Polyphenol Oleuropein on Human Health. *Int. J. Mol. Sci.* , 15, pp.18508-18524.

Bemporad, F. & Chiti, F., 2012. Protein misfolded oligomers: experimental approaches, mechanism of formation, and structure-toxicity relationships. *Chem Biol.* , 19, pp.315-27.

Bjerrum, O.W. & Plesner, T., 1985. Beta-2-microglobulin: a valuable parameter of stage, prognosis and response to treatment in myelomatosis,. *Scand J Haematol* , 35, pp.22-25.

Bjorkman, P.J. et al., 1987. Structure of the human class-I histocompatibility antigen,Hla-A2. *Nature* , 329, pp.506–512.

Blommaart , E.F.C. et al., 1995. Phosphorylation of ribosomal protein S6 is inhibitory for autophagy in isolated rat Hepatocytes. *Journal of Biological Chemistry* , 270, pp.2320–2326.

Bokvist, M., Lindström, F., Watts, A. & Gröbner, G., 2004. Two types of Alzheimer's beta-amyloid (1-40) peptide membrane interactions: aggregation preventing transmembrane anchoring versus accelerated surface fibril formation. *J Mol Biol.* , 335, pp.1039-1049.

Bonifati, V. et al., 2003. DJ-1(PARK7), a novel gene for autosomal recessive, early onset parkinsonism. *Neurol Sci.*, 24, pp.159-60.

Booth, D.R. et al., 1997. Instability, unfolding and aggregation of human lysozyme variants underlying amyloid fibrillogenesis. *Nature*, 385, pp.787–793.

Bourquelot, E. & Vintilesco, J.C.R., 1908. Sur l'oleuropein, nouveau principe de nature glucosidique retré de l'olivier (Olea europaeaL.). *Compt. Rend. Hebd. Acad. Sci.* , 147, pp.533-535.

Bové, J., Martínez-Vicente, M. & Vila, M., 2011. Fighting neurodegeneration with rapamycin: mechanistic insights.. *Nat. Rev. Neurosci.*, 12, pp.437-52.

Braak, H. et al., 2003. Staging of brain pathology related to sporadic Parkinson's disease. *Neurobiol Aging.*, 24, pp.197-211.

Breydo, L. & Uversky, V.N., 2015. Structural, morphological, and functional diversity of amyloid oligomers. *FEBS Lett.*, 589, pp.2640-48.

Brown, E.A. & Gower, P.E., 1982. Joint problems in maintenance haemodialysis. *Clin Nephrol* , 18, pp.247-250.

Bucciantini, M. et al., 2012. Toxic effects of amyloid fibrils on cell membranes: the importance of ganglioside GM1. *FASEB J.* , 26, pp.818–831.

Burré, J. et al., 2010. Alpha-synuclein promotes SNARE-complex assembly in vivo and in vitro. *Science*, 329, pp.1663-67.

Burré, J. et al., 2013. Properties of native brain α-synuclein. *Nature*, 498, pp.4-6.

Bychkova , V.E., Pam , R.H. & Ptitsyh, O.B., 1988. The molten globule state is involved in the traslocation of protein across membranes. *FEBS Lett.* , 238, pp.231-234.

Cai , Z. et al., 2012. Roles of AMP-activated Protein Kinase in Alzheimer's Disease. *Neuromol Med* , 14, pp.1–14.

Calamai, M. & Pavone, F.S., 2013. Partitioning and confinement of GM1 ganglioside induced by amyloid aggregates. *FEBS Lett.* , 587, pp.1385-1391.

Canale, C., Oropesa-Nuñez, R., Diaspro, A. & Dante, S., 2018. Amyloid and membrane complexity: The toxic interplay revealed by AFM. *Semin Cell Dev Biol.*, 73, pp.82-94.

Canale, C. et al., 2006. Natively folded HypF-N and its early amyloid aggregates interact with phospholipid monolayers and destabilize supported phospholipid bilayers. *Biophys J.*, 91(12), pp.4575-88.

Carluccio, M.A. et al., 2003. Olive oil and red wine antioxidant polyphenols inhibit endothelial activation: antiatherogenic properties of Mediterranean diet phytochemicals. *Arterioscler Thromb Vasc Biol* , 23, pp.622-29.

Casamenti, F. et al., 2015. Oleuropein Aglycone: A Possible Drug against Degenerative Conditions. In Vivo Evidence of its Effectiveness against Alzheimer's Disease. *J Alzheimers Dis.* , 45, pp.679- 688.

Casamenti, F. & Stefani, M., 2017. Olive polyphenols: new promising agents to combat aging-associated neurodegeneration. *Expert Rev Neurother.*, 17, pp.345-58.

Cassuto, J.P. et al., 1978. *Lancet* , 2, pp.108-109.

Chamberlain, A.K. et al., 2000. Ultrastructural organization of amyloid fibrils by atomic force microscopy. *Biophys J.* , 79, pp.3282-3293.

Chapman, M.R. et al., 2002. Role of Escherichia coli curli operons in directing amyloid fiber formation. *Science* , 295, pp.851–55.

Chernoff, Y.O., 2004. Amyloidogenic domains, prions and structural inheritance: rudiments ofearly life or recent acquisition?. *Curr. Opin. Chem. Biol.* , 8, pp.665–71.

Cheynier, V., Sarni-Manchado, P. & Quideau, S., 2012. Recent advances in polyphenol research. *John Wiley & Sons* .

Chiti, F. et al., 2001. Solution conditions can promote formation of either amyloid protofilaments or mature fibrils from the Hypf N-temrinal domani. *Protein Sci.* , 10, pp.2541-2547.

Chiti, F. & Dobson, C.M., 2006. Protein misfolding, functional amyloid, and human disease. *Annu Rev Biochem.* , 75, pp.333-66.

Chiti, F. & Dobson, C.M., 2017. Amyloid Formation, and Human Disease: A Summary of Progress Over the Last Decade. *Annu Rev Biochem.* , 20(86), pp.27-68. doi: 10.1146/annurev-biochem-061516-045115.

Claessen, D. et al., 2003. A novel class of secreted hydrophobic proteins is involved in aerial hyphae formation in Streptomyces coelicolor by forming amyloid-like fibrils. *Genes Dev.* , 17, pp.1714–1726.

Codogno , P. & Meijer , A.J., 2003. Signaling pathways in mammalian autophagy. *Autophagy* .

Connors, L.H. et al., 1985. *Biochem Biophys Res Commun* , 131, pp.1063-1068.

Corazza, A. et al., 2004. Properties of some variants of human beta2-microglobulin and amyloidogenesis. *J Biol Chem.* , 279, pp.9176-89.

Corona, G. et al., 2007. Inhibition of p38 CREB phosphorylation and COX-2 expression by olive oil polyphenols underlies their anti-proliferative effects. *Biochem.Biophys. Res. Commun.* , 362 , pp.606-611.

Cuervo, A.M., 2004. Many paths to the same end. *Molecular and Cellular Biochemistry* , 263, pp.55–72.

Cuervo, A.M., 2008. Autophagy and aging: keeping that old broom working. *Trends Genet.*, 24, pp.604-12.

Cuervo, A.M. & Dice, J.F., 1998. Lysosomes, a meeting point of proteins, chaperones, and proteases. *J Mol Med* , 76, pp.6-12.

Daccache, A. et al., 2011. Oleuropein and derivatives from olives as Tau aggregation inhibitors. *Neurochem Int.*, 58, pp.700-07.

Damtoft, S., Franzyk, H. & Jensen, S.R., 1993. Biosynthesis of secoiridoid glucosides in Oleaceae. *Phytochemistry* , 34, pp.1291–1299.

Danzer, K.M. et al., 2009. Seeding induced by alpha-synuclein oligomers provides evidence for spreading of alpha-synuclein pathology. *J Neurochem.*, 111, pp.192-203.

Dauer, W. & Przedborski, S., 2003. Parkinson's disease: mechanisms and models. *Neuron.*, 39, pp.889-909.

De Duve, C., 1963. The lysosome. *Sci Am* , 208, pp.64-72.

De Franceschi, G. et al., 2009. Molecular insights into the interaction between alpha-synuclein and docosahexaenoic acid. *J Mol Biol.*, 20, pp.94-107.

De la Puerta, R. et al., 2001. Effects of olive oil phenolics on scavenging of reactive nitrogen species and upon nitrergic neurotransmission. *Life Sci.* , 69, pp.1213–1222.

De Leonardis, A., Macciola, V. & Defelice, M., 1998. Rapid determination of squalene in virgin olive oils using gas-liquid chromatography. *Ital. J. Food Sci.* , 10, pp.75-80.

de Rijk, M.C. et al., 1997. Prevalence of parkinsonism and Parkinson's disease in Europe: the EUROPARKINSON Collaborative Study. European Community Concerted Action on the Epidemiology of Parkinson's disease.. *J Neurol Neurosurg Psychiatry.*, 62, pp.10-5.

Dedmon , M.M., Patel , C.N., Young , G.B. & Pielak , G.J., 2002. F1gM gains structure in living cells. *Proc. Natl. Acad. Sci.* , 99, pp.12681-12684.

Dedmon, M.M. et al., 2005. Mapping long-range interactions in alpha-synuclein using spin-label NMR and ensemble molecular dynamics simulations. *J Am Chem Soc.*, 127, pp.476-7.

Dennis , P.B. et al., 2001. Mammalian TOR: a homeostatic ATP sensor. *Science*, 294, pp.1102–1105.

Dice, J.F., 200. Lysosomal Pathways of Protein Degradation. *Landes Bioscience* , p.107.

Dinner, A.R. et al., 2000. Understanding protein folding via free-energy surfaces from theory and experiment. *Trends Biochem Sci.*, 25, pp.331-39.

Diociaiuti, M. et al., 2006. Calcitonin forms oligomeric pore-like structures in lipid membranes. *Biophys J.* , 91, pp.2275-2281.

Diomede, L. et al., 2013. Oleuropein aglycone protects transgenic C.elegans strains expressing Aβ 42 by reducing plaque load and motor deficit. *PLoS ONE* , 8, p.e58893.

Dobson , C.M., Sali , A. & Karplus , M., 1998. Protein folding: a perspective from theory and experiment Angew. *Chem. Int. Ed. Eng.* , 37, pp.868–893.

Dobson, C.M., 2001. The structural basis of protein folding and links with human disease. *Phil. trans. R. soc Lond. B* , 356, pp.133-145.

Dobson, C.M., 2003. Protein folding and misfolding. *Nature*, 18, pp.884-90.

Dorsey, E.R. et al., 2007. Projected number of people with Parkinson disease in the most populous nations, 2005 through 2030. *Neurology.*, 68, pp.384-86.

Dufty, B.M. et al., 2007. Calpain-cleavage of alpha-synuclein: connecting proteolytic processing to disease-linked aggregation. *Am J Pathol.* , 170, pp.1725-38.

Dunlop , E.A. & Tee , A.R., 2009. Mammalian target of rapamycin complex 1: signalling inputs, substrates and feedback mechanisms. *Cell Signal* , 21, pp.827-35.

Ebeling, W. et al., 1974. Proteinase K from Tritirachium album Limber. *Eur J Biochem.*, 47, pp.91-97.

Eliezer, D., Kutluay, E., Bussell, R. & Browne, G., 2001. Conformational properties of alpha-synuclein in its free and lipid-associated states. *J Mol Biol.*, 307, pp.1061-73.

Ellis , R.J., 2001. Macromolecular crowding: an important but neglected aspect of the intracellular enviroment. *Cun. Opin. Struct. Biol.* , 11 , pp.114-119.

Engel, M.F., 2009. Membrane permeabilization by Islet amyloid polypeptide. *Chem. Phys. Lipids* , 160, pp.1-10.

Escrich, E. et al., 2007. Molecular mechanisms of the effects of olive oil and other dietary lipids on cancer. *Mol Nutr Food Res* , 51, pp.1279- 1292.

Escrich, E., Solanas, M. & Moral, R., 2006. Olive oil, and other dietary lipids, in cancer: experimental approaches. *Olive oil and health* , pp.317-374.

Eskelinen, E.L., 2005. Maturation of autophagic vacuoles in mammalian cells. *Autophagy* , 1, pp.1-10.

Esposito, G. et al., 2000. Removal of the N-terminal hexapeptide from human beta2-microglobulin facilitates protein aggregation and fibril formation. *Protein Sci* , 9 , pp.831-845.

Esposito, G. et al., 2008. The controlling roles of Trp60 and Trp95 in beta2-microglobulin function, folding and amyloid aggregation properties. *J Mol Biol* , 378, pp.887-897.

Esteban-Martín, S., Silvestre-Ryan, J., Bertoncini, C.W. & Salvatella, X., 2013. Identification of fibril-like tertiary contacts in soluble monomeric α-synuclein. *Biophys J.*, 105, pp.1192-98.

Evangelisti, E. et al., 2012. Membrane lipid composition and its physicochemical properties define cell vulnerability to aberrant protein oligomers. *J Cell Sci.*, 10(125), pp.2416-27.

Fang, X. et al., 2000. Phosphorylation and inactivation of glycogen synthase kinase 3 by protein kinase A. *PNAS*, 97, pp.11960–65.

Fares, M.B. et al., 2014. The novel Parkinson's disease linked mutation G51D attenuates in vitro aggregation and membrane binding of α-synuclein, and enhances its secretion and nuclear localization in cells. *Hum Mol Genet.*, 23, pp.4491-509.

Fleming , A., Noda , T., Yoshimori , T. & Rubinsztein , D.C., 2011. Chemical modulators of autophagy as biological probes and potential therapeutics. *Nat Chem Biol* , 7, pp.9-17.

Fontana, A. et al., 2004. Probing protein structure by limited proteolysis. *Acta Biochim Pol.* , 51, pp.299-321.

Fowler, D.M. et al., 2006. Functional amyloid formation within mammalian tissue. *PLoS Biol* , 4, pp.1-6.

Frid, P., Anisimov, S.V. & Popovic, N., 2007. Congo red and protein aggregation in neurodegenerative diseases. *Brain Res Rev.* , 53, pp.135-160.

Fulop , T., Larbi , A. & Douziech , N., 2003. Insulin receptor and ageing. *Pathol Biol.* , 51, pp.574-580.

Furukawa, K. et al., 2011. Regulatory mechanisms of nervous systems with glycosphingolipids. *Neurochem. Res.* , 36, pp.1578–1586.

Ganley, I.G., 2013. Autophagosome maturation and lysosomal fusion. *Essays Biochem.*, 55, pp.65-78.

Gasset, M. et al., 1995. Thermal unfolding of the cytotoxin alpha-sarcin: phospholipid binding induces destabilization of the protein structure. *Biochim Biophys Acta.* , 1252, pp.126-134.

Gejyo, F., Homma, N., Suzuki, Y. & Arakawa, M., 1986. *N Engl J Med* , 314, pp.585-586.

Gellermann, G.P. et al., 2005. Raft lipids as common components of human extracellular amyloid fibrils. *Proc. Natl. Acad. Sci. USA* , 102, pp.6297–6302.

Gill, S.C. & von Hippel, P.H., 1989. Calculation of protein extinction coefficients from amino acid sequence data. *Analytical Biochemistry*, 182, pp.319-26.

Giorgetti, S. et al., 2009. *Nephrol Dial Transplant* , 24, pp.1176-1181.

Glenner, G.G., 1980. Amyloid deposits and amyloidosis, The fl-fibrilloses. *N Engl J Med* , 302, pp.1333-1342.

Glick, D., Barth, S. & Macleod, K.F., 2010. Autophagy: cellular and molecular mechanisms. *J Pathol.* , 22, pp.3–12.

Goedert, M., Spillantini, M.G., Del Tredici, K. & Braak, H., 2013. 100 years of Lewy pathology. *Nat Rev Neurol.*, 9, pp.13-24.

Gorevic, P.D., Munoz, P.C. & Casey, T.T., 1986. Polymerization of intact beta-2 microglobulin in tissue causes amyloidosis in patients on chronic hemodialysis. *Proc Natl Acad Sci USA* , 83, pp.7908-7912.

Gowrikumar, S., Palanivel, C., Ramar, M. & Ganapasam, S., 2014. Hesperidin induces apoptosis and triggers autophagic markers through inhibition of Aurora-A mediated phosphoinositide-3-kinase/Akt/mammalian target of rapamycin and glycogen synthase kinase-3 beta signalling cascades in experimental colon carcinogenesis. *European Journal of Cancer*, 50, pp.2489-507.

Grossi, C. et al., 2013. The polyphenol oleuropein aglycone protects TgCRND8 mice against Aß plaque pathology. *PLoS One* , 8, p.71702.

Guijarro, J.I. et al., 1998. Amyloid fibril formation by an SH3 domain. *Proc Natl Acad Sci U S A.* , 95, pp.4224-4228.

Gutierrez-Rosales, F. et al., 2010. Metabolites involved in Oleuropein accumulation and degradation in fruits of Olea europaea L. Hojiblanca and Arbequina Varieties. *J. Agric. Food Chem.*, 58, pp.12924–33.

Hakomori, S. et al., 1998. New insights in glycosphingolipid function: "glycosignaling domain," a cell surface assembly of glycosphingolipids with signal transducer molecules, involved in cell adhesion coupled with signalling. *Glycobiology* , 8, pp.11-14.

Harper , J.D., Lieber, C.M. & Lansbury, P.T., 1997. Atomic force microscopic imaging of seeded fibril formation and fibril branching by the Alzheimer's disease amyloid-beta protein. *Chem Biol.* , 4, pp.951-959.

Hartl, F.U. & Hayer-Hartl, M., 2002. Molecular chaperones in the cytosol: from nascent chain to folded protein. *Science* , 295, pp.1852-1858.

Hashimoto, M. et al., 1999. Oxidative stress induces amyloid-like aggregate formation of NACP/alpha-synuclein in vitro. *Neuroreport.* , 10, pp.717-21.

Hawe, A., Sutter, M. & Jiskoot, W., 2008. Extrinsic Fluorescent Dyes as Tools for Protein Characterization. *Pharmaceutical Research*, 25, pp.1487-99.

Hong, D.P., Fink, A.L. & Uversky, V.N., 2008. Structural characteristics of alpha-synuclein oligomers stabilized by the flavonoid baicalein. *J Mol Biol.*, 31, pp.214-23.

Hurst, N.P. et al., 1989. *Ann Rheum Dis* , 48, pp.409-420.

Ibáñez, P. et al., 2004. Causal relation between alpha-synuclein gene duplication and familial Parkinson's disease. *Lancet.*, 364, pp.1169-71.

Iconomidou, V.A. et al., 2006. Amyloid fibril formation propensity is inherent into the hexapeptide tandemly repeating sequence of the central domain of silkmoth chorion proteins of the A-family. *J Struct Biol.* , 156, pp.480-488.

Inoki , K., Zhu , T. & Guan , K.L., 2003. TSC2 mediates cellular energy response to control cell growth and survival. *Cell* , 115, pp.577-590.

Jahn, T.R. & Radford , S.E., 2005. *The Yin and Yang of protein folding.* FEBS J.

Jahn, T.R. & Radford, S.E., 2005. *the Yin and Yang of protein folding*. FRBS J.

Jares-EriJman, E.A. & Jovin, T.M., 2006. Imaging molecular interactions in living cells by FRET microscopy. *Curr. Opin.Chem. Biol.*, 10, pp.409-16.

Javitch, J.A., D'Amato, R.J., Strittmatter, S.M. & Snyder, S.H., 1985. Parkinsonism-inducing neurotoxin, N-methyl-4-phenyl-1,2,3,6 -tetrahydropyridine: uptake of the metabolite N-methyl-4-phenylpyridine by dopamine neurons explains selective toxicity. *Proc Natl Acad Sci U S A.*, 82, pp.2173-77.

Johansen, T. & Lamark, T., 2011. Selective autophagy mediated by autophagic adapter proteins. *Autophagy* , 7, pp.279–296.

Jones, S., Smith, D.P. & Radford, S.E., 2003. Role of the N and C-terminal strands of beta 2- microglobulin in amyloid formation at neutral pH. *J Mol Biol.* , 330, pp.935-941.

Jung , C.H. et al., 2010. mTOR regulation of autophagy. *FEBS Letters* , 584, pp.1287–1295.

Jung, C.H. et al., 2010. mTOR regulation of autophagy. *FEBS Letters* , 584, pp.1287–1295.

Kaida, K., Ariga, T. & Yu, R.K., 2009. Antiganglioside antibodies and their pathophysiological effects on Guillain-Barre syndrome and related disorders. *Glycobiology* , 19, pp.676–692.

Kalanj-Bognar, S., 2006. Ganglioside catabolism is altered in fibroblasts and leukocytes from Alzheimer's disease patients. *Neurobiol. Aging.* , 27, pp.1354–1356.

Karube, H. et al., 2008. N-terminal region of alpha-synuclein is essential for the fatty acid-induced oligomerization of the molecules. *FEBS Lett.*, 582, pp.3693-700.

Kayed, R. et al., 2003. Common structure of soluble amyloid oligomers implies common mechanism of pathogenesis. *Science*, 300, pp.486-489.

Kiely, A.P. et al., 2013. α-Synucleinopathy associated with G51D SNCA mutation: a link between Parkinson's disease and multiple system atrophy? *Acta Neuropathol.*, 125, pp.753-69.

Kisilevsky, R. et al., 1986. What factors are necessary for the induction of AA amyloidosis?. *Amy-loidosis* , pp.301-310.

Kitada, T. et al., 1998. Mutations in the parkin gene cause autosomal recessive juvenile parkinsonism. *Nature*, 392, pp.605-08.

Klionsky, D.J. et al., 2003. A unified nomenclature for yeast autophagy-related genes. *Dev. Cell* , 5, pp.539–545.

Klionsky, D.J. et al., 2007. How shall I eat thee. *Autophagy* , 3, pp.413–416.

Konno , K., Hirayama , C., Yasui , H. & Nakamura , M., 1999. Enzymatic activation of oleuropein: a protein crosslinker used as a chemical defense in the privet tree. *Proc Natl Acad Sci* , 96, pp.9159–9164.

Konno, T. et al., 2016. Autosomal dominant Parkinson's disease caused by SNCA duplications. *Parkinsonism Relat Disord.*, 22, pp.S1-6.

Kourie, J.I., 2001. Mechanisms of amyloid beta protein-induced modification in ion transport systems: implications for neurodegenerative diseases. *Cell. Mol. Neurobiol.* , 21, pp.173-213.

Kourie, J.I. & Henry, C.L., 2002. Ion channel formation and membrane-linked pathologies of misfolded hydrophobic proteins: the role of dangerous unchaperoned molecules. *Clin Exp Pharmacol Physiol.* , 29, pp.741-753.

Kourie, J.I. & Shorthouse, A.A., 2000. Properties of cytotoxic peptide-formed ion channels. *Am J Physiol Cell Physiol.* , 278, pp.1063-1087.

Krüger, R. et al., 1998. Ala30Pro mutation in the gene encoding alpha-synuclein in Parkinson's disease. *Nat Genet.*, 18, pp.106-08.

La Vecchia, C., 2004. Mediterranean Diet and cancer. *Public Health Nutr* , 7, pp.965-968.

La Vecchia, C. et al., 1995. Olive oil, other dietary fats, and the risk of breast cancer. 6, pp.545- 550.

Lancet, D., Parham, P. & Strominger, J.L., 1979. *Proc Natl Acad Sci USA* , 76, pp.3844- 3848.

Langston, J.W., Ballard, P., Tetrud, J.W. & Irwin, I., 1983. Chronic Parkinsonism in humans due to a product of meperidine-analog synthesis. *Science.*, 219, pp.979-80.

Lashuel, H.A. et al., 2002. Neurodegenerative disease: amyloid pores from pathogenic mutations. *Nature* , 418.

Lashuel, A., Overk, C.R., Oueslati, A. & Masliah, E., 2013. The many faces of α-synuclein: from structure and toxicity to therapeutic target. *Nat Rev Neurosci.*, 14, pp.38-48.

Laurine, E. et al., 2003. Lithostathine quadruple-helical filaments form proteinase K-resistant deposits in Creutzfeldt-Jakob disease. *J Biol Chem.* , 278, pp.51770-51778.

LaVoie, M.J. & Hastings, T.G., 1999. Dopamine quinone formation and protein modification associated with the striatal neurotoxicity of methamphetamine: evidence against a role for extracellular dopamine.. *J Neurosci.*, 19, pp.1484-91.

Layfield, R., Alban, A., Mayer, R.J. & Lowe, J., 2001. he ubiquitin protein catabolic disorders. *Neurophatal Appl. NeuroBiol.* , 27, pp.171-179.

Le Vine , H., 1999. Quantification of β-sheet amyloid fibril structures with thioflavin T. *Methods in Enzymology*, 309, pp.274-84.

Ledeen, R.W. & Wu, G., 2008. Nuclear sphingolipids: metabolism and signalling. *J. Lipid Res* , 49, pp.1176-1186.

Lee-Huang, S. et al., 2007. Discovery of small-molecule HIV-1 fusion and integrase inhibitors oleuropein and hydroxytyrosol: Part I. Integrase inhibition. *Biochem. Biophys. Res. Commun.* , 354, pp.872–878.

Lee, J.Y. et al., 2010. HDAC6 controls autophagosome maturation essential for ubiquitin-selective quality-control autophagy. *EMBO*, 29, pp.969–980.

Lemkau, L.R. et al., 2012. Mutant protein A30P α-synuclein adopts wild-type fibril structure, despite slower fibrillation kinetics. *J Biol Chem.*, 287, pp.11526-32.

Leri, M. et al., 2016. Molecular insights into cell toxicity of a novel familial amyloidogenic variant of β2-microglobulin. *J. Cell. Mol. Med.*, 20, pp.1443-56.

Leri, M. et al., 2016. The polyphenol Oleuropein aglycone hinders the growth of toxic transthyretin amyloid assemblies. *Journal of Nutritional Biochemistry*, 30, pp.153-66.

Leri, M. et al., 2018. Oleuropein aglycone: A polyphenol with different targets against amyloid toxicity. *Biochim Biophys Acta Gen Subj.*, 1862, pp.1432-42.

LeVine, H., 1993. Thioflavine T interaction with syntetic Alzheimer's disease beta-amyloid peptides: detection of amyloid aggregation in solution. *Protein Sci.* , 2, pp.404-10.

Levinthal , C., 1968. Are there pathways for protein folding?. *J. Chem. Phys* , 85, pp.44-45.

Linke, R.P. et al., 1986. Amyloid kidney stones of uremic patients consist of beta2-microglobulin fragments. *Biochem Biophys Res Commun* , 136, pp.665-671.

Litvinovich, S.V. et al., 1998. Formation of amyloid-like fibrils by self-association of a partially unfolded fibronectin type III module. *J Mol Biol.* , 280, pp.245-258.

Lopez-Miranda, J. et al., 2010. Olive oil and health: Summary of the II International Conference on Olive Oil and Health consensus report, Jaen and Cordoba (Spain) 2008. *Nutr Metab Cardiovasc Diseases* , 20, pp.284- 294.

Lorenzen, N. et al., 2014. How epigallocatechin gallate can inhibit α-synuclein oligomer toxicity in vitro. *J Biol Chem.* , 289, pp.21299-310.

Macario, A.J.L. & De Macario, E.C., 2001. ick chaperones and agenig: a perspective agening. *Res. Rev* , 1, pp.295-311.

Mackay, J.P. et al., 2001. The hydrophobin EAS is largely unstructured in solution and functionsby forming amyloid-like structures. *Structure* , 9, pp.83–91.

Makarov, D.E. & Plaxco, K.W., 2003. The topomer search model: A simple, quantitative theory of two-state protein folding kinetics. *Protein Science*, 12, pp.17-26.

Makin, O.S. & Serpell, L.C., 2005. Structures for amyloid fibrils. *FEBS J.* , 272, pp.5950-5961.

Mangione, P.P. et al., 2013. Structure, folding dynamics, and amyloidogenesis of D76N β2-microglobulin: roles of shear flow, hydrophobic surfaces, and α-crystallin. *J Biol Chem.*, 25, pp.30917-30.

Martinez-Lopez, N. et al., 2013. Autophagy proteins regulate ERK phosphorylation. *Nature Communication*, 4, p.2799.

Martin, A., Joseph, J. & Cuervo, A., 2002. Stimulatory effect of vitamin C on autophagy in glial cells. *J Neurochem* , 82, pp.538–549.

Marygold , S.J. & Leevers , S.J., 2002. Growth signaling: TSC takes it place. *Current Biology* , 12, pp.785–787.

Masuda, M. et al., 2006. Small molecule inhibitors of alpha-synuclein filament assembly. *Biochemistry.*, 45, pp.6085-94.

Masuda, M. et al., 2006. Small molecule inhibitors of alpha-synuclein filament assembly. *Biochemistry.*, 45, pp.6085-94.

Mattila, S.O., Tuusa, J.T. & Petäjä-Repo, U.E., 2016. The Parkinson's-disease-associated receptor GPR37 undergoes metalloproteinase-mediated N-terminal cleavage and ectodomain shedding. *J Cell Sci.*, 129, pp.1366-77.

Maury, C.P.J., 1988. Amyloidosis. *Scand J Rheum* , S74, pp.33 -39.

Maury, C.P.J., Helve, T. & Sjblom, C., 1982. *Rheumatol Int* , 2, pp.145-49.

McKnight, N.C. & Zhenyu, Y., 2013. Beclin 1, an Essential Component and Master Regulator of PI3K-III in Health and Disease. *Current Pathobiology Reports* , 1, pp.231–238.

Meijer , A.J. & Codogno , P., 2004. Regulation and role of autophagy in mammalian cells. *The International Journal of Biochemistry & Cell Biology* , 36, pp.2445–2462.

Memmott, R.M. & Dennis, P.A., 2009. Akt-dependent and -independent mechanisms of mTOR regulation in cancer. *Cell Signal.*, 21, pp.656-64.

Menendez, J.A. et al., 2008. tabAnti-HER2 (erbB-2) oncogene effects of phenolic compounds directly isolated from commercial Extra-Virgin Olive Oil (EVOO). *BMC Cancer.* , 8, p.377.

Miller, D.W. et al., 2004. Alpha-synuclein in blood and brain from familial Parkinson disease with SNCA locus triplication. *Neurology.*, 62, pp.1835-38.

Minguez-Mosquera, M.I., Gandul-Rojas, B., Garrido-Fernàndez, J. & Gallardo-Guerrero, L., 1990. Pigments present in virgin olive oil. *JAOCS* , 67, pp.192-196.

Mizushima, N., Levine , B., Cuervo , A.M. & Klionsky , D.J., 2008. Autophagy fights disease through cellular self-digestion. *Nature* , 451, pp.1069–1075.

Mizushima, N., Levine, B., Cuervo, A.M. & Klionsky, D.J., 2008. Autophagy fights disease through cellular self-digestion. *Nature*, 451, pp.1069–1075.

Mizushima, N., Yoshimori, T. & Ohsumi, Y., 2011. The role of Atg proteins in autophagosome formation. *Annu Rev Cell Dev Biol.* , 27, pp.107-32.

Mortimore , G.E. & Kadowaki , M., 1994. Autophagy: Its mechanism and regulation. *Cellular proteolytic systems* , pp.65–87.

Mortimore, G.E. & Schworer, C.M., 1977. Induction of autophagy by amino-acid deprivation in perfused rat liver. *Nature*, 270, pp.174-76.

Muangpaisan, W., Hori, H. & Brayne, C., 2009. Systematic review of the prevalence and incidence of Parkinson's disease in Asia. *J Epidemiol.*, 19, pp.281-93.

Munishkina, L.A. & Fink, A.L., 2007. Fluorescence as a method to reveal structures and membrane-interactions of amyloidogenic proteins. *Biochim. Biophys. Acta.* , 1768 , pp.1862- 1885.

Mutoh, T. et al., 2006. Role of glycosphingolipids and therapeutic perspectives on Alzheimer’s disease. *CNS Neurol. Disord. Drug Targets* , 5, pp.375–380.

Nakahira, K. & Choi, A.M., 2013. Autophagy: a potential therapeutic target in lung diseases. Am J Physiol Lung Cell. *Mol Physiol.*, 305, pp.93-107.

Nakatogawa, H., Suzuki, K., Kamada, Y. & Ohsumi, Y., 2009. Dynamics and diversity in autophagy mechanisms: lessons from yeast. *Nat. Rev. Mol. Cell Biol.* , 10, pp.458–467.

Nilson, M.R., 2004. Techniques to study amyloid fibril formaions in vitro. *Methods* , 34, pp.151-160.

Nosi, D. et al., 2012. A molecular imaging analysis of Cx43 association with Cdo during skeletal myoblast differentiation. *Journal of Biophotonics*, 6, pp.612-21.

O'Keefe, L. & Denton, D., 2018. Using Drosophila Models of Amyloid Toxicity to Study Autophagy in the Pathogenesis of Alzheimer's Disease. *Biomed Res Int.*, 20, pp.5195-416.

Okubadejo, N.U., Bower, H.J., Rocca, W.A. & Maraganore, D.M., 2006. Parkinson's disease in Africa: A systematic review of epidemiologic and genetic studies. *Mov Disord.*, 21, pp.2150-56.

Omar, S.H., 2010. Oleuropein in olive and its pharmacological effects. *Sci Pharm.* , 78, pp.133-54.

Oropesa-Nuñez, R. et al., 2016. Interaction of toxic and non-toxic HypF-N oligomers with lipid bilayers investigated at high resolution with atomic force microscopy. *Oncotarget*, 7(29), pp.44991-5004. doi: 10.18632/oncotarget.10449.

Ozawa, D. et al., 2011. *J. Biol. Chem.* , 286, pp.9668–9676.

Palazzi, L. et al., 2018. Oleuropein aglycone stabilizes the monomeric α-synuclein and favours the growth of non-toxic aggregates. *Sci Rep.* , 29, pp.1-39.

Pedersen, L.O. et al., 1994. *Scand J Immunol* , 39, pp.64–72.

Pernber, Z. et al., 2012. Altered distribution of the Gangliosides GM1 and GM2 in Alzheimer's disease. *Dement. Geriatr. Cogn. Disord* , 33, pp.174–188.

Perrin, R.J., Woods, W.S., Clayton, D.F. & George, J.M., 2001. Exposure to long chain polyunsaturated fatty acids triggers rapid multimerization of synucleins. *J Biol Chem.*, 276, pp.41958-62.

Peterson, P.A., Cunningham, B.A., Berggård, I. & Edelman, G.M., 1972. *Proc Natl Acad Sci U S A* , 69, pp.1697-1972.

Piazza, R. et al., 2006. Micro- heterogeneity and aggregation in Beta2-microglobulin solutions: affects of temperature, pH, and conformational variant addition. *Eur Biophys J* , 35, pp.439-445.

Poirier, M.A. et al., 2002. Huntingtin spheroids and protofibrils as precursors in polyglutamine fibrilization. *J Biol Chem* , 277, pp.41032-41037.

Polverino de Laureto, P. et al., 2003. Protein aggregation and amyloid fibril formation by an SH3 domain probed by limited proteolysis. *J Mol Biol.*, 334, pp.129-41.

Polymeropoulos, M.H. et al., 1997. Mutation in the alpha-synuclein gene identified in families with Parkinson's disease. *Science*, 27, pp.2045-47.

Pringsheim, T., Jette, N., Frolkis, A. & Steeves, T.D., 2014. The prevalence of Parkinson's disease: a systematic review and meta-analysis. *Mov Disord.*, 29, pp.1583-90.

Quintas, A. et al., 2001. Tetramer dissociation and monomer partial unfolding precedes protofibril formation in amyloidogenic transthyretin variants. *J Biol Chem.* , 276, pp.27207-27213.

Ramakrishnan, M., Yensen, P.H. & Marsh, D., 2006. Association of alpha-synuclein and mutants with lipid membranes: spin-label ESR and polarized IR. *Biochemistry*, 45, pp.3386-95.

Ramirez Tortosa, M.C., Granados, S. & Quiles, J.L., 2006. Chemical composition, types and characteristics of olive oil. *Olive oil and health* , 2, p.45.

Rashid, S.A., Axon, A.T.R., Bullen, A.W. & Cooper, E.H., 1981. *Clin Chim Acta* , 114, pp.83-91.

Renner, M. et al., 2010. Deleterious effects of amyloid beta oligomers acting as an extracellular scaffold for mGluR5. *Neuron* , 66, pp.739–754.

Rigacci , S. & Stefani, M., 2016. Nutraceutical Properties of Olive Oil Polyphenols. An Itinerary from Cultured Cells through Animal Models to Humans. *Int J Mol Sci.*, 17.

Rigacci, S. & Berti, A., 2011. Oleuropein aglycon: the bitter treasure of extra virgin olive oil. *Olive Oil and Health* , pp.221-240.

Rigacci, S. et al., 2011. Aβ (1-42) aggregates into non toxic Amyloid Assemblies in the Presence of the Natural Poliphenol. Oleuropein Aglycon. *Curr res Alzheimer* , 8, pp.841-852.

Rigacci, S. et al., 2011. Aβ(1-42) aggregates into non-toxic amyloid assemblies in the presence of the natural polyphenol oleuropein aglycon. *Curr Alzheimer Res.*, 8, pp.841-582.

Rigacci, S. et al., 2010. Oleuropein aglycon prevents cytotoxic amyloid aggregation of human amylin. *J Nutr Biochem.*, 21, pp.726-35.

Rigacci, S. et al., 2015. Oleuropein aglycone induces autophagy via the AMPK/mTOR signalling pathway: a mechanistic insight. *Oncotarget* , p. .

Riss , T.L. et al., 2013. Cell Viability Assays. *Assay Guidance Manual*.

Rizzo, M. et al., 2017. Antioxidant activity of oleuropein and semisynthetic acetyl-derivatives determined by measuring malondialdehyde in rat brain. *J Pharm Pharmacol.*, 69, pp.1502-12.

Rodríguez-Morató, J. et al., 2015. Potential role of olive oil phenolic compounds in the prevention of neurodegenerative diseases. *Molecules.*, 20, pp.4655-8460.

Rohde , J., Heitman , J. & Cardenas , M.E., 2001. The TOR kinases link nutrient sensing to cell growth. *Journal of Biological Chemistry* , 276, pp.9583–9586.

Rozengurt, E., 2007. Mitogenic signaling pathways induced by G protein-coupled receptors. *J Cell Physiol.*, 213, pp.589-602.

Rozengurt, E., Sinnett-Smith, J. & Kisfalvi, K., 2010. Crosstalk between insulin/insulin-like growth factor-1 receptors and G protein-coupled receptor signaling systems: a novel target for the antidiabetic drug metformin in pancreatic cancer. *Clin Cancer Res.*, 16, pp.2505-11.

Rubinsztein , D.C., Mariño , G. & Kroemer , G., 2011. Autophagy and aging. *Cell* , 146, pp.682- 95.

Rubinsztein, D.C., 2006. The roles of intracellular protein-degradation pathways in neurodegeneration. *Nature* , 443, pp.780-786.

Rubinsztein, D.C., Mariño, G. & Kroemer, G., 2011. Autophagy and aging. *Cell*, 146, pp.682-95.

Russell, R.C. et al., 2013. ULK1 induces autophagy by phosphorylating Beclin-1 and activating Vps34 lipid kinase. *Nature Cell Biology* , 15, pp.741–750.

Rutherford, N.J., Moore, B.D., Golde, T.E. & Giasson, B.I., 2014. Divergent effects of the H50Q and G51D SNCA mutations on the aggregation of α-synuclein. *J Neurochem.*, 131, pp.859-67.

Saija, A. & Uccella, N., 2011. Olive biophenols: functional effects on human well-being. *Trends Food Sci Technol.* , 11, pp.357-363.

Salmona, M. et al., 1997. A neurotoxic and gliotrophic fragment of the prion protein increases plasma membrane microviscosity. *Neurobiol Dis* , 4, pp.47-57.

Sano, K. et al., 2018. Prion-Like Seeding of Misfolded α-Synuclein in the Brains of Dementia with Lewy Body Patients in RT-QUIC. *Mol Neurobiol.*, 55, pp.3916-30.

Saper, M.A., Bjorkman, P.J. & Wiley, D.C., 1991. Refined structure of the human histocompatibility antigen HLA-A2 at 2.6 A resolution.. *J Mol Biol.* , 219, pp.277-319.

Sarolic', M., Gugić, M., Marijanović, Z. & Šuste, M., 2014. Virgin olive oil and nutrition. *Food in health and disease, scientific-professional journal of nutrition and dietetics*, 3, pp.38-43.

Sartiani, L. et al., 2016. Biochemical and Electrophysiological Modification of Amyloid Transthyretin on Cardiomyocytes. *Biophysical Journal*, 111.

Schoenberg, B.S. et al., 1988. Comparison of the prevalence of Parkinson's disease in black populations in the rural United States and in rural Nigeria: door-to-door community studies. *Neurology.*, 38, pp.645-46.

Schwarz, A. et al., 1984. Carpal tunnel syndrome: a major complication in longterm haemodialysis patients. *Clin Nephrol* , 22, pp.133-137.

Seglen , P.O. & Bohley , P., 1992. Autophagy and other vacuolar protein degradation mechanisms. *Experientia* , 48, pp.158–172.

Serpell, L., 2014. *Amyloid structure*. Essay In Biochemistry.

Serpell, L.C. et al., 2000. The protofilament substructure of amyloid fibrils. *J. Mol. Biol.* , 300, pp.1033-1039.

Servili, M. & Montedoro, G.F., 2002. Contribution of phenolic compounds to virgin olive oil quality. *Eur. J. Lipid Sci. Technol.* , 104, pp.1095-1108.

Simons, K. & Toomre, D., 2000. Lipid rafts and signal transduction. *Nat. Rev. Mol. Cell Biol.* , 1, pp.31–39.

Snead, D. & Eliezer, D., 2014. Alpha-synuclein function and dysfunction on cellular membranes. *Exp Neurobiol.* , 23, pp.292-313.

Sparr, E. et al., 2004. Islet amyloid polypeptide-induced membrane leakage involves uptake of lipids by forming amyloid fibers. *FEBS Lett.*, 5, pp.117-20.

Spillantini, M.G. et al., 1998. alpha-Synuclein in filamentous inclusions of Lewy bodies from Parkinson's disease and dementia with lewy bodies. *Proc Natl Acad Sci U S A.*, 95, pp.6469-73.

Stefani, M., 2004. Protein misfolding and aggregation: new examples in medicine and biology of the dark side of the protein world. *Biochim Biophys Acta.* , 1739 , pp.5-25.

Stefani, M., 2008. Protein folding and misfolding on surfaces. *Int. J. Mol. Sci.* , 9, pp.2515- 2542.

Stefani, M. & Dobson, C.M., 2003. Protein aggregation and aggregate toxicity: new insights into protein folding, misfolding diseases and biological evolution. *J. Mol. Med.* , 81, pp.678- 699.

Sunde, M. et al., 1997. Common core structure of amyloid fibrils by synchrotron X-ray diffraction. *J Mol Biol.* , 273, pp.729-739.

Sun, J. et al., 2018. Inhibition of p70 S6 kinase activity by A77 1726 induces autophagy and enhances the degradation of superoxide dismutase 1 (SOD1) protein aggregates. *Cell Death and Disease*, 9, p.407.

Suresh, N.S., Verma, V., Sateesh, S. & Clement, J.P., 2018. Neurodegenerative diseases: model organisms, pathology and autophagy. *Journal of Genetics*, 97, pp.679–701.

Swuec, P. et al., 2018. *Cryo-EM structure of cardiac amyloid fibrils from an immunoglobulin light chain (AL) amyloidosis patient.* ORCID. https://doi.org/10.1101/444901.

Tagliavini, F. et al., 2001. Studies on peptide fragments of prion proteins. *Adv Protein Chem.* , 57, pp.171-201.

Thielemans, C. et al., 1988. Continuous ambulatory peritoneal dialysis vs haemodialysis: a lesser risk of amyloidosis. *Nephrol Dial Transplant* , 3, pp.291-294.

Thomas, P.J., Qu, B.H. & Pedersen, P.L., 1995. Defective protein folding as a basis of human disease. *Trends Biochem. Sci.*, 20, pp.456-459.

Trichopoulou, A., Lagiou, P., Kuper, H. & Trichopoulos, D., 2000. Cancer and Mediterranean Dietary traditions. *Cancer Epidemiol Biomarkers Prev* , 9, pp.869-873.

Ullman, O., Fisher, C.K. & Stultz, C.M., 2011. Explaining the structural plasticity of α-synuclein. *J Am Chem Soc.* , 133, pp.19536-46.

Uversky , V.N., 2002. Natively unfolded proteins: a point where biology waits for physics. *Protein Sci.* , 11, pp.739-756.

Uversky, V.N., 2007. Neuropathology, biochemistry, and biophysics of alpha-synuclein aggregation. *J Neurochem.* , 103, pp.17-37.

Uversky, V.N. & Fink, A.L., 2004. Conformational constraints for amyloid fibrillation: the importance of being unfolded. *Biochim Biophys Acta.* , 1698, pp.131-153.

Uversky, V.N., Li, J. & Fink, A.L., 2001. Evidence for a Partially Folded Intermediate in □-Synuclein Fibril Formation. *Journal of Biological Chemistry*, 276, pp.10737–44.

Valleix, S. et al., 2012. Hereditary systemic amyloidosis due to Asp76Asn variant β2-microglobulin. *N Engl J Med*, 366, pp.2276-8223.

van Maarschalkerweerd, A. et al., 2014. Protein/lipid coaggregates are formed during α-synuclein-induced disruption of lipid bilayers. *Biomacromolecules.*, 15, pp.3643-54.

van Rheenen, J., Langeslang, M. & jalink, K., 2004. *Correcting confocal acquisition to optimize imaging of fluorescence resonance energy transfer by sensitized emission.* Biophys.J.

Van Sluijters , D.A., Dubbelhuis , P.F., Blommaart , E.F. & Meijer , A.J., 2000. Amino-acid- dependent signal transduction. *Biochem. J* , pp.545-550.

Vendal, L.L., Cragg, S.j., Buchman, V.L. & Martins, R.W., 2010. *alpha Synuclein and dopamine at the crossroad of Parkinson's disease*. Trends Neurosci.

Vilchez, D., Saez, I. & Dillin, A., 2014. The role of protein clearance mechanisms in organismal ageing and age-related disease. *Nat. Commun.* , 5, p.5659.

Vincent, C., Pozet, N. & Revillard, J.P., 1980. *Acta. Clin. Belg.*, 35, pp.2- 13.

Visioli , F., Bellomo, G. & Galli, C., 1998. Free radical-scavenging properties of olive oil polyphenols. *Biochem. Biophys. Res. Commun.* , 247, pp.60–64.

Visioli, F., Galli, C., Galli, G. & Caruso, D., 2002. Biological activities and metabolic fate of olive oil phenols. *Eur J Lipid Sci Technol.*, pp.677–684.

Volles, M.J. et al., 2001. Vesicle permeabilization by protofibrillar alpha-synuclein: implications for the pathogenesis and treatment of Parkinson's disease. *Biochemistry* , 40, pp.7812-7819.

Wakabayashi, M. & Matsuzaki, K., 2009. Ganglioside-induced amyloid formation by human islet amyloid polypeptide in lipid rafts. *FEBS Lett.* , 583, pp.2854–2858.

Walsh, P. et al., 2014. The Mechanism of Membrane Disruption by Cytotoxic Amyloid Oligomers Formed by Prion Protein(106 –126) Is Dependent on Bilayer Composition. *Journal of Biological Chemistry*, 289, pp.10419–30.

Warren, D.J. & Otieno, L.S., 1975. Carpal tunnel syndrome in patients on intermittent hemodialysis. *Postgrad Med J* , 51, pp.450- 454.

Wetzel, R., 2002. Ideas of order for amyloid fibril structure. *Structure* , 10, pp.1031-1036.

Wibell, L., Evrin, P.E. & Berggfird, I., 1973. Serum/32-microglobulin in renal disease. *Nephron* , 10, pp.320-331.

Woo, P., O'Brien, J., Robson, M. & Ansell, B.M., 1987. A genetic marker for systemic amyloidosis in juvenile arthritis. *Lancet* , 2, pp.767-769.

Wooten, G.F. et al., 2004. Are men at greater risk for Parkinson's disease than women? *J Neurol Neurosurg Psychiatry.*, 75, pp.637-39.

Wright , P.E. & Dyson , H.J., 1999. Intrinsically unstructured proteins: reassessing the protein structure-function paradigm. *J. Mol.Biol* , 293, pp.321-331.

Yang , Y., Liang , Z., Gu , Z. & Qin , Z., 2005. Molecular mechanism and regulation of autophagy. *Acta Pharmacologica Sinica* , 26, pp.1421-1434.

Yu, R.K., Nakatani, Y. & Yanagisawa, M., 2009. The role of glycosphingolipid metabolism in the developing brain. *J. Lipid Res.* , 50, pp.S440–S445.

Yu, R.K., Tsai, Y.T. & Ariga, T., 2012. Functional roles of gangliosides in neurodevelopment: an overview of recent advances. *Neurochem. Res.* , 37, pp.1230–1244.

Yu, R.K., Tsai, Y.T., Ariga, T. & Yanagisawa, M., 2011. Structures, biosynthesis, and functions of gangliosides--an overview. *J Oleo Sci.*, 60, pp.537-44.

Zarranz, J.J. et al., 2004. The new mutation, E46K, of alpha-synuclein causes Parkinson and Lewy body dementia. *Ann Neurol.*, 55, pp.164-73.

Zhu, M. et al., 2002. Surface-catalyzed amyloid fibril formation. *J Biol Chem.* , 277, pp.50914-50922.

Ringraziamenti

Il primo grande ringraziamento va al mio maritino adorato, fonte inesauribile di supporto ed esempio di tenacia, grazie per credere in me più di quanto faccia io stessa! Ti amo tanto!
Ringrazio tantissimo anche la mia famiglia, i miei straordinari genitori, dispensatori di ottimi consigli che con il loro esempio mi hanno insegnato a rispettare gli altri ma anche me stessa. Non è così scontato quindi grazie mille, vi voglio tanto bene!
Impossibile dimenticare il mio fratellino che mi manca tantissimo ma, nonostante la lontananza sa essere presente nei momenti che contano per questo lo ringrazio e gli mando un bacione pieno d'affetto! Gracias hermano te quiero mucho!
Se sono arrivata alla fine di questo viaggio è anche grazie alle vibrazioni positive inviatemi dalla dolcissima Alex! Merci beaucoup Alex pour votre soutien et vos vibrations positives, elles étaient indispensables! Je t'envoie un gros bisou à toi aussi! Andrea est un garçon très chanceux.

Un grande grazie va al professor Massimo Stefani e alla professoressa Monica Bucciantini i quali mi hanno permesso di proseguire e terminare in maniera serena il mio dottorato di ricerca. Durante questi tre anni ho imparato tantissimo e il merito è della professoressa Bucciantini, ma anche della mia collega Manuela, tutor instancabile! Manuela, insieme a Marzia (non dimenticherò le nostre chiacchierate e risate), Camilla, Giulia, Erica, Alessandra, Lorenzo, Simone, Gianluca e la dolcissima Vlada hanno contribuito a rendere l'esperienza del dottorato, a volte difficile, un viaggio divertente e stimolante! Grazie ragazzi spero davvero di poter continuare a lavorare con voi!
Vorrei ringraziare anche la Professoressa Degl'Innocenti che, nonostante non sia il mio tutor ha saputo insegnarmi molto, non solo sulla Biochimica.

Se come me si viene da un'altra città può essere difficile ambientarsi ma grazie a Luca e Sabrina, io e Simo non ci siamo mai sentiti soli! Grazie ragazzi per averci accolti siete dei carissimi amici!
Ringrazio Chiara, come mi capisci tu nessuno! La nostra amicizia iniziata all'asilo e ancora salda, nonostante la forte lontananza, è una delle cose più preziose che ho! Ti voglio tanto bene!

L’ultimo pensiero va alla creaturina che sta crescendo dentro di me! Hai reso la stesura di questa tesi non poco problematica tra nausee mattutine, stanchezza infinita e grandi spaventi ma sei stata anche fonte di grande determinazione. Mamma e papà non vedono l’ora di conoscerti e ti vogliono già tantissimo bene!